Understanding Electro-Selective Fermentation of *Scenedesmus acutus* and its Effect on Lipids Extraction and Biohydrogenation

by

Yuanzhe Liu

A Dissertation Presented in Partial Fulfillment
of the Requirements of the Degree
Doctor of Philosophy

Approved November 2019 by the
Graduate Supervisory Committee:

Bruce E. Rittmann, Chair
César I. Torres
Rosa Krajmalnik-Brown

ARIZONA STATE UNIVERSITY

December 2019

ABSTRACT

Electro-Selective Fermentation (ESF) combines Selective Fermentation (SF) and a Microbial Electrolysis Cell (MEC) to selectively degrade carbohydrate and protein in lipid-rich microalgae biomass, enhancing lipid wet-extraction. In addition, saturated long-chain fatty acids (LCFAs) are produced via β-oxidation. This dissertation builds understanding of the biochemical phenomena and microbial interactions occurring among fermenters, lipid biohydrogenaters, and anode respiring bacteria (ARB) in ESF. The work begins by proving that ESF is effective in enhancing lipid wet-extraction from *Scenedesmus acutus* biomass, while also achieving "biohydrogenation" to produce saturated LCFAs. Increasing anode respiration effectively scavenges short chain fatty acids (SCFAs) generated by fermentation, reducing electron loss. However, the effectiveness of ESF depends on biochemical characteristics of the feeding biomass (FB). Four different FB batches yield different lipid-extraction performances, based on the composition of FB's cellular structure. Finally, starting an ESF reactor with a long solid retention time (*SRT*), but then switching it to a short *SRT* provides high lipid extractability and volumetric production with low lipid los. Lipid fermenters can be flushed out with short a *SRT*, but starting with a short *SRT* fails achieve good results because fermenters needed to degrading algal protective layers also are flushed out and fail to recover when a long *SRT* is imposed. These results point to a potentially useful technology to harvest lipid from microalgae, as well as insight about how this technology can be best managed.

DEDICATION

It is deep fall in San Jose, California, yet still green in Tempe, Arizona. As I come to the finale of this chapter of my life, I think of a Chinese phrase, “三十而立", which roughly translates to “a person stands when he turns 30”. Yet I am, reaching this milestone of my life, exactly as I turn 30. I have my deepest gratitude for my parents, my father, my mother, you gave your everything, and made me the person I am today. For my parents-in-law, who love and care about me like their own son and gave me incredible richness in my life. Especially my father-in-law, who is a great teacher and senior in Environmental Geology, I always learn from you.

For my wife, Yi Hu, you have my deepest apologies and gratitude, thank you for your understanding across all these 5 years we had to separate. You are my best other part and soul mate, and whenever we meet you become my best partner in crime. I am beyond happy to be able for our Rendezvous after these incredible adventures in these 5 years, and we are expecting much more.

And for Ellie, our upcoming little angel, I’ll see you next January. 待会见!

ACKNOWLEDGEMENTS

I thank Dr. Bruce Rittmann for his constant support, and guidance in my Ph. D studies. I, first, must be grateful for the initial opportunity to meet Dr. Rittmann in Shenzhen, China back in 2015 at an academic meeting, when I received the very first teachings of him. I was fortunately enough to have grasped this opportunity to join the Biodesign Swette Center of Environmental Biotechnology, and have learned much more onwards. As Dr. Rittmann said, his main job is to delete words. In all these years I had worked at the BSCEB on manuscripts, reports, and assignments, I had many words deleted. But these deleted words have deeply inscribed in my mind, helping my progress so much in both writing in academic English concisely, and my understanding on Environmental Biotechnology. I also greatly appreciate and admire Dr. Rittmann's teachings in his class of Advanced Environmental Biotechnology, group meetings, and in-person meetings: his innate passion and exuberance on Environmental Engineering has evoked my hearty admiration. I hope I can bring on his knowledge, as well as passion and energy in my future work and study: to think like a microbe and follow the electrons. Yes, these are my take home lessons from my Ph. D studies.

I thank Dr. Cesar Torres and Dr. Rosa Krajmalnik-Brown for being my committee members. Dr. Torres helped me build the base of Microbial Electrochemical Cell with his class, and Dr. Rosy put in the bricks of biotransformation in my project. Their insightful questions have brought forth and fortified my research greatly. I thank you both for all the hard work you put in my research and studies.

I also wish to thank Dr. Prathap Parameswaran for initiating the idea of "Electro-Selective Fermentation" by combining Selective Fermentation and Microbial Electrolysis Cell. In the first year of my Ph. D program, I was confused when I had to put supernatant of SF in the MEC, and calculate coulombic efficiency: to me it didn't bear much value! Thanks to Dr. Parameswaran's idea, I put algae biomass in the MEC's anode chamber, and started the unforgettable journey of ESF. Dr. Yen-jung Sean Lai for all the wholeheartedly support and help with experiment, understanding the results, via many many discussions. Thank you Dr. Michelle Young for your valuable questions after every meeting that helped my whole project shape.

Thank you to Diana Hagner, Carole Flores and Sarah Arrowsmith for managing the office and lab, helping managing item orders, and maintain a safe and well-organized lab environment. And thank you for organizing so many wonderful parties and birthday cake celebrations – yum!

Thank you to two of my undergraduate students, Neil Rastogi and Steven Nguyen, who I enjoyed to mentor. They took and analyzed batches and batches of samples, with great responsibility and enthusiasm to the project.

My work was generously supported by the National Science Foundation (NSF Award 1509933), the Biodesign Swette Center of Environmental Biotechnology at Arizona State University.

TABLE OF CONTENTS

Page

CHAPTER Page

CHAPTER Page

CHAPTER Page

LIST OF TABLES

LIST OF FIGURES

Figure Page

Figure Page

Figure Page

Figure Page

Figure Page

Figure Page

LIST OF ABBREVIATIONS

AEM	Anion exchange membrane
ARB	Anode respiring bacteria
COD	Chemical oxygen demand
DAG	Diacylglyceride
EET	Extracellular electron transfer
ESF	Electro-selective fermentation
FAME	Fatty acid methyl esters
HRT	Hydraulic retention time
LCFA	Long-chain fatty acids
MEC	Microbial electrolysis cell
MxC	Microbial electrochemical cell
PCoA	Principal Coordinates Analysis
PBS	Phosphate buffer solution
SCFA	Short-chain fatty acids
SCOD	Soluble chemical oxygen demand
SF	Selective fermentation
SRT	Solid retention time
TAG	Tricylglyceride
TCOD	Total chemical oxygen demand
TSS	Total suspended solids
WAS	Waste activated sludge

CHAPTER 1 INTRODUCTION

1.1 Algae-Based Biodiesel as a Replacement for Fossil Fuel

Human society has depended on fossil-fuel for a long time. The United States consumed 8×10^{13} W of energy in 2017 (U.S. Energy Information Administration, 2018), of which 78% was from fossil fuel. This dependency has increasingly become a threat to humanity itself, due to its large contribution the built up of greenhouse gases in the atmosphere and the consequent global warming. Combustion of fossil fuel moves carbon embedded in the Earth's crust to the atmosphere in the form of the greenhouse gas CO_2. The CO_2 concentration in the atmosphere has increased from ~320 ppm_v in 1960 to ~405 ppm_v in 2018 (US Department of Commerce, 2019). Consequently, the global temperature has also registered a 1.8℃ increase from 1940 to 2018 (National Centers for Environmental Information, 2019). Multiple measures must be taken to slow and ultimately reverse the ongoing global warming: reducing CO_2 emission by replacing fossil sources of energy and sequestering CO_2 from the atmosphere (Sayre, 2010). Reducing CO_2 emission will require sustainable non-fossil energy sources at large scale.

Photosynthetic microorganisms, including algae and cyanobacteria, can fix atmospheric CO_2 and synthesize lipids as energy-storage substances that can replace petroleum. The lipids can be a major feedstock for bio-diesel production, since microalgae, including *Scenedesmus*, *Chlorella*, *Nannochloropsis*, and *Chlamydomonas*, can reach up to 60% of their cell dry weight as lipids (Wang et al., 2013a). Moreover, microalgae enjoy high areal productivity compared to macrophyte crops. For example, microalgae with 30% oil by dry weight theoretically can achieve 130 times the rate of biofuel production rate as

soybeans and ~10 times the rate of oil palm (Chisti, 2007). Furthermore, microalgae can be grown in non-arable land or in wastewater stream; thus, microalgae need not compete with food crops. For these reasons, biodiesel production based on microalgal lipids is considered one of the new source of renewable non-fossil energy (Chisti, 2007).

The application of microalga-derived biodiesel has been hampered by difficulties in lipid extraction. Lipids in algae cells are mostly triacylglycerols (TAGs) enclosed in intracellular structures. They are highly protected by the cell wall and cell membrane; thus, effective extraction of intracellular lipids requires that the solvents penetrate to the cell's interior.

Two strategies provide potential solutions to the extraction difficulties: using strong solvents or using pretreatment to disrupt the cell wall and membrane. Strong solvents, such as Folch (1:1 v/v chloroform : methanol) and Bligh & Dyer (1:1:0.5 v/v/v chloroform : methanol : water), can break down the matrix of the cell wall and membrane to achieve effective extraction. However, chloroform has been classified as a Group B2 carcinogen (possibly carcinogen) by the U.S. EPA, hence its use is restricted (Andersen, 2002). Pretreatment methods that disrupt cellular structures can improve lipid accessibility by overcoming cellular resistance to solvent penetration. Pretreatments, which include acid/base addition, pulse-electric fields (PEF), and ultrasound, have been reported to be effective towards enhancement of lipids extraction with "green solvents" like hexane, ethyl acetate and isopropanol (Ehimen et al., 2009; Halim et al., 2011). However, these pretreatment techniques are energy-intensive and capital-expensive. A pretreatment technology that requires less energy would be highly valuable.

1.2 Selective Fermentation (SF)

Selective Fermentation (SF) is a technology, introduced by Lai et al. (2016b), to enhance microalgal-lipids extraction with low-energy input. SF exploits the fact that carbohydrates, proteins, and lipids in microalgae cells have different degradation kinetics in anaerobic conditions. Lipid fermentation is relatively slow, compared to fermentations of carbohydrate and protein (Rittmann and McCarty, 2001); hence, bacteria that specialize in lipid fermentation require a longer retention time to avoid being washed out of the fermentation system. By properly reducing the solids retention time (*SRT*), one can manage the microbial community so that it effectively ferments carbohydrates and proteins, but leaves lipids intact. This has the added benefit of allowing easier lipid-extraction due to the removal of the carbohydrate- and protein-based protection of the microalgae's intracellular structures.

SF also has demonstrated another benefit, biohydrogenation of the lipids (Lai et al., 2016a); biohydrogenation produced more-saturated long-chain fatty acids and their respective fatty acid methyl esters (FAME). Microalgae such as *Chlorella, Scenedesmus,* and *Nannochloropsis* are known to produce and accumulate unsaturated fatty acids, such as C16:1, C18:1 and C18:3 (Taipale et al., 2013). From the perspective of biofuel production, unsaturated fatty acids are not desired, because they are susceptible to oxidation and lower octane value, which undermine combustion performance. Ideal microalgae-derived lipids for biodiesel have low unsaturated lipids and high saturated lipids. SF converted unsaturated lipids to saturated forms via biohydrogenation (Lai et al., 2016b).

1.3 Electro-Selective Fermentation (ESF)

For my PhD research, I introduce the concept of Electro-Selective Fermentation (ESF). It is a combination of SF and a Microbial Electrolysis Cell (MEC). In MECs, anode-respiring bacteria (ARB) form a biofilm on the anode, oxidize short-chain fatty acids (SCFAs), and transfer the extracted electrons to the anode via extracellular electron transfer (EET) (Reguera et al., 2005; Torres et al., 2009b; Torres et al., 2009a; Yang et al., 2012). Electrons travel through the external circuit to the cathode, where they are captured by water molecules to form H_2, which evolves as a gas from the cathode. The MEC is a promising means for enhancing protein biodegradation within complex organic substrates (Lu et al., 2012). Hence, I hypothesize that the combination of MEC and SF, i.e., ESF, should be able to enhance microalgae degradation more than SF by increasing degradation of protein that makes up algae cellular structures, therefore rupturing the cell wall and membrane and exposing intracellular lipids for easier extraction. The removal of short-chain fatty acids by ARBs also can lower the concentrations of SCFAs, therefore lowering thermodynamic barriers to the fermentation reactions and promoting faster fermentation. Low concentration of SCFAs also can mitigate inhibition of fermentation reactions (Kaspar and Wuhrmann, 1977; Siegert and Banks, 2005). Thus, I also hypothesize that ESF will provide the added benefit of producing more saturated fatty acids than was demonstrated by SF. A schematic that links the proposed mechanisms occurring ESF is shown in Figure 1.1.

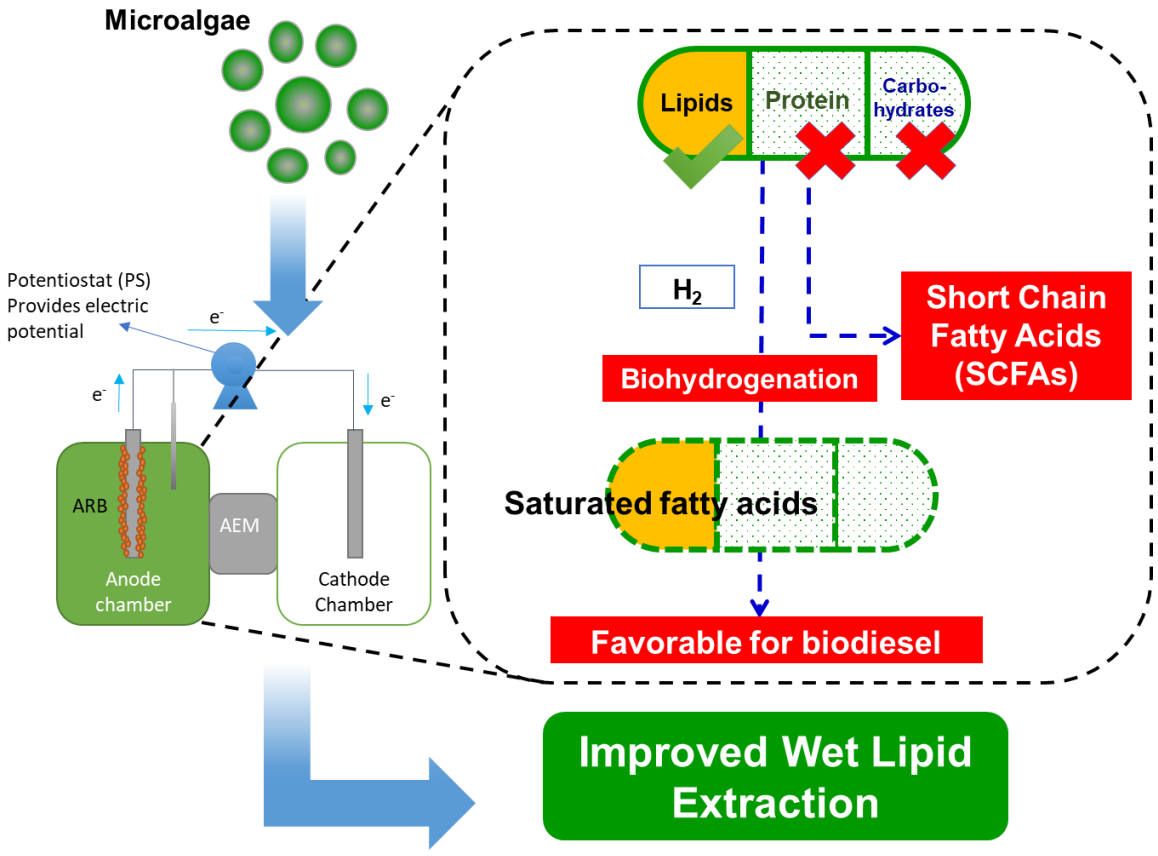

Figure 1.1 Schematic of mechanism hypothesized to occur in the anode chamber during ESF. The outcomes are selectively removing carbohydrates and protein; retaining lipids; biohydrogenation; and improved wet lipid extraction.

1.4 Objectives

The main objective of my work is to evaluate if ESF enhances lipid wet extraction and biohydrogenation of algal biomass. In particular, I seek to understand the mechanisms that act in the ESF system to enhance lipid extraction and biohydrogenation.

My dissertation is organized as the following chapters:

1. In Chapter 2, I introduce and document the phenomena associated with ESF. I demonstrate the ESF improves lipid wet extraction from ESF-treated *Scenedesmus* biomass, compared to fresh feeding biomass and SF-treated biomass. I also document biohydrogenation and identify the mechanism that led to the accumulation of saturated long-chain fatty acids (LCFAs) after ESF. This chapter is published in *Algal Research* (doi: 10.1016/j.algal.2018.101397)
2. In Chapter 3, I expand on the benefits of ESF treatment of *Scenedesmus* biomass by applying an improved ESF-reactor design, one with a much larger anode surface area, to maximize the oxidation of short-chain fatty acids that accumulated in ESF effluents in Chapter 2. I also used two different solvents, Hexane : Isopropanol (1:1 v/v, HI) and 100% hexane, to evaluate their extraction efficiency of lipids, as well as their selectivity towards saturated and unsaturated LCFA. The result show that the new flat-plate ESF reactor (with enlarged anode area) can enhance lipids wet extraction, although the anode accumulated algal biomass and lipids. Hexane proved to be strongly selective towards saturated LCFA extraction. This chapter is published in *Renewable Energy*. (doi: 10.1016/j.renene.2019.10.043)

3. In Chapter 4, I analyze the effects of different batches of algae feedstock on ESF. I carry out semi-continuous experiments in the same flat-plate ESF reactors used in Chapter 3.

   I perform a semi-continuous experiment for 102 days, compared to 30 days in Chapter 2. Over the 102 days, I evaluate four different batches of *S. acutus* feedstock. I evaluate changes to the lipid profiles, saturation ratio, extractable lipids, carbohydrate- and protein-removal rates, and ESF performances in terms of current generation and coulombic efficiency. I find that, although ESF can be effective for enhancing lipid wet-extraction, some *S. acutus* batches are relatively recalcitrant to ESF treatment, with lipid extraction in these batches' effluents nearly zero. Production of additional saturated LCFAs in the "recalcitrant" feeding biomasses is very limited, indicating enhanced lipid extraction and saturated LCFA production are coincident. I also analyze microbial communities in the different batches' effluents and ARB biofilms and find FB endogenous microbial community is less likely the cause of differentiating performance among batches, but FB biochemical composition is more likely the cause.

4. In Chapter 5, I explore effects of different solid retention times (*SRT*) on ESF solid retention times and, consequently, on ESF performance and microbial community structure and function. I point out that three *SRT*s are present in the ESF due to the existence of an ARB-biofilm: the biofilm-*SRT*, the planktonic-*SRT*, and the overall-*SRT*. I estimate that hydraulic retention time (*HRT*) is

accurate on estimating overall-*SRT* with model calculation. I find that, starting the ESF with long *SRT* yields high lipid extraction ratio with strong biohydrogenation, and switching to short *SRT* increases lipid volumetric productivity. In contrast, starting with a short *SRT* and then switching to a long *SRT* yielded poor results. I performed microbial community analysis and found fermenters that caused advanced protein degradation leading to enhanced lipid extraction. Thus, I recommend starting the ESF with longer *SRT* to incubate a strong fermenting microbial community, then switching to a short *SRT* to maximize lipid output.

5. In Chapter 6, I summarize my results and findings in my Ph. D work. I also propose potential further work to (1) pursue higher lipid extraction ratio; (2) find out the mechanism of the anode biofilm enhancing protein degradation that lead to enhanced lipid extraction; and (3) find out the cause of why different feeding biomass batches lead to different lipid extracting performance.

CHAPTER 2 ELECTRO-SELECTIVE FERMENTATION ENHANCES LIPID EXTRACTION AND BIOHYDROGENATION OF *SCENEDESMUS ACUTUS* BIOMASS

This work, in a slightly modified format, is published in Algal Research*, titled:*

Liu Y, Lai Y-JS, Barbosa TS, Chandra R, Parameswaran P, Rittmann BE. 2019. Electro-selective fermentation enhances lipid extraction and biohydrogenation of *Scenedesmus acutus* biomass. *Algal Res.* **38**. doi: 10.1016/j.algal.2018.10139

2.1 Introduction

Non-fossil energy sources need to be developed on a large scale. Among non-fossil candidates, microalgae-derived biofuel is promising due to the microalgae's high biomass production per unit area, their potentially high weight ratio of lipids, and that they do not compete for arable land (Adeniyi et al., 2018; Chisti, 2007; Hallenbeck et al., 2016; Rittmann, 2008). Despite its advantages, biofuel from microalgae has not had commercial success due in part to technical and economic problems associated with algae harvesting and lipids extraction. Pretreatment measures, such as acid/alkaline hydrolysis, pulsed electric fields and ultrasound, work, but usually are too energy intensive and, thus, economically prohibitive (Cho et al., 2013; Lai et al., 2014; Laurens et al., 2015; Sheng et al., 2011a; Zbinden et al., 2013). Likewise, extraction by Folch (1:1 chloroform : methanol, v/v) and Bligh & Dyer (1:1:0.5 chloroform : methanol : water, v/v) solvents, the current "gold standards" for lipids extraction, must be replaced by non-toxic "green"

solvents to reduce environmental and worker hazards. An example of non-toxic solvent is a 1:1 (v/v) mixture of hexane plus isopropanol (Lai et al., 2014; Lai et al., 2016a).

Selective fermentation (SF) is a novel biological approach to make lipid extraction simpler and more economically attractive (Lai et al., 2016b). SF exploits the fact that lipids are generally more slowly biodegraded than carbohydrate and protein in anaerobic conditions: Bacteria that ferment lipids, being slow growers (Christ et al., 2000; Rittmann and McCarty, 2001), can be washed out of a reactor having a relatively short solids retention time (*SRT*) (Lai et al., 2016b). Thus, SF allows fermentation of carbohydrate and protein in microalgae cells and leaves lipids intact, but in a state much easier to extract due to the removal of carbohydrate and protein "protection" (Lai et al., 2016b). Protein fermentation is slower than carbohydrate fermentation (Lu et al., 2010), making it a possible bottleneck in SF.

Another benefit of SF is biohydrogenation, in which the dominant lipid groups on long-chain fatty acids (LCFAs) are converted to saturated forms, such as C18:0, C16:0, and C14:0. Saturated fatty acids are beneficial for producing transportation fuel, as they provide more energy value, a higher octane number for better combustion efficiency, and greater resistance to oxidation (Knothe, 2011).

Biohydrogenation can occur by two distinct routes. One route is direct reduction of the unsaturated bonds to saturated bonds; in this route, H_2 is the electron donor, and the number of carbon atoms in the LCFA molecule does not change (Lai et al., 2016). An example of direct biohydrogenation is the reduction of C18:1 to C18:0: $C_{18}H_{33}O_2^- + H_2 \rightarrow C_{18}H_{35}O_2^-$. Direct biohydrogenation can be thermodynamically inhibited by a low H_2

concentration, and an increased concentration of H_2 can accelerate direct biohydrogenation (Cavaleiro et al., 2016; Lai et al., 2016a). Strains in the genera *Butyrivibrio* and *Pseudobutyrivibrio* (both in the order *Clostridiales*) can directly biohydrogenate C18:2 n-6 and C18:3 n-3 to C18:0 (Wallace et al., 2006; van de Vossenberg and Joblin, 2003). *In vivo* studies with ruminants suggest that the families *Porphyromonodaceae* (Order *Bacteroides*) and *Ruminococcaceae* (Order *Clostridiales*) are active in direct biohydrogenation (Castro-Carrera et al., 2014; Huws et al., 2011).

The second route occurs when an unsaturated LCFA molecule is transformed to a saturated LCFA molecule with the loss of two C atoms, as in acetate loss via β-oxidation (Cavaleiro et al., 2016). An example of the second route is transformation of C18:1 to C16:0:

$C_{18}H_{33}O_2^- + 2H_2O \rightarrow C_{16}H_{31}O_2^- + CH_3COO^- + H_2 + H^+$. This route does not need an external source of H_2, and it generates H_2. In principle, reactions that consume acetate, H_2, or both, could provide a thermodynamic boost to this second route of biohydrogenation (Cavaleiro et al., 2016).

Lipid conservation varies with the two biohydrogenation routes. β-oxidation reduces saturated LCFA chain length by two C atoms per step, and the loss is more substantial if multiple steps of β-oxidation occur. An example is the transformation from C16:0 to C14:0: $C_{16}H_{31}O_2^- + H_2O \rightarrow C_{14}H_{27}O_2^- + CH_3COO^- + 2H_2 + H^+$, which produces 2 moles of H_2 and 1 mole of acetate per 1 mole of C14:0 produced.

In Microbial Electrolysis Cells (MECs), Anode Respiring Bacteria (ARB) form a biofilm on the anode, oxidize short-chain fatty acids (SCFAs) generated from fermentation and β-oxidation, and transfer the extracted electrons to the anode via extracellular electron transfer (EET) (Reguera et al., 2005; Torres et al., 2009b; Torres et al., 2009a; Yang et al., 2012). Electrons travel through the external circuit to the cathode, where they are captured by water molecules to form H_2, which evolves as a gas from the cathode. The MEC is a promising means for enhancing protein biodegradation within complex organic substrates (Lu et al., 2012).

In this chapter, I combine MEC and SF to create *electro-selective fermentation* (ESF). Our goal is to improve carbohydrate and protein conversions, while making the lipids more wet-extractable. According to previous studies, MECs have the potential to accelerate protein fermentation (Lu et al., 2012; Velasquez-Orta et al., 2009). Increased removal of protein may disrupt hydrogen bonding between membrane protein and lipids, thereby rupturing the cell membrane and exposing intracellular lipids for easier extraction (Cooney et al., 2009; Sheng et al., 2011b).

In this study, I evaluated ESF in an MEC operated in a semi-continuous mode and fed with *Scenedesmus acutus* biomass. I compared the performance of ESF to that of SF by evaluating the fate of the carbohydrate, protein, and lipid components of *S. acutus* biomass; lipid extraction by hexane/isopropanol (1:1, v/v); and the degree to which the lipids were bio-hydrogenated. I quantitatively evaluated whether or not anode respiration in ESF enhanced fermentation of carbohydrate and protein, lipid bioavailability, and

biohydrogenation. I also determined whether or not ESF boosts β-oxidation, which harms lipid conservation.

2.2 Materials and Methods

2.2.1 *Scenedesmus acutus* Biomass Characterization

Scenedesmus acutus biomass, harvested from a pilot-scale photobioreactor at the Arizona Center for Algal Technology and Innovation (AzCATI, Mesa, AZ, USA), had a Volatile Suspended Solids (VSS) concentration of ~1.5 g VSS /L. It was harvested in a nutrient-depleted stage, which means that it was enriched in lipids in the form of triacylglyderides (TAGs) (Griffiths and Harrison, 2009; Rodolfi et al., 2009). It was immediately transported to the Biodesign Swette Center Environmental Biotechnology at the Tempe Campus of Arizona State University (BSCEB, Tempe, AZ, USA) and stored in a cold room at 4°C to allow sedimentation. After 5 days, the supernatant was removed, and the settled algal solids were transferred to a 5-L high-density polyethylene carboy and thoroughly mixed. Before addition to the ESF and SF reactors, the settled algae solids were sparged with N_2 gas for 15 minutes to remove dissolved oxygen. The algae slurry had a VSS concentration of 8.1 ± 0.2 g VSS/L. A potential electron acceptor, nitrate, was not detected in the supernatant of the algae slurry, which is consistent with the algae's nutrient-depleted status. Other biomass characteristics after settling -- Total Suspended Solids (TSS), Chemical Oxygen Demand (COD), and COD breakdown -- are shown in Tables 2.S1 in the Supplemental Information. All Supplemental Information for Chapter 2 are attached to the end of Chapter 2.

2.2.2 ESF Setup and Operation

ESF was carried out in two MECs, in which hydrogen gas (H_2) was generated at a cathode not exposed to oxygen. Each H-type MEC (Lee et al., 2008b; Miceli et al., 2014; Parameswaran et al., 2010) had one anode compartment and one cathode compartment made by connecting two 250-mL serum bottles (VWR, Randor, PA, USA) via a glass extension on the side of each bottle. The MEC was divided by an Anion Exchange Membrane (AEM) (AMI-7001, Membranes International, Glen Rock, NJ, USA). Because the extensions added approximately 130 mL to each compartment, both compartments had working volumes of 340 mL and a headspace of 40 mL. Serving as electrodes were identical-graphite rods with a square cross-section (approximately 6 cm in length, 0.64 cm^2 in cross-section area, 10.4 cm^2 exposed area) and mounted on an aluminum wire through a cavity screwed through a hole drilled (about 1-mm diameter) approximately 3 mm from the rod's end; they were fixed with rubber tubes. Two graphite rods were installed in each compartment, making the total area of electrodes in each compartment 20.8 cm^2. The rods were brushed with fine sandpaper and rinsed with diluted nitric acid prior to installation. An Ag/AgCl reference electrode (BASI Electrochemistry, West Lafayette, IN, USA) was installed in the anode chamber approximately 0.5 cm from each anode rod. A potentiostat (VSP model, Bio-Logic SAS, Claix, France) was used to poise the anode potential at -0.3V vs Ag/AgCl, which corresponds to -0.078 V vs the standard hydrogen electrode (SHE). The reactor was kept in a temperature-controlled room with a stable temperature of 30°C. Current, current density, power, and coulombs collected by the potentiostat were monitored and recorded by the EC-Lab software (V10.44, Bio-Logic SAS, Claix, France).

Prior to the startup of the experiment with *S. acutus*, 335 mL of a synthetic medium (1970 mg/L sodium acetate, 380 mg/L sodium propionate, 200 mg/L sodium butyrate, 90 mg/L glucose, 140 mg/L Bovine Serum Albumin, and 1 mL of trace element solution (Lee et al., 2008b) in a 40-mM phosphate buffer solution having a starting pH of 7.5) was added to the anode compartment. Then, 5 mL of anaerobic digester sludge (Mesa Northwest Water Reclamation Plant, Mesa, AZ, USA) was added to inoculate an ARB biofilm. The anode compartment was constantly stirred with a 2.5-cm magnetic stirrer at a rate of 400 rpm. It took approximately 7 days to form an ARB biofilm that achieved a current density of ~7 A/m^2. Then, the previous synthetic medium was replaced by fresh medium and inoculated for another period of 7 days to enrich the biofilm in ARB. The cathode chamber was filled with 340 mL of NaOH solution with pH = 12.

To start the ESF process, 310 mL of *S. acutus*, at a concentration of 8.1 g VSS /L, was fed to the anode compartment of the MEC seeded with 30 mL of Waste Activated Sludge (WAS) from Mesa Northwest Wastewater Reclamation Plant (MNWWRP, Mesa, AZ, USA). The WAS was added to ensure that fermenting bacteria were present in the anode chamber. The anode's biofilm was retained. NaH_2PO_4 and Na_2HPO_4 (Fisher Chemical, Fair Lawn, NJ, USA) were added to achieve a 40-mM phosphate buffer solution with a starting pH of 7.5. The anode compartment was sparged with N_2 gas for 15 minutes, and the MEC was immediately moved to the temperature-controlled room. Stirring in the anode compartment was with a 2.5-cm magnetic stirrer at 400 rpm.

The MEC fed with *S. acutus* initially was run in batch mode for 7 days. After that and on a daily basis, the MEC was temporarily disconnected from the potentiostat, 68 mL of the liquid content was withdrawn from the anode compartment, and 68 mL of algae feedstock (stored in a 4°C cold room and then mixed with 40 mM PBS, no WAS) was added to replace the withdrawn liquid. After every replacement, the anode chamber was sparged with N_2 for 15 min and then returned to the stirrer and reconnected to the potentiostat.

Slurry samples were taken at days 8, 13, 20, 25, and 30 for microbial-community analysis. At the end of the run (day 30), the anode's biofilm was scrapped from the electrode surface using a nuclease-free 50µL pipette tip and transferred to a RNA-free 2-mL Eppendorf tube.

2.2.3 SF Setup and Operation

SF was evaluated in one semi-continuous fermenter that was a 500-mL screw cap serum bottle (VWR, Radnor, PA, USA) modified with an added side sampling port for gas measurement; the port was sealed with butyl-rubber stopper. The reactor was initially fed with 400 mL of *S. acutus* biomass (8.1 g VSS/L). It was then inoculated with 40 mL of WAS obtained from MNWWRP, and 40 mM of PBS was added to establish a pH of 7.5, thus making the working volume 440 mL. The reactor was sparged with N_2 for 15 min, sealed with a rubber stopper penetrated with two PTFE tubes (Kimber Chase, Vineland, NJ, USA) for sampling and sparging, and well mixed in an incubator at 210 rpm and kept at 30°C. After 7 days of batch reaction, the SF reactor was shifted to the semi-continuous mode, where 88 mL of SF effluent were withdrawn from the reactor, and the same volume of *S. acutus* feeding biomass buffered with 40 mM PBS at a pH of 7.5 was reinjected. The reactors were then sparged with N_2 for 15 minutes and moved back to the incubator for mixing. This operation was repeated daily until day 30. Samples were taken on the same day as when ESF samples were taken.

2.2.4 Analytical Methods

Slurry samples were assayed directly for total chemical oxygen demand (TCOD), total suspended solids (TSS), volatile suspended solids (VSS), total carbohydrate, and total protein. TSS and VSS were determined by dry weight according to sections 2540 B and E, respectively, of *Standard Methods*(APHA, 2016). Total COD were measured using a HACH COD kit (concentration range 10-1,500 mg/L); NO_3^- was measured using HACH Nitrate kit (concentration range 1 – 60 NO_3^- /L) (HACH Co., Loveland, CO, USA). Carbohydrate and protein were analyzed by a phenol-sulfuric acid colorimetric method (DuBois et al., 1956) and the Bicinchoninic acid (BCA) method (Brown et al., 1989), respectively; concentrations were determined using calibration curves with glucose and bovine serum albumin standards, respectively. Short-chain fatty acids (SCFAs) were assayed after 0.2-μm membrane filtration (Pall Science, NY, USA). SCFA concentrations were measured with an high-performance liquid choromatography (HPLC) (Shimadzu Corp, Columbia, MD, USA) equipped with an Aminex HPX-87H column (Parameswaran et al., 2009). Gas samples of CH_4 and H_2 were analyzed by gas chromatography (GC) (Parameswaran et al., 2009).

I adopted the approach of Lai et al. (2016b) to quantify the total and extractable lipids in the biomass as fatty acid methyl esters (FAMEs). 1 mL of slurry sample was dispensed into screw-cap glass tube, and these samples were frozen in a -20°C freezer, then freeze-dried using a FreeZone Benchtop instrument (Labconco, MO, USA). The freeze-dried biomass was mixed with 2 mL of 3-N Methanolic-HCl (Sigma-Aldrich, St. Louis, MO, USA) and incubated at 85°C for 2.5 h for direct trans-esterification. Then, I added 1.55

mL of hexane (HPLC-Grade, Sigma-Aldrich, St. Louis, MO) to the trans-esterified sample and vortexed the mixture for 1 minute. The non-aqueous phase was then assayed on a gas chromatograph (GC, Shimadzu Corporation, Columbia, MD, USA) for FAMEs concentrations. The FAMEs concentrations were converted to COD concentrations. The saturation ratios of the feeding biomass (FB), ESF, and SF biomasses were quantified by dividing the sum of COD values of saturated LCFAs by the total LCFA-COD value (Eq. 2.S3).

Lipids extracted from biomass were quantified as FAMEs. Triplicate 1-mL biomass samples were mixed with 3 mL of a mixture of hexane and isopropanol (1:1, v/v) and vortexed for 1 min (Scientific Industries Inc., Bohemia, NY, USA) at room temperature. 1-mL non-aqueous phase supernatant samples were transferred to clean tubes and air dried in a fume hood overnight.

2 mL of Methanolic-HCl was added to the tube, then the tubes were sealed with screw-caps and heated at 85 °C for 2.5 hours. After cooling, 0.5 mL of DI water was added to each sample to produce an emulsion of resulting FAME in the aqueous phase. 1.55 mL of Hexane was added to the emulsion, then capped and vortexed for 1 min to transfer the FAME to the non-aqueous phase.

Cell morphology was visualized by Transmission Electron Microscopy (TEM). Feeding and effluent slurry samples were first fixed in 2% glutyraldehyde in 50-mM PBS solution at pH 7.2. Then, a 1% osmium tetroxide solution was added to the fixed biomass as a post-fix agent. The post-fixed samples were dehydrated with Acetone, embedded in an agarose resin, and polymerized at 60 °C for 36 h. Polymerized samples were cut in a

square section of 60-nm dimension and post-stained with uranyl acetate and lead citrate. TEM images were taken using a Philips CM12 TEM (Philips North America, Andover, MA, USA) operated at 80 kV with a Gatan model 791 camera (Gatan Inc, Pleasanton, CA, USA).

Centrifuged pellets and scrapped anode biofilm were used for DNA analysis. DNA extraction was performed with PowerSoil DNA isolation Kits (MoBio Laboratories, Inc, Carslbad, CA, USA). Amplification, and sequencing were performed by the Microbiome Analysis Laboratory, Arizona State University, using a MiSeq Illumina Sequencer, targeting the V4 Region of the 16S rRNA gene with primer set 515f/806r. 16S rRNA gene sequences were analyzed using the Quantitative Insights into Microbial Ecology software package (QIIME, version 1.9, http://qiime.org/) (Lai et al., 2016) and deposited to the online database
(submission ID: SUB3753583).

2.2.5 Calculations

COD distributions of the feeding biomass and the ESF and SF effluent samples were established by calculating COD equivalences of the measured carbohydrate, protein, lipids (as Long-chain Fatty Acids, LCFAs), and SCFAs. COD conversion coefficients were adopted from previous studies (Lee et al., 2008a; Miron et al., 2000): carbohydrate, 1.07 g COD / g; protein,
1.5 g COD /g; acetate, 1.07 g COD / g; propionate, 1.51 g COD / g, and butyrate, 1.82 g COD / g. H_2 and CH_4 are 0.62 and 2.46 g COD / mL at 30 °C, respectively. For LCFAs, the respective names, codes, and COD conversions are listed in Table. 2.1.

For total and extractable LCFA concentrations in slurry samples, the FAME concentration in the hexane solvent was converted to its LCFA concentration by a molecular-weight conversion and a volume conversion (ratios shown in Table 2.1). Then, I calculated the final concentration of LCFAs as COD equivalents in the feeding biomass or ESF biomass. The calculation methods are shown as Eq. 2.S1 and Eq. 2.S2 in the Supporting Information. Saturation ratios were calculated by dividing the total COD equivalent concentration of saturated LCFAs in the slurry by the total LCFA - COD equivalent concentration, as shown in Eq. 2.S3 in the supporting information.

Table 2.1. Names, codes, FAME-LCFA and COD-conversion ratios of detected LCFAs in *S. acutus* biomass

Name of LCFA	Code Nomenclature[§]	FAME to LCFA conversion ratio (g LCFA / g FAME	COD conversion ratio (g COD /g LCFA)
Lauric Acid	C12:0	0.93	2.72
Myristic Acid	C14:0	0.94	2.81
Palmitic Acid	C16:0	0.95	2.88
Palmitoleic Acid	C16:1	0.95	2.83
Stearic Acid	C18:0	0.95	2.93
Oleic Acid	C18:1	0.95	2.89
Linoleic Acid	C18:2	0.95	2.86
Archidic Acid	C20:0	0.96	2.97
Gondoic Acid	C20:1	0.96	2.99

§ In LCFA nomenclature (e.g., C 16:0), the number before the colon is the number of carbons in the LCFA molecule, and the number after the colon is the number of double bonds in the molecule.

2.3 Results and Discussion

2.3.1 Steady-State Performances for ESF and SF

The current densities and cumulative Coulombs collected in one of the ESF reactors are shown in Figure 2.1 (a). Similar current densities and coulombs collected of the duplicate reactor are shown in Figure 2.S1. The initial current density quickly reached 4.8 A/m^2, since an ARB biofilm was previously accumulated on the anode. In batch mode, the current gradually declined to about 0.5 A/m^2 between day 2 and day 5 as the organic donor was depleted. Semi-continuous feeding of *S. acutus* biomass began on day 7, and the current density immediately increased to about 1 A/m^2. With long-term semi-continuous feeding, the current density rose, and, at day 14, the current density had increased to a peak around 2.5 A/m^2. A pseudo steady state was achieved from days 20 – 25, with the average current density around 1.8 A/m^2. I focus on the performance from days 20 to day 25, when the current density was stable , although modest compared to maximum current densities of > 10 A/m^2 with simple soluble substrates like acetate (Torres et al., 2008).

TCOD, SCOD, and pH values for ESF, SF, and FB are shown in Figure 2.1 (b). At pseudo steady state (days 20 – 25), ESF achieved 12 ± 2 % TCOD removal and 17 ± 0 % conversion to SCOD; the corresponding values for SF were 2 ± 0 % TCOD removal and 11 ± 0% SCOD production. The effluent TCOD was less than the influent TCOD from day 8 to day 23; this was caused by the visible accumulation of lipid solids on the surfaces of the anode compartment, as shown in Figure 2.S2 and 2.S3 in the Supplemental Information at the end of this chapter.

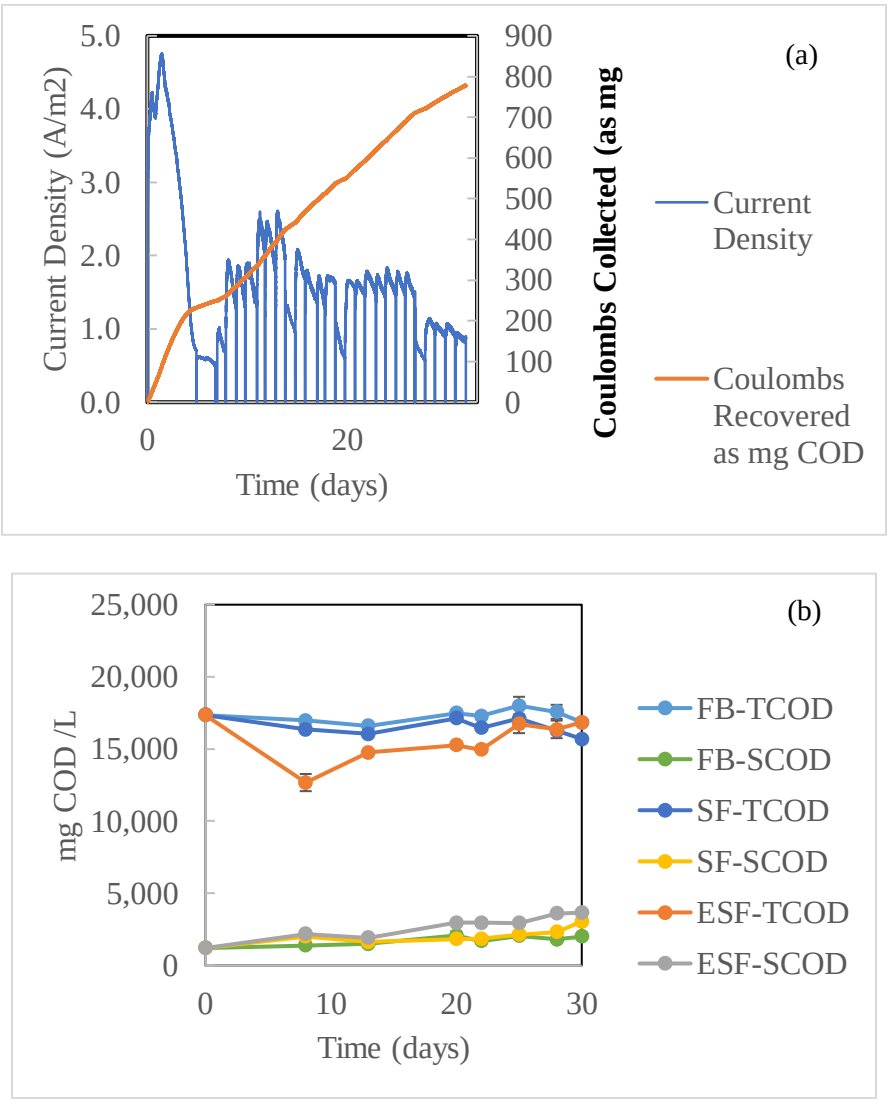

Figure 2.1. (a) Performance of ESF fed with *S. acutus* biomass: current density and cumulative Coulombs recovered as mg COD. Staggered current density was a result of daily removal and injection of feeding biomass as a part of the semi-continuous regime. The results in each cycle were stable from day 20 to day 26. (b) COD performance for ESF and SF. Error bars indicate high and low values for duplicate reactors in ESF; duplicate samples in SF and FB. FB stands for Feeding Biomass; SF stands for Selective-Fermentation and ESF stands for Electro-Selective Fermentation. TCOD is total Chemical Oxygen Demand, and SCOD is soluble Chemical Oxygen Demand.

Figure 2.2. (a) shows 45 ± 4% removal of total protein and 42 ± 10% removal of total carbohydrate in ESF, while the SF showed about 10 ± 3% total protein removal and 43 ± 10% carbohydrate removal. Thus, ESF clearly had greater removals rates of TCOD and protein, as well as conversion of TCOD to SCOD, although carbohydrate removals were nearly identical.

COD (i.e., electron-equivalent) mass balances are shown in Figure 2.2 (b), which presents average values between day 20 - 25. Electrical current was a minor component in the COD balance for ESF, accounting for <0.4% of the total COD. The reason for current being a minor sink is the small specific surface area of the anode (20.8 cm^2/340 cm^3 = 6.1 m^{-1}), even though the current density was moderate (~1.8 A/m^2). H_2 was not detected in the headspace of the SF or of the ESF anode, and CH_4 also was minor in both reactors, accounting for 0.3% and 0.5% of the total COD for ESF and SF, respectively. H_2 generated by fermentation was scavenged by ARB or methanogens, or it was used for LCFA biohydrogenation (Lai et al., 2016b; Parameswaran et al., 2011). Some of the loss of TCOD in ESF was due to the attachment of algal-biomass solids on the reactor's wall and electrodes.

The major sink of COD lost from protein and carbohydrate was SCFA, mostly acetate and propionate and a small portion of n-butyrate. High SCFAs in the effluent of the ESF are consistent with minimal current generation due to the very low anode specific surface area, since previous research showed that ARB are able to oxidize SCFAs at a fast rate (Ki et al., 2015). More accumulation of SCFA in ESF paralleled its enhanced degradation of protein in ESF, which may have been promoted by robust H_2 scavenging

(Ramsay and Pullammanappallil, 2001). The two nearly identical carbohydrate removals (35% for ESF and 36% for SF) were similar to the 30% maximum carbohydrate loss in *S. acutus* reported earlier (Lai et al., 2016a) for SF. SCFAs with more than 5 carbons were not detected.

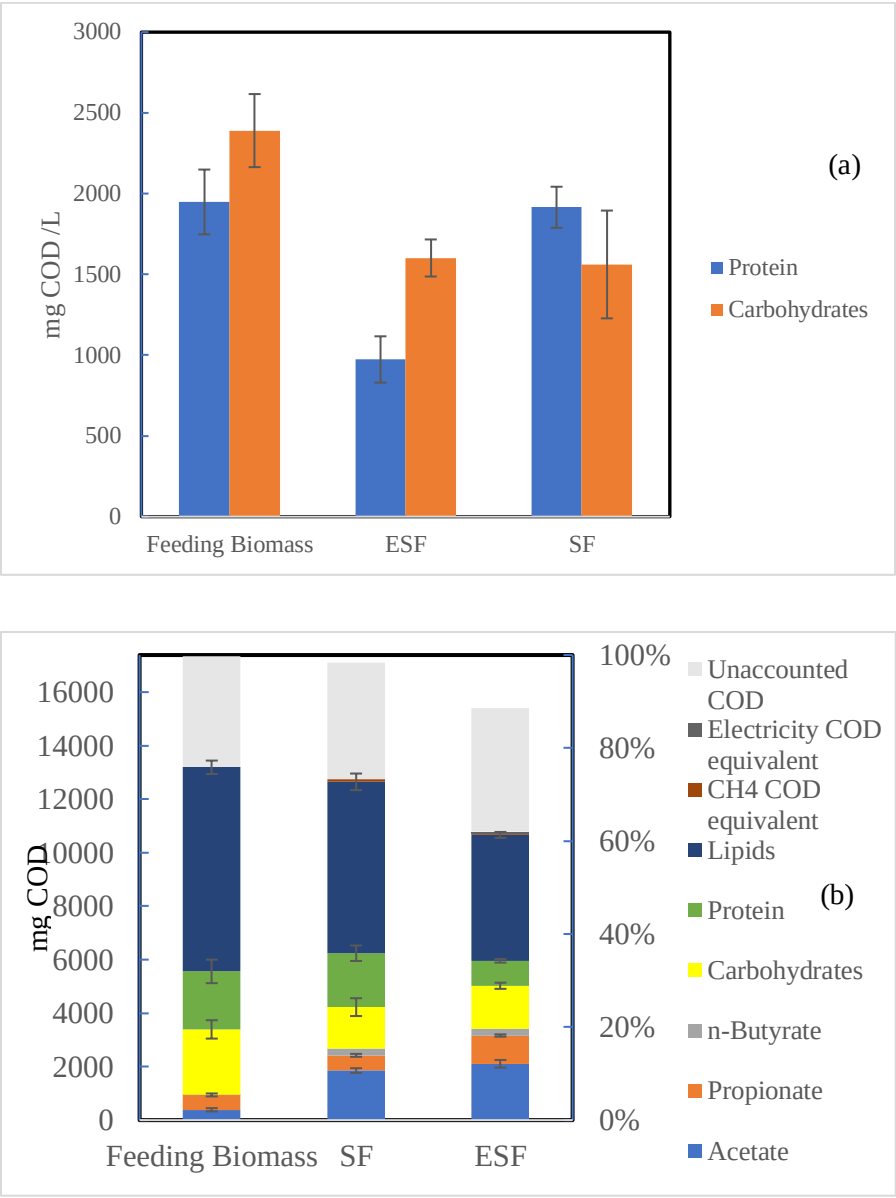

Figure 2.2. (a) Total protein and carbohydrate concentrations for SF and ESF at pseudo-steady state (average values between days 20 and 25) compared to the feeding biomass (day 0). Error bars indicate the high and low values for duplicate reactors in ESF, and duplicate samples in SF and FB. (b) COD mass balances for feeding biomass, SF effluent, and ESF effluent. Values are averages between day 20 and day 25. FB value set to 100%. Error bars indicate high and low values.

2.3.2 FAME Conservation and Biohydrogenation

Major changes to the distribution of lipids during ESF and SF are clearly documented in Figure 2.3, which is for day 25. The data for day 20, shown in Figure 2.S4, are almost the same as for day 25. For total LCFA, ESF recovered 62% of the lipids present in the feeding biomass, while SF recovered 83%. Lipid extraction of the feeding biomass by hexane/isopropanol yielded ~4% of the total lipids from the feeding biomass, but the yield was 12% for the SF effluent and 37% for the ESF effluent. Thus, ESF led to some loss of total FAME, but had a strongly positive impact on lipid extractability, increasing extractability by about three-fold over SF and almost 10-fold over the feeding biomass. The loss of total FAME caused by ESF can be attributed to β-oxidation (discussed below) and to the accumulation of solid lipids attached to the anode electrode and reactor surface; the accumulations are shown in Figures 2.S2 and 2.S3 of SI.

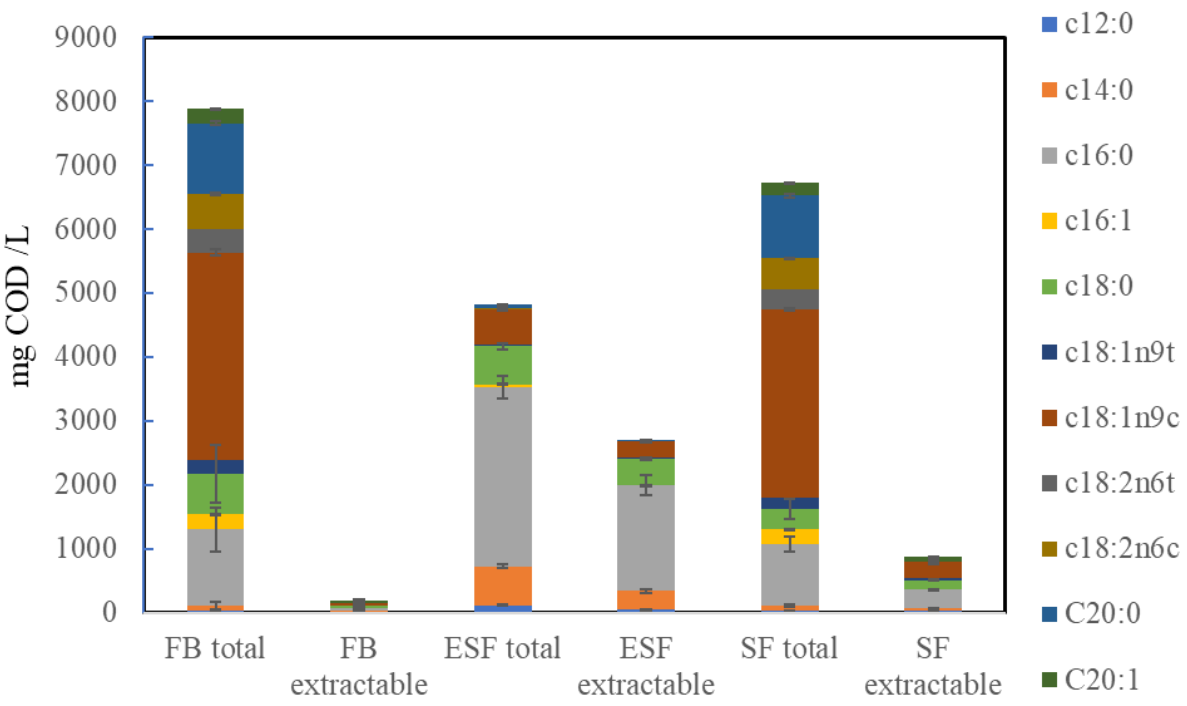

Figure 2.3. Profiles of total and extractable lipids for FB, ESF effluent, and SF effluent on day 25. Data from day 20 are shown in Fig. 2.S4 and are almost the same.

The saturation ratio increased for the total and extractable lipids in the ESF effluent, but not for the SF effluent. The saturation ratio was 36% in the feeding biomass's lipids and 34% in the SF-effluent lipids, but it increased to 92% in ESF total lipids. This means that biohydrogenation was important during ESF. The most abundant LCFA species changed from C18:1n9c in the feeding biomass and SF effluent to C16:0 in the ESF effluent. C18:2, although small in FB, completely disappeared.

Despite improvement in lipid-extraction efficiency and biohydrogenation, ESF led to the net loss of lipid mass, and the losses were largely consistent with biohydrogenation

coupled to β-oxidation. For example, loss of C18:1 was accompanied by accumulation of C16:0 and C14:0 in ESF. Biohydrogenation coupled to β-oxidation also is consistent with negligible H_2 concentration in the ESF anode headspace and no increase in C18:0.

I analyzed the fate of carbon in LCFA to delineate which biohydrogenation route was occurring in ESF and SF. To do this, I introduce ΔCOD/ΔC, which is the ratio of decreased LCFA-COD to the decrease of the concentration of carbon contained in LCFA (LCFA-C). Details of the ΔCOD/ΔC computation are provided in SI. The direct and β-oxidation routes have different ratios. For example, β-oxidation of a fully saturated LCFA - e.g., C18:0 to C16:0 or C16:0 to C14:0 – has a ΔCOD/ΔC values of 4 g COD/g C. Transformation of an unsaturated LCFA to a saturated LCFA - e.g., C18:1 to C16:0 - by β-oxidation has a smaller ΔCOD/ΔC of 3.3 g COD/g C, since conversion of the unsaturated bond to a saturated bond is a net reduction. Direct biohydrogenation does not have a ΔCOD/ΔC ratio, as it loses no LCFA-C. However, a degree of direct biohydrogenation will decrease the overall ΔCOD/ΔC ratio value by increasing the total LCFA-COD, thus decreasing the ΔCOD value of total LCFAs. Thus, biohydrogenation with β-oxidation will move the overall ΔCOD/ΔC ratio upwards towards 4, while direct biohydrogenation will move the overall ratio to a smaller value.

In our experiments, ESF had a ΔCOD/ΔC value of 3.7, while SF had a higher value, 3.8. This supports that both systems were dominated by biohydrogenation associated with β-oxidation (values not far from 4), but ESF had more direct biohydrogenation, perhaps along with β-oxidation that also saturated the LCFA, as its overall ratio was smaller.

These trends are supported by the decreases of total LCFA concentrations in ESF and SF (Figure 2.3).

2.3.3 Cell Morphology

Figure 2.4 showed TEM images of *S. acutus* cells of the (a) FB, (b) ESF effluent, and (c) SF effluent. FB cells have distinct white borders, while cells in the ESF and SF effluent show grey borders. The less-distinct cell borders imply that the cells were compromised during ESF and SF, leading to the loss of cell wall and membrane integrity. Also, the grey globule-like particles in the cytoplasm of FB cells, which are lipid inclusions (Wang et al., 2013b), lost distinct boundaries after SF and ESF treatment (Figs. 2.4 (b) and (c)). White spots in FB cells, which represent starch stained by TEM fixation chemicals (glutaraldehyde and osmium tetroxide), grew bigger in SF- and ESF-treated cells. This indicates that more starch was in ESF- and SF-treated cells. Thus, ESF and SF inflicted clear disruptions on *S. acutus* cells, similar to observations of *Scenedesmus* cells before and after pulsed-electric field (PEF) treatment (Lai et al., 2014).

While SF and ESF led to cell disruption, Figs. 2.4 (b) and (c) show that ESF caused more organelle disruption: ESF had no visible organelle structures, but SF still possessed large organelles, although the lipid globules disappeared. These observations agree with the improved lipid extractability with ESF in this study (Figure 2.3).

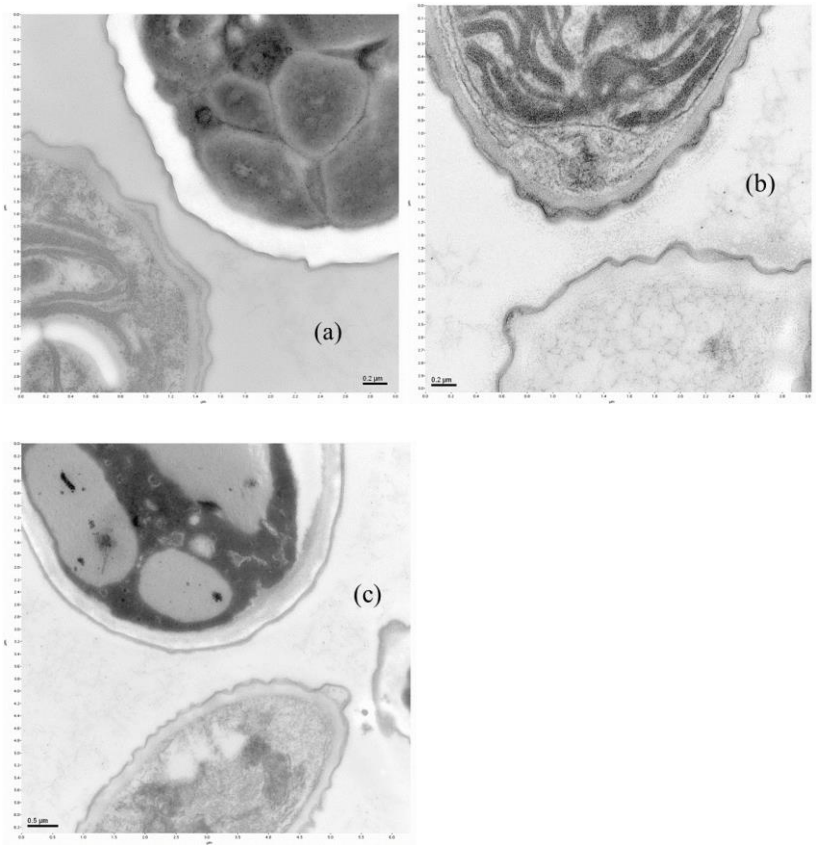

Figure 2.4. TEM images of (a) *Scenedesmus* feeding biomass; (b) ESF effluent; and (c) SF effluent. Disappearance of globule-like structures and organelles is evident in (b).

2.3.4 Microbial Communities

Microbial community structures in ESF (suspension and biofilm), SF, and FB are shown at the family level in Figure 2.5. The community structure of the ESF biofilm was obviously different from the structures of effluent suspensions and the FB. In the ESF biofilm, the largest number of sequences belonged to the family *Geobacteraceae*, solely represented by the genus *Geobacter* (30.4%), a widely recognized ARB (Bond, 2002; Holmes et al., 2004; Jung and Regan, 2007; Miceli et al., 2014). Another typical ARB, genus *Desulfovibrio* of the order *Desulfovibrioceae* (4.5%), (Parameswaran et al., 2011),

also was important. These genera were barely represented in the ESF effluent suspension (0.3% and 0.7% respectively), and they were absent in the SF effluent suspension and the *S. acutus* FB. Thus, the anode provided strong selective pressure in favor of the ARB biofilm. The genus *Erysipelotrichaceae RFN20* of family *Erysipelotrichaceae*, which accumulates in lipid-rich environments (Greiner and Bäckhed, 2011), also was significant on the ESF anode's biofilm (8.5%). This is consistent with observable lipids accumulation on the anode, shown in Figures 2.S2 and 2.S3 in SI.

In the ESF effluent suspension, the family *Bacteroidaceae* was the most abundant group (35.7%), and it was solely represented by the genus *Bacteroides,* which potentially is a protein degrader (Bermingham et al., 2017). In contrast, the SF effluent suspension only had 5.5% *Bacteroides,* which is consistent with the low degree of protein degradation in SF (13%) compared to ESF (45%).

Multiple potential carbohydrate fermenters were detected in the ESF and SF effluents. The families *Porphyromonadaceae* (5% in ESF and 25% in SF) and *Veillonellaceae* (17% in ESF and 25% in SF) were the dominant groups. *Veillonellaceae,* also present in *S. acutus* feeding biomass (17%), are reported to lead to H_2 production (Lee and Rittmann, 2009; Ramsay and Pullammanappallil, 2001).

Since ESF and SF had minimal H_2 concentrations, the two systems must have had strong H_2-scavenging mechanisms. In ESF, H_2 could have been scavenged by ARB (about 2% abundance in suspension, 31% abundance in biofilm) or methanogens (~1% abundance in suspension and biofilm), as well as the biohydrogenaters that used the direct route. The latter agrees with the enrichment of *Porphyromonadaceae* in ESF. The high abundance of *Porphyromonadaceae* in SF, which is consistent with Lai et al. (2016b), suggests that they were important in fermentation, since biohydrogenation was less important.

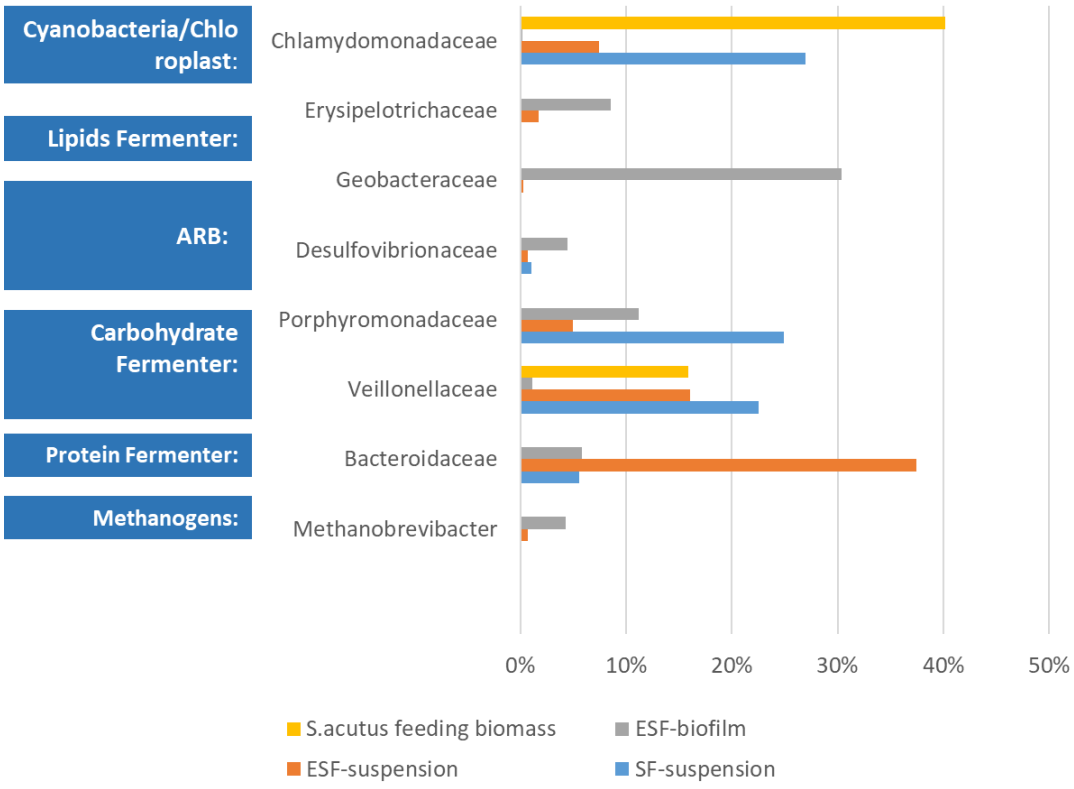

Figure 2.5. Phylogenetic profiling of the ESF and SF effluent suspension, the ESF biofilm, and the *S. acutus* FB at the family level. The horizontal-axis values represent the percentage abundance of the families. Functions known to be associated with each family are shown to the left.

2.4 Conclusions

ESF led to superior hydrolysis of protein of *S. acutus* biomass over SF. ESF also exhibited a higher LCFA saturation ratio, shifting from C18:1 to C16:0 and C14:0, and improved lipid extractability by 3-fold compared to SF and 10-fold compared to the feeding biomass. Improved lipid extractability was associated with disruption of the cell wall and oil globules in the cytoplasm. The biofilm anode in ESF was enriched in ARB, particularly *Geobacteraceae*, while the suspended biomass in ESF was enriched in protein degraders (family *Bacteroidaceae*) and potential biohydrogenaters (family *Porphyromonadaceae*). Overall, ESF improved lipid extractability and biofuel quality.

Supplemental Information for Chapter 2

2. S1. Biomass Characteristics After Settling

Table 2.S1. Key parameters for Feeding Biomass and ESF and SF effluents at steady state on days 20 and 25. Units are in g/L except pH.

	Day 20			
	VSS	TCOD	SCOD	pH
Feeding biomass	8.1 ± 0.0	17.0 ± 0.1	2.1 ± 0.3	6.6
ESF	5.3 ± 0.0	15.0 ± 0.0	3.0 ± 0.0	6.4
SCF	7.7 ± 0.0	17.1 ± 0.1	1.8 ± 0.1	6.9

	Day 25			
	VSS	TCOD	SCOD	pH
Feeding Biomass	7.7 ± 0.1	18.0 ± 0.6	2.1± 0.2	7.0
ESF	5.7 ± 0.0	15.5 ± 0.2	2.9±0.1	6.2
SF	7.4 ± 0.0	17.1 ± 0.0	2.1±0.1	7.0

2.S2. Calculations for Lipids Concentration

To calculate the total lipid concentrations in ESF and SF effluents, I started from the concentration of FAME in the hexane solution obtained from GC signal intensities. The concentration (expressed in mg FAME/ mL hexane) was multiplied by 1.55 mL of hexane to obtain the total mass of FAME (mg FAME). Since this mass of FAME came directly from the transesterification of LCFAs in 1 mL of effluent, the effluent FAME concentration was obtained by dividing FAME mass by 1 mL of effluent solution (mg FAME /mL effluent). Finally, concentrations of corresponding LCFA were obtained from doing a molecular weight conversion (conversion ratios shown in Table 2.1), followed by a conversion of molecular weight to COD. The equation for effluent total lipids concentration to mg COD /L is summarized in Equation 2.S1:

Total LCFA concentration (mg COD /L) = (concentration of LCFA in hexane (mg FAME/ mL hexane)/*1.55 mL hexane / 1 mL effluent * LCFA/FAME conversion ratio (mg LCFA/mg FAME) * COD/LCFA conversion ratio (mg COD/mg LCFA) *1000 mL /L *(Eq. 2.S1)*

For extractable lipids concentration, I started from the FAME concentration obtained from GC signal intensity (mg FAME / mL hexane) and multiplied it by 1.55 mL hexane to get the total FAME mass (mg FAME). When I did the extractions, I injected 3 mL of isopropanol: hexane (1:1) into 1 mL effluent slurry samples; after mixing, isopropanol entered the aqueous phase, and the non-aqueous phase was 1.5 mL of hexane, which I transferred 1 mL to a clean tube for drying. Thus, the FAME mass I obtained only represented the FAME in 1 mL of hexane, and I multiplied that value by 1.5 to obtain the

total mass of FAME extracted from 1 mL of effluent slurry. The equation is summarized in Equation 2.S2.

Extractable LCFA concentration (mg COD /L) = (concentration of LCFA in hexane (mg FAME/ mL hexane)/*(1.55 mL hexane * 1.5 mL effluent / mL hexane)/ (1 mL effluent) * (LCFA/FAME conversion ratio (mg LCFA/mg FAME)) * (COD/LCFA conversion ratio (mg COD/mg LCFA))*(1000 mL /L) *(Eq. 2.S2)*

The saturation ratio was calculated by dividing the COD concentration of saturated LCFAs in the effluent (mg COD/L) by the COD concentration of total LCFAs in effluent. It is expressed in percentage. The equation is summarized in Equation (2.S3).

Saturation (%) = [Saturated LCFA COD (mg COD /L)] / [Total LCFA COD (mg COD/L)] * 100% *(Eq. 2.S3)*

2.S3. Current Density and Cumulative Coulombs Collected by ESF Reactor #2

The current densities and cumulative Coulombs (expressed in mg COD) in ESF reactor #2 are shown in Figure 2.S1.

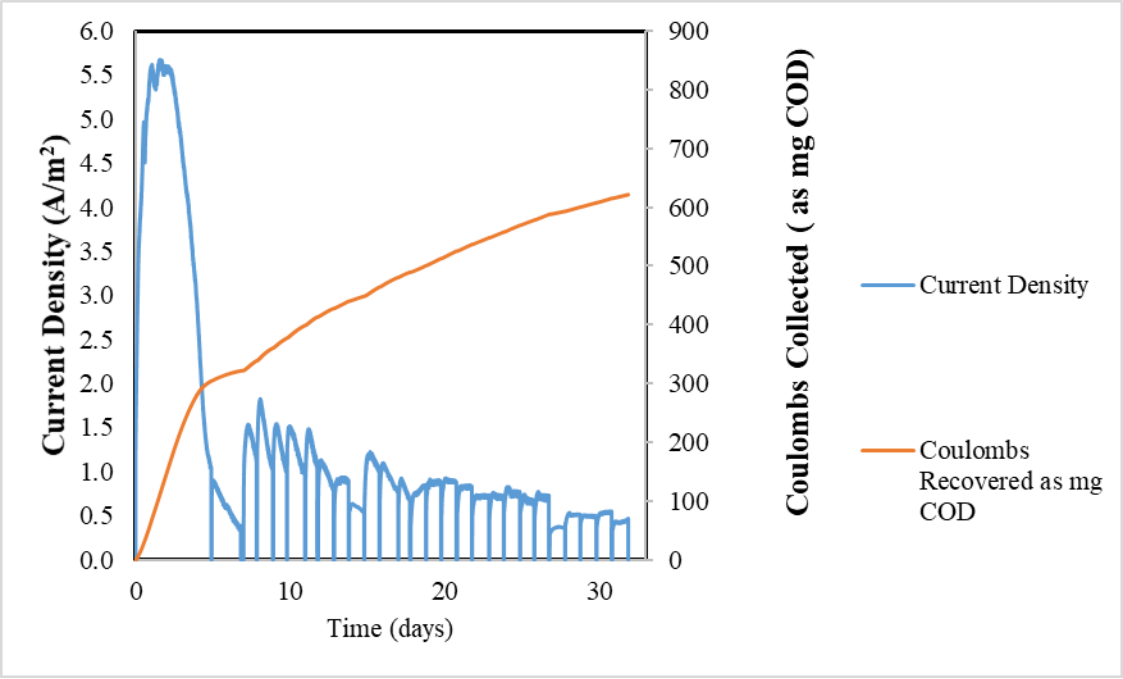

Figure 2.S1. (a) Performance of ESF fed with S. acutus biomass: current density and cumulative Coulombs recovered as mg COD. Staggered current density was a result of daily removal and injection of feeding biomass as a part of the semi-continuous regime. The results in each cycle were stable from day 20 to day 26;

2.S4. Lipids Residue on Electrodes and Reactor Wall Surface

Figure 2.S2 shows that white matter was attached to anode electrodes and reactor wall surfaces at the end of the experiment. The white matter was transferred with 50uL RNA-free pipette tip to a clean boroscilicate glass tube and then freeze-dried for 2 d in a Labconco freeze dryer (Labconco, Kansas City, MO, USA). The freeze-dried sample were then trans-esterified and extracted with HPLC-grade hexane (100%) for GC analysis. Figure 2.S3 shows the peak intensities of the GC result. Calculation concluded 8 mg total of identifiable LCFA was present in the collected white matter (not all white matter from the reactor collected).

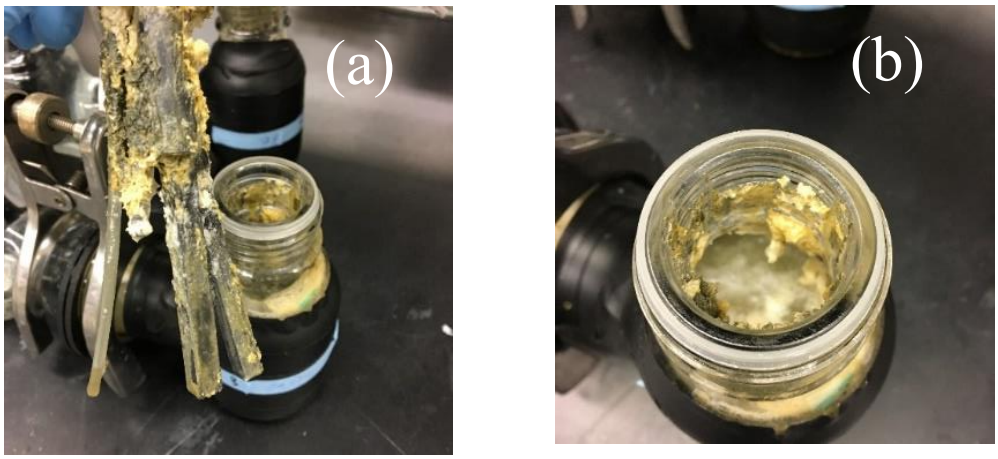

Figure 2.S2. Lipids accumulation on anode surface (a) and on reactor wall (b).

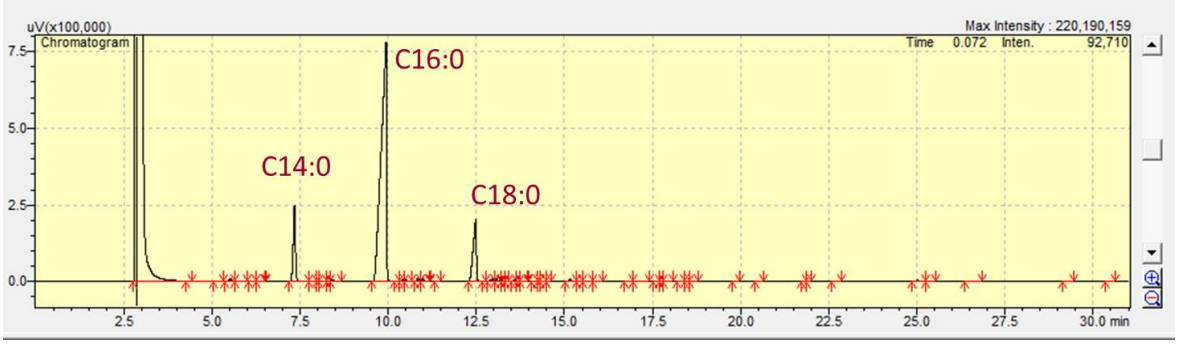

Figure 2.S3. Peaks intensities of lipid test results from the white matter collected from surface of electrodes and reactor wall.

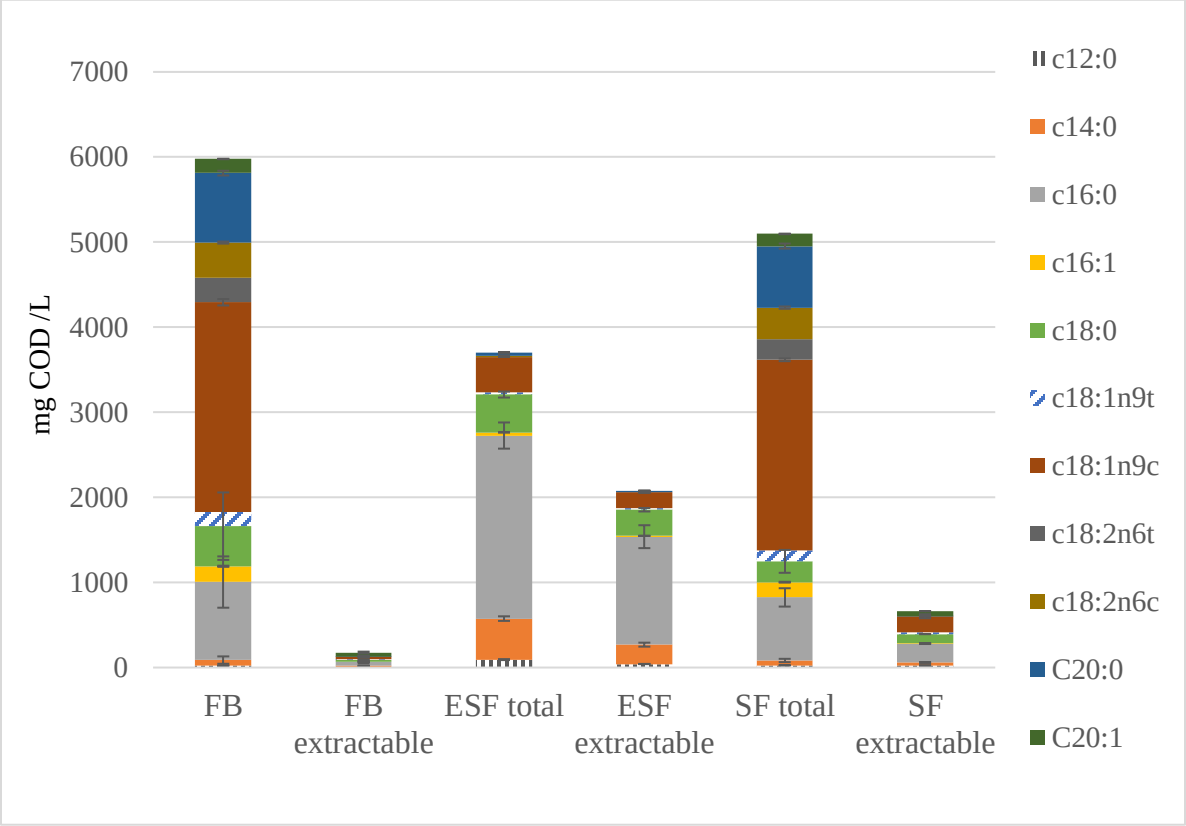

Figure 2.S4. Profiles of total and extractable lipids for FB, ESF effluent, and SF effluent on day 20.

2.S5. Equations and ΔCOD/ΔC Values Calculations for LCFA Degradation

Equation 2.S4 is an example of biohydrogenation reactions with carbon loss due to β-oxidation, from C18:1 to C16:0; Equation 2.S5 is an example of saturated LCFA degradation via β-oxidation, from C18:0 to C16:0. Calculations of the corresponding ΔCOD / ΔC values a are shown in Table 2.S2.

$$C_{18}H_{33}O_2^- + 2H_2O \rightarrow C_{16}H_{31}O_2^- + CH_3COO^- + H^+ + H_2$$

(Eq. 2.S4)

$$C_{18}H_{35}O_2^- + 2H_2O \rightarrow C_{16}H_{31}O_2^- + CH_3COO^- + H^+ + 2H_2$$

(Eq. 2.S5)

Table 2.S2. Calculations of ΔCOD / ΔC values for LCFA biohydrogenation with β-oxidation corresponding to Equations 2.S4 (top) and 2.S5 (bottom).

	$C_{18}H_{33}O_2^-$	$2H_2O$	→	$C_{16}H_{31}O_2^-$	CH_3COO^-	H^+	H_2	ΔCOD or ΔC ×	ΔCOD / ΔC ×
COD (g COD/mol)	816			736	64		16	80	3.3
C (g C/mol)	216			192				24	
	$C_{18}H_{35}O_2^-$	H_2O	→	$C_{16}H_{31}O_2^-$	CH_3COO^-	H^+	$2H_2$	ΔCOD or ΔC ×	ΔCOD / ΔC ×
COD (g COD/mol)	832			736	64		32	96	4
C (g C/mol)	216			192				24	

× Only LCFAs (C18:1, C18:0, and C16:0) are included in the calculation of ΔCOD, ΔC, and ΔCOD/ ΔC values. SCFAs and hydrogen are excluded.

Table 2.S3 shows an example of calculating the ΔCOD / ΔC values for SF and ESF effluents at Day 25.

Table 2.S3. Example of Calculation of ΔCOD / ΔC from experimental results

	COD (mgCOD/L)	C (mg C/L)	ΔCOD	ΔC	ΔCOD / ΔC
FB	7380	1945	-	-	-
ESF	4600	1200	3230	740	3.74
SF	6100	1610	1730	340	3.80

CHAPTER 3 INCREASED ANODE RESPIRATION ENHANCES UTILIZATION OF SHORT-CHAIN FATTY ACID AND LIPID WET-EXTRACTION FROM *SCENEDESMUS ACUTUS* BIOMASS IN ELECTRO-SELECTIVE FERMENTATION

This work, in a slightly modified format, is published in Renewable Energy, *titled:*
Liu Y, Lai Y-JS, Rittmann BE. 2019. Increased anode respiration enhances utilization of short-chain fatty acid and lipid wet-extraction from *Scenedesmus acutus* biomass in Electro-Selective Fermentation, *Renewable Energy, In press, doi: 10.1016/j.renene.2019.10.043*

3.1 Introduction

Renewable fuel must be developed at large scale to combat the rising concentration of atmospheric CO_2 and global warming (IPCC, 2018). Biodiesel from microalgae is a potential candidate for large-scale renewable biofuel production, thanks to its high unit-area production and ability to accumulate lipids in oleosomes (Chisti, 2007; Hu et al., 2008; Rittmann, 2008). However, the high costs associated with producing and harvesting biomass, as well as oil extraction, have prevented large-scale application (Markou and Nerantzis, 2013). I focus on economical oil extraction, which would go far towards making microalgae biodiesel a viable option.

Economical oil extraction from microalgae biomass might be possible by using strong solvents that penetrate the cell wall and membrane. Folch (1:1 Methanol : Chloroform v/v) (Folch et al., 1957) and Bligh & Dyer (1 : 1 : 0.5 chloroform : methanol : water v/v) (Bligh and Dyer, 1959) are effective, but they present acute environmental and human

toxicity (Dejoye et al., 2011). A second approach to bring about good oil extraction involves pretreatment to disrupt the cell wall and membrane. Acid/alkali-catalyzed hydrolysis, ultrasonication, and pulsed-electric fields (PEF) have proven to be effective (Sheng et al., 2011a; Zbinden et al., 2013), but they also are associated with high energy and capital cost. Here, I seek a more economically feasible pre-treatment method that can be coupled with an environmental friendly solvent, such as ethyl acetate, isopropanol, or hexane.(Dong et al., 2016; Laurens et al., 2015)

Selective Fermentation (SF) is a new approach to enhance lipids extraction from microalgal biomass (Lai et al., 2016b). SF is based on the fact that lipids are generally biodegraded more slowly than carbohydrate and protein in anaerobic conditions (Lai et al., 2016b; Rittmann and McCarty, 2001; Siegert and Banks, 2005). Bacteria that ferment lipids require a longer solid retention time (*SRT*) than those that ferment carbohydrates and proteins; the lipid fermenters can be washed out of the system if the *SRT* is short enough (Lai et al., 2016b). SF promoted lipid extraction with a hexane/isopropanol solvent (Hexane : Isopropanol 1:1 v/v, HI): more than a 5000-fold increase in lipid extraction from *Scenedesmus acutus 0401* after SF treatment at neutral pH, compared to untreated biomass (Lai et al., 2016a). SF also provided the added benefit of biohydrogenation, where unsaturated LCFA were converted to saturated LCFA in a biological process. The saturation ratio of *S. acutus* lipids increased from 20% to 80% after SF treatment. As saturated lipids are desired for biodiesel production, biohydrogenation is a desirable benefit (Knothe, 2011).

Despite its benefits, SF presents a few weaknesses that need to be overcome. One is the accumulation of short-chain fatty acids (SCFAs): The chemical oxygen demand (COD) from SCFAs were about 1800 mg /L in the SF effluent with a 6-day *SRT* (Lai et al., 2016b). Accumulated SCFAs represent a waste of electrons from the feeding biomass, and a high-enough concentration of SCFAs also can inhibit the fermentation process directly and by lowering the pH (Siegert and Banks, 2005). Thus, a highly efficient SCFA scavenger would remove the inhibitory effect.

Microbial Electrolysis Cells (MECs) are devices that use Anode Respiring Bacteria (ARB), which live as a biofilm on an anode, where they oxidize SCFAs and respire the electrons to the anode (Ki et al., 2015; Parameswaran et al., 2009; Torres et al., 2007). The electrons are transported from the ARB cells to the anode via extracellular electron transfer (EET) (Reguera et al., 2005; Torres et al., 2009a), conducted through an electrical circuit to a cathode, and used to reduce H_2O to H_2 gas, which evolves from the cathode (Guo et al., 2017; Logan et al., 2008; Rozendal et al., 2008). The MEC is a promising means to scavenge the SCFAs that accumulate in SF.

A second weakness of SF occurs because fermentation usually is slower at biodegrading protein compared to carbohydrate (Lu et al., 2010; Siegert and Banks, 2005). An MEC also may be valuable for enhancing the biodegradation of protein. Lu et al. (2010) was able to use an MEC to produce a high H_2 yield (21 mmol H_2 / g COD) using Bovine Serum Albumin (BSA) with a batch cycle of 3 days, with 60% of the total nitrogen released as ammonium-N (Lu et al., 2010). Later research by the same authors showed

increased protein degradation from Waste Activated Sludge (WAS) using an MEC (Lu et al., 2012).

With the goal of overcoming the weaknesses of SF, I created *electro-selective fermentation* (ESF) by integrating an MEC with SF (Liu et al., 2019a). In particular, I sought to improve carbohydrate and protein biodegradation of algae biomass, while making the biomass's lipids more available for wet-extraction using the more environmentally friendly solvents hexane or isopropanol. Accelerating protein biodegradation should disrupt hydrogen bonding between membrane protein and lipids, thus exposing intracellular oleosomes to the solvent and allowing much easier extraction (Sheng et al., 2011c).

Conducting "ESF vs. SF" experiments with *Scenedesmus acutus* biomass, Liu et al. (2019a) showed that ESF enhanced lipid extraction by 3-fold and protein degradation by 4-fold (Liu et al., 2019a). However, the COD equivalent of the coulombs collected by the anode in the ESF process was less than 1% of the total feeding COD, and SCFAs accumulated (>1500mg COD /L) in the ESF's anode chamber. The reason for SCFAs accumulation was the small anode area (20.8 cm^2 in an anode-chamber volume of 340 mL), which allowed only a small amount of ARB biomass on the anode surface.

To eliminate these shortcomings, I employed a flat-plate MEC design with a higher anode area for this research. This design should increase the coulombic conversion efficiency and provide better SCFA-scavenging. Rapid scavenging of SCFA, provided by a large amount of ARB biofilm, can quickly lower the SCFA concentration in the anode chamber. Since SCFAs are products of fermentation from monomers like

monosaccharides, amino acids, and long chain fatty acids (LCFAs), the removal of SCFA in the anode chamber may be able to accelerate the fermentation process of monomers by creating a syntrophic relationship between the fermenters and the ARB;(Gao et al., 2014; Parameswaran et al., 2009).

Here, I investigate the effects of the larger anode area in ESF. In particular, I quantify the SCFA-scavenging ability of ARB on the anode; the effects of ESF on wet lipid-extraction using 100% hexane (Hex) and 1:1 (v/v) hexane : isopropanol (HI); "biohydrogenation" of long chain fatty acids during ESF via β-oxidation, and accelerated protein fermentation caused by ESF.

3.2 Material and Methods

Scenedesmus acutus 0401 biomass was freshly harvested from a bench-scale photobioreactor located on the Tempe Campus of Arizona State University (Tempe, AZ, USA). It had a volatile solids (VSS) concentration of ~1.5 g VSS /L upon harvesting. After sedimentation in a 4°C cold room, the concentration was ~6.6 g VSS /L.

The design of the flat-plate MEC followed Ki et al. (2017), but with removal of the serpentine structure in the cathode chamber. A picture of the flat-plate MEC is shown in Figure 3.1. The MEC was constructed using acrylic plates (McMaster-Carr, Santa Fe Springs, CA, USA). The anode chamber had a working volume of 200 mL, and the cathode chamber, with the serpentine design removed, had a working volume of 60 mL. The anode was carbon fiber (0.01-mm strand diameter, 2000 filaments, Goodfellows Cambridge Limited, Huntingdon, England) woven through a perforated titanium-plate mesh. The cathode was made of stainless-steel mesh (SS, type 316, mesh 80 * 80, 0.014cm of wire diameter, McMaster-Carr, Santa Fe Springs, CA, USA). The anode and cathode had geometric areas of 49 cm^2, but the actual area for biofilm attachment was greater than the geometric area of the graphite anode (20.8 cm^2) due to the high specific area of the carbon fiber. An Ag/AgCl reference electrode (BASI Electrochemistry, West Lafayette, IN, USA) was installed at the center of the anode chamber from the top through a butyl-stopper with its tip ~3 cm above the bottom of the anode chamber and ~1cm from the surface of the carbon-fiber anode. An Anion-Exchange membrane (AEM) (AMI - 7001, Membranes International, New Jersey, USA) was used to separate the anode and the cathode. Duplicate reactors were used for ESF experiments.

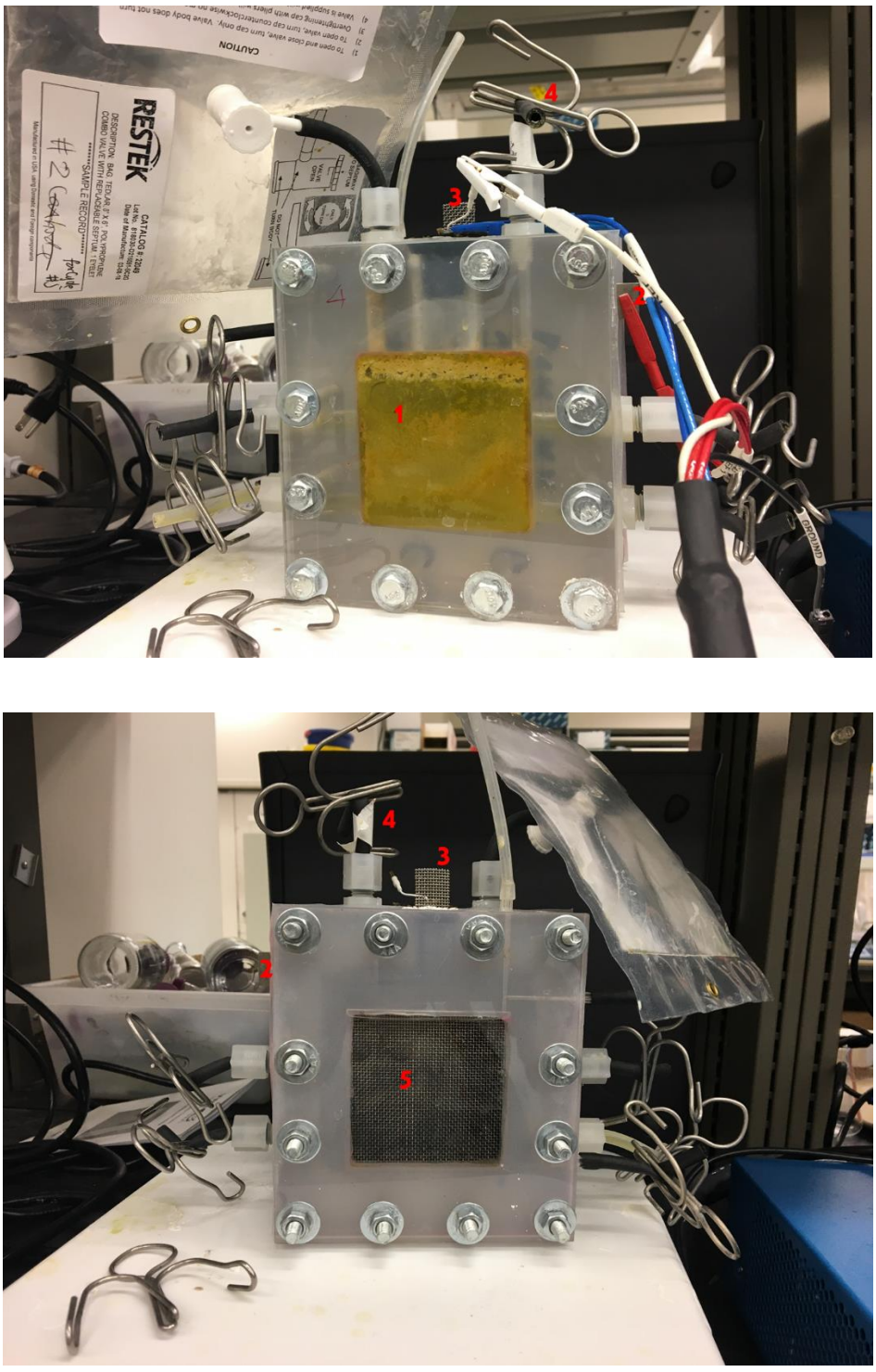

Figure 3.1. Photograph of the flat-plate MEC. Visible are the anode chamber (1), anode connection (2), cathode connection (3), sampling port (4), cathode chamber (5).

To accumulate ARB on the anode, the anode chamber of the flat-plate MEC reactor was fed with synthetic medium (1970 mg/L sodium acetate, 380 mg/L sodium propionate, 200 mg/L sodium butyrate, 90 mg/L glucose, 140 mg/L Bovine Serum Albumin, and 1 mL/L of trace element solution (Lee et al., 2008b) in a 80-mM Phosphate Buffer (pH = 7.5). Condensed anaerobic digestor sludge from Mesa Northwest Water Reclamation Facility (MNWWRP, Mesa, AZ) was used as the inoculum. Acclimation was in batch mode with the anode potential set at -0.3 V (vs Ag/AgCl, -0.078V vs SHE) using a VSP potentiostat (BioLogic Science Instruments SAS, Claix, France). EC-Lab software (v 11.21, Bio-Logic SAS) was used to set the electrical parameters and record current density, coulombs collected, and power data during operation of the MEC. Startup was rapid, with current densities of the two MECs reaching 5 A/m^2 after 7 days. At this time, the two ESF reactors were hydraulically connected to form a lead-lag system; the lead reactor was fed the same synthetic medium continuously at a flow rate of 0.08 mL/min, with its effluent going to the lag reactor. Steady currents of ~5 A/m^2 were achieved in approximately 30 days' continuous operation for both MECs, as acetate was present (by design) at a high concentration is both MECs.

After acclimation, the ESF process was initiated by adding to the anode chambers 180 mL of concentrated *S. acutus* biomass (6.6 g VSS /L) and 20 mL of Waste Activated Sludge (WAS, WNWWRP, Mesa, AZ). NaH_2PO_4 and $NaHPO_4$ were added to the starting pre-inoculated biomass to achieve an 80-mM phosphate buffer with a starting pH of 7.0. The feeding biomass with WAS inoculation and PBS was sparged with N_2 gas for 15 minutes to remove dissolved oxygen. It was then transferred to the MEC anode

chamber using a 60-mL syringe. The anode chamber was then sparged with N_2 gas for 15 minutes and moved to a room with a stable temperature (25 ± 1.0°C). Stirring in the anode chamber was provided by a 2.5-cm magnetic stirring rod driven by a stirrer at 450 rpm. The cathode chamber was filled with 60 mL of NaOH solution at pH 12, and the cathode chamber was refilled on a daily basis. For SCFA and ammonium-N analyses, 1-mL liquid samples were taken from both replicate reactors beginning on day 0.5. For carbohydrate, protein, and lipids analyses, one liquid sample was taken from each duplicate reactor on day 0 and day 9, when the experiment was stopped.

Total chemical oxygen demand (COD), total suspended solids (TSS), volatile suspended solids (VSS), total carbohydrate, total protein, and total and extractable lipids were directly assayed and analyzed from unfiltered liquid samples taken on days 0 and 9. ammonium-N and SCFAs were measured from filtered samples taken on day 0.5, 1, 2, 3, 5, 7, 9. TSS and VSS were determined by methods described in sections 2540 B and E of *Standard Methods* (Rice et al., 2012), respectively. Total COD was measured using a HACH COD kit (concentration range 10-1,500 mg/L); NH_4^+ was measured using HACH ammonium-N kit (concentration range 2 – 47 NH_4^+-N /L) (HACH Co., Loveland, CO, USA). Total carbohydrates were determined by a modified phenol-sulfuric acid method developed by Chen et al. (2012). Total protein was determined by the Bio-Rad protein kit (Bio-Rad, Hercules, CA, USA). Total and extractable lipids, characterized as fatty acid methyl esters (FAME), were quantified using the method of Lai et al. (2016a), where direct-transesterification was used to convert algal triacylglycerides and diacylglycerids (DAGs) to FAME. The FAME-COD concentrations for each LCFA

species were then converted to their corresponding TAGs with three identical LCFA tails. Two solvents, pure hexane and hexane : isopropanol (1:1 v/v), were used to quantify extractable lipids and compare the wet-extraction effects of two different solvents. Short-chain fatty acids (SCFAs) were assayed after 0.2-μm membrane filtration (Pall Science, NY, USA). SCFAs were measured with an high-performance liquid chromatography (HPLC) (Shimadzu Corp, Columbia, MD, USA) equipped with an Aminex HPX-87H column (Parameswaran et al., 2009). SCFAs, total protein, total carbohydrates, and total FAME concentrations obtained from these methods were converted into the unified units of mg COD /L to quantify the electron distribution.

3.3 Results and Discussion

Current densities and collected coulombs for the two batch-mode flat-plate ESF reactors are shown in Figure 3.2. Both reactors had similar trends: the current densities rose to >2.5A/m^2 in less than 2 days, but slowly declined thereafter. At day 9, when the batch experiment ended, the current densities had declined to around 0.5 A / m^2. SCFAs in the effluent had been largely depleted; fermentation of *S. acutus* biomass was not providing as large flow of SCFAs for the ARB biofilm. About 6000 C and 5000 C were collected in duplicate ESF #1 and #2 respectively, and they correspond to about 2500 mg COD/L and 2000 mg COD /L of electrons transported to the cathode.

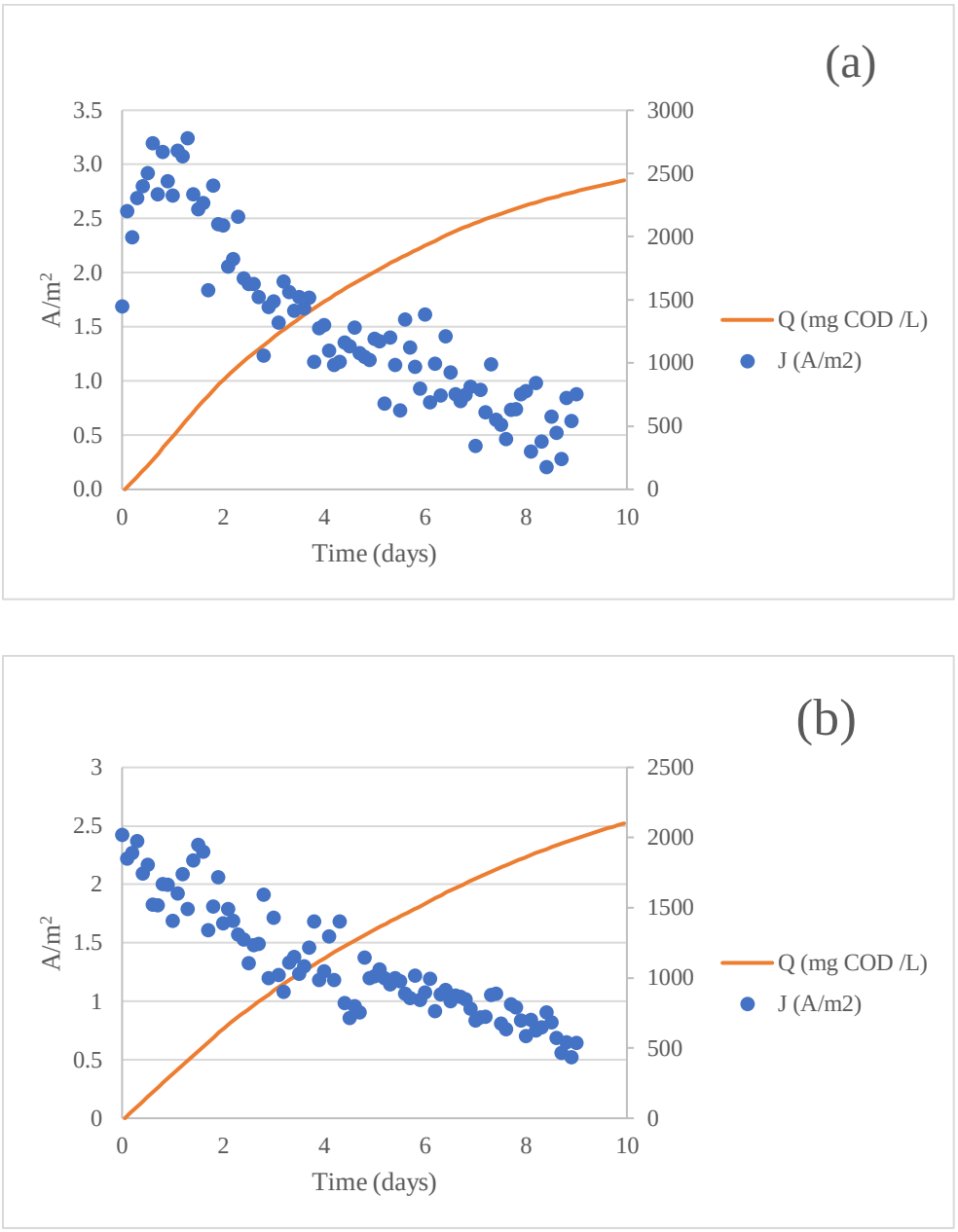

Figure 3.2. Batch-reaction performance of the ESFs fed with *S. acutus* biomass: current density (J, A/m^2) and cumulative Coulombs recovered as mg COD /L (Q, mg COD /L). (a) ESF reactor #1; (b) ESF reactor #2.

The breakdown of the COD for the feeding biomass (FB) at day 0 and the average values of effluents from two ESF reactors are shown in Figure 3.3. Compared to the FB, 9 days of batch ESF treatment achieved 50 ± 2 % TCOD removal, and < 1% was converted to and remained in the form of SCFA. Because of its much higher specific anode-surface area, the flat-plate ESF reactor had much higher conversion of FB COD to Coulombs (17% of FB TCOD) than with the H-type ESF reactors (<1 %) used by Liu et al. (2019a). The consequence was that SCFA accumulation was minimal (<1%), compared to ~18% of TCOD retained as SCFAs in the H-type ESF reactor (Liu et al., 2019a). This confirms that the ESF anode can be a strong SCFA sink as long as it has enough area and accumulation of ARB biomass.

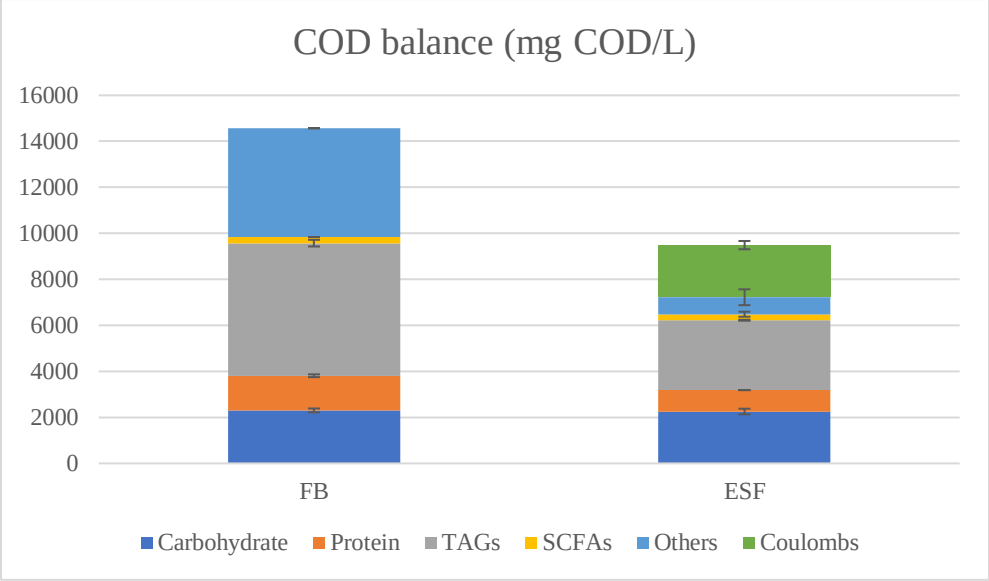

Figure 3.3. COD mass balances for the feeding biomass (FB) and ESF effluent. Values for FB are averages of two duplicate samples; values for ESF are averages between two

reactors and two duplicate samples for each reactor (4 in total). Error bars indicate high and low values for FB and standard deviation for ESF.

SCFA concentrations, expressed in mg COD /L, were monitored throughout the batch experiment and are summarized in Figure 3.4, along with cumulative Coulombs collected. Acetate, propionate, butyrate, and valerate, which were the only significant SCFAs, increased and then decreased over time, although each with its own timing. Acetate reached its peak on day 1, ~150 mg COD /L; valerate reached its peak on the same day as acetate, ~220 mg COD /L. For propionate and butyrate, the peak concentrations were ~550 and ~390 mg COD /L, at days 2 and 5 respectively. The fast depletion of acetate supports that it was rapidly oxidized by ARB, a well-known phenomenon (Gao et al., 2014; Miceli et al., 2012; Parameswaran et al., 2009). The slight and brief accumulation of propionate and butyrate implies that they also were substrates for the ARB – fermenter syntrophic pair. *Geobacter*, a common ARB, cannot directly utilize butyrate (Miceli et al., 2014), which support that butyrate was first fermented to acetate, then oxidized by ARB, leading to the observed low acetate concentration in the system.

By day 9, the total SCFA concentration had declined to ~250 mg COD /L, only 1.6% of initial feed COD. Hence, ESF oxidized SCFA, converting their electrons equivalents to electrical current equivalent to ~2300 mg COD/L (18% of total FB COD) by day 9.

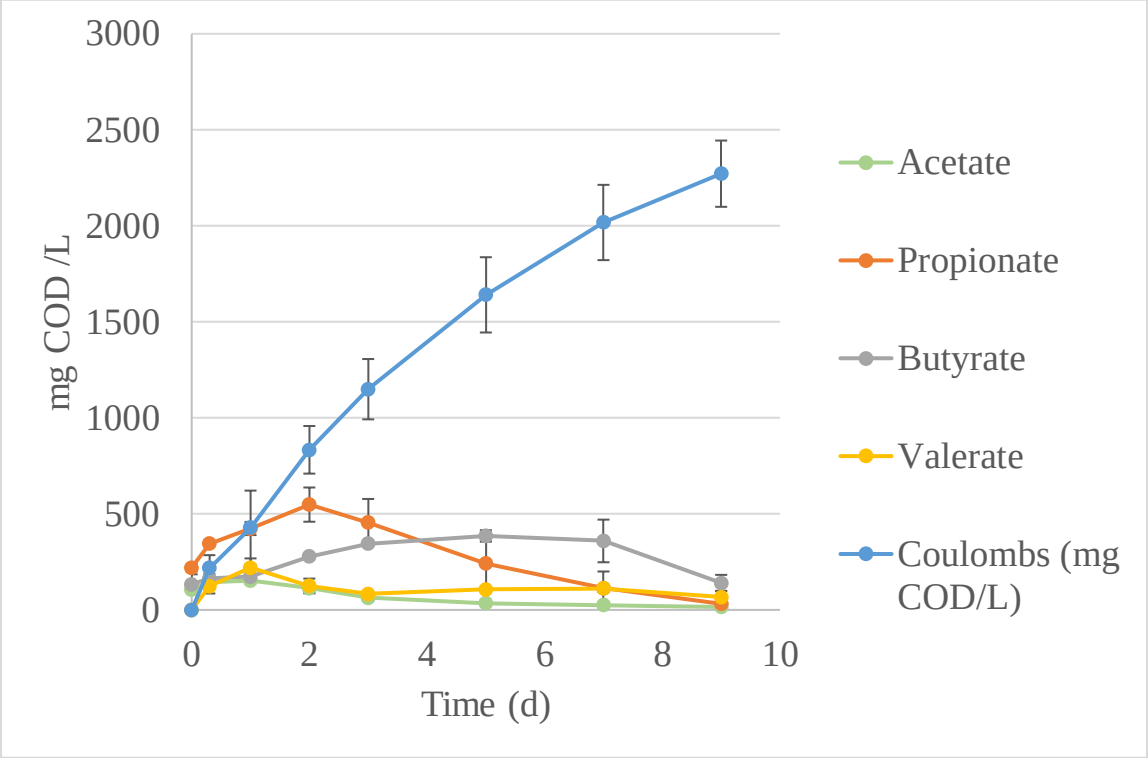

Figure 3.4. Trends of SCFA and coulomb accumulation in ESF. Values are averages from both reactors; error bars represent high and low values. All species are presented in units of mg COD /L.

Protein degradation by ESF can be tracked by the release of ammonium-N into the medium, shown in Figure 3.5. ESF showed ~38% protein degradation, which was slightly greater than the results of Lu et al. (2010): 20 - 35%. The decrease of protein concentration of ~1500 mg COD /L to ~930 mg COD/L yielded an ammonium-N concentration of 90 mg /L. This corresponds to 90 mg N/L released when ~570 mg COD/L of protein was hydrolyzed and fermented. Since 570 mg /L of protein COD translates to 380 mg /L of protein, the hydrolysis of protein yielded ammonium-N with a ratio of 0.24 g N / g protein. Chen et al. (2017) reported that the Kjeldahl nitrogen

releases for crop residues ranges from 0.22 to 0.25g N / g protein, with an average value of 0.236 g N / g protein. For microalgae, a value of 0.21 g N / g protein often is used (Laurens et al., 2012), although Templeton et al. (2015) found a range of 0.23 to 0.33, based on the amino-acid profiles of 21 different algal biomass samples. Based on the g N/ g protein values, most of the ammonium-N accumulated in the medium was the result of protein degradation ESF showed faster protein degradation kinetics compared to SF (Lai et al., 2016b). Whereas no significant degradation of *S. acutus* protein was detected in the first 20 days of the SF experiments (Lai et al., 2016b), ESF degraded 38% of the total protein in *S. acutus* within 9 days.

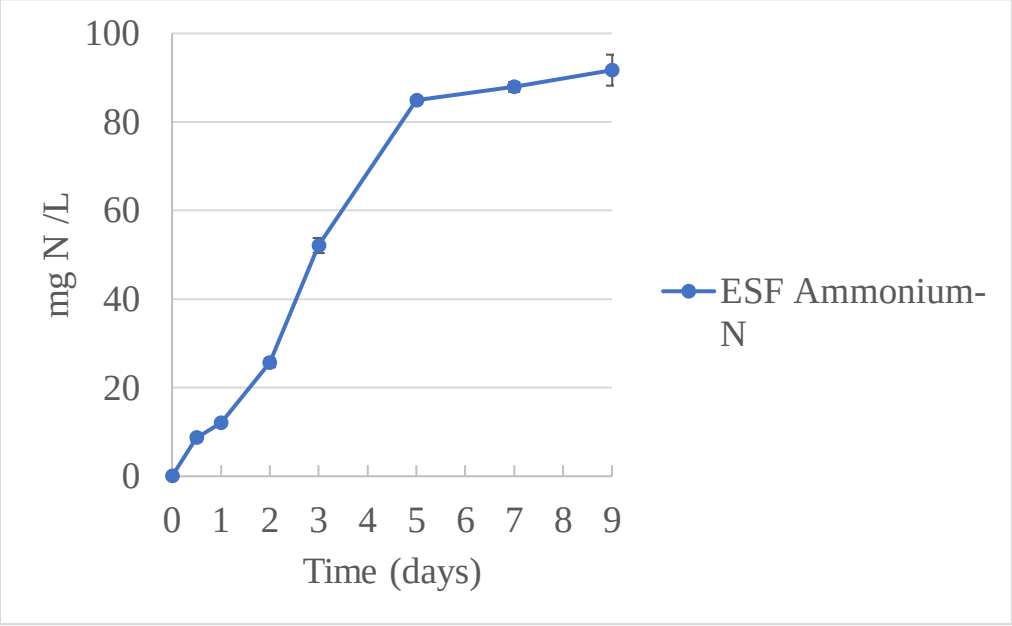

Figure 3.5. Ammonium-N accumulation during ESF. The total N of the FB was 240 mg N/L.

As pointed out by Lu et al. (2010), protein hydrolysis/fermentation can be the "choke" point in an anaerobic fermentation process if fermentation products accumulate. When the anode of an MEC oxidizes SCFAs, it can eliminate the choke point by creating an efficient syntrophic interaction in which SCFAs are rapidly oxidized by ARB. For example, Gao et al. (2014) documented a syntrophy among ARB, fermenters, and homoacetogens in a biofilm anode treating anaerobic digestate; SCFA concentrations were negligible, and methanogenesis was suppressed (Gao et al., 2014). An advantage of increased protein hydrolysis is that it can aid the extractability of lipids by breaking down cellular structures and increasing the exposure TAG-containing oleosomes to the solvent. This might include break down of oleosin, a protein embedded in the intracellular membrane of oleosomes (Huang, 1996).

Profiles of total and extractable lipids using two solvents (Hexane : Isopropanol 1:1 v/v, HI; Hexane 100%, Hex) are documented in Figure 3.6, which compares the FAME profile of the feeding biomass on day 0 against the FAME profile for ESF on day 9. On the one hand, ESF led to a loss of total lipids, assayed by direct transesterification: ESF recovered 53 ± 1 % of the total FAME. This trend is consistent with the COD balance in Figure 3. On the other hand, ESF greatly increased the amount of FAME that could be extracted. While wet-extraction of the FB using either solvent registered minimal recovery (< 1%), extraction efficiency after ESF was 21% to 24% for HI and 43% to 55% using hexane. Thus, ESF greatly increased the wet-extractability of FAME, particularly when using 100% hexane as the solvent.

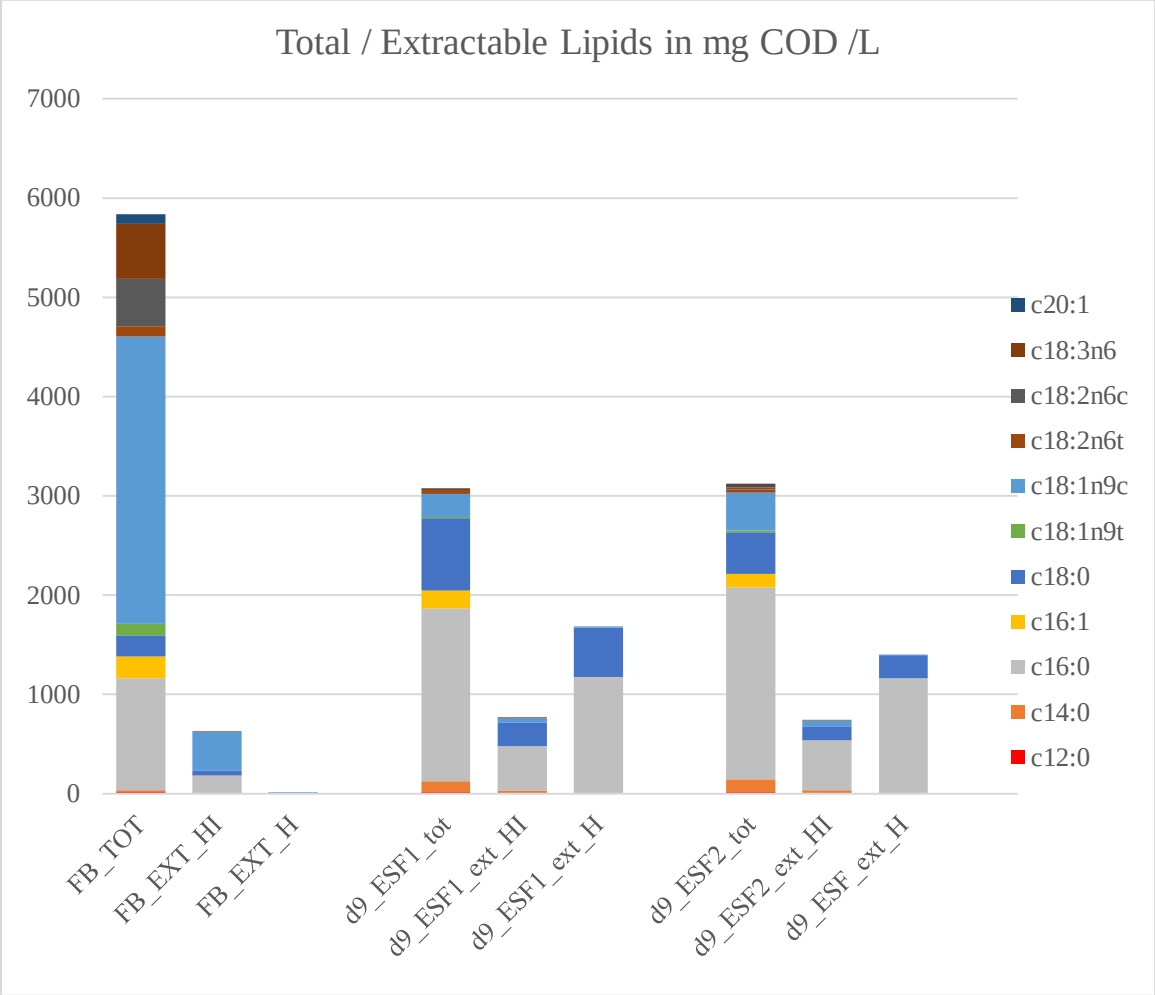

Figure 3.6. Profiles of total (TOT) and extractable (EXT) lipids for feeding biomass (FB) and the two ESF reactors. Extraction effects are for the two solvents: 1 : 1 (v/v) hexane : isopropanol (HI) and 100% hexane (H).

The COD percentages of extractable lipids, normalized to the COD of the total lipids, are shown in Figure 3.7. ESF enriched the lipids in saturated FAME, particularly C18:0 and C16:0. Thus, the saturation ratio of total FAME increased in ESF: The saturation ratio was 24 ± 0% in the FB FAME, but increased to 82 ± 2% in ESF total FAME. This reinforces the important role that "biohydrogenation" via β-oxidation plays in ESF, and it

is consistent with Chapter 2. Furthermore, the saturation effect was even stronger for extracted FAME: The HI extract had a 98 ± 1% saturation ratio in ESF medium, and hexane-extracted FAME was 100% saturated, with a strong preference for C16:0. In parallel with the increases in the saturation degree via "biohydrogenation", the SCFA concentrations were reduced to minimum levels. As noted by Cavaleiro et al. (2016) and Liu et al. (2019a), "biohydrogenation" of unsaturated LCFA can be achieved by β-oxidation: An unsaturated LCFA molecule is transformed to a saturated LCFA molecule with the loss of two carbon atoms, forming an acetate molecule (Cavaleiro et al., 2016): e.g. $C_{18}H_{33}O_2^- + 2H_2O \rightarrow C_{16}H_{31}O_2^- + CH_3COO^- + H^+ + H_2$, $\Delta G°' = -28$ kJ/mol. In ESF, acetate oxidation by ARB consumed the acetate.

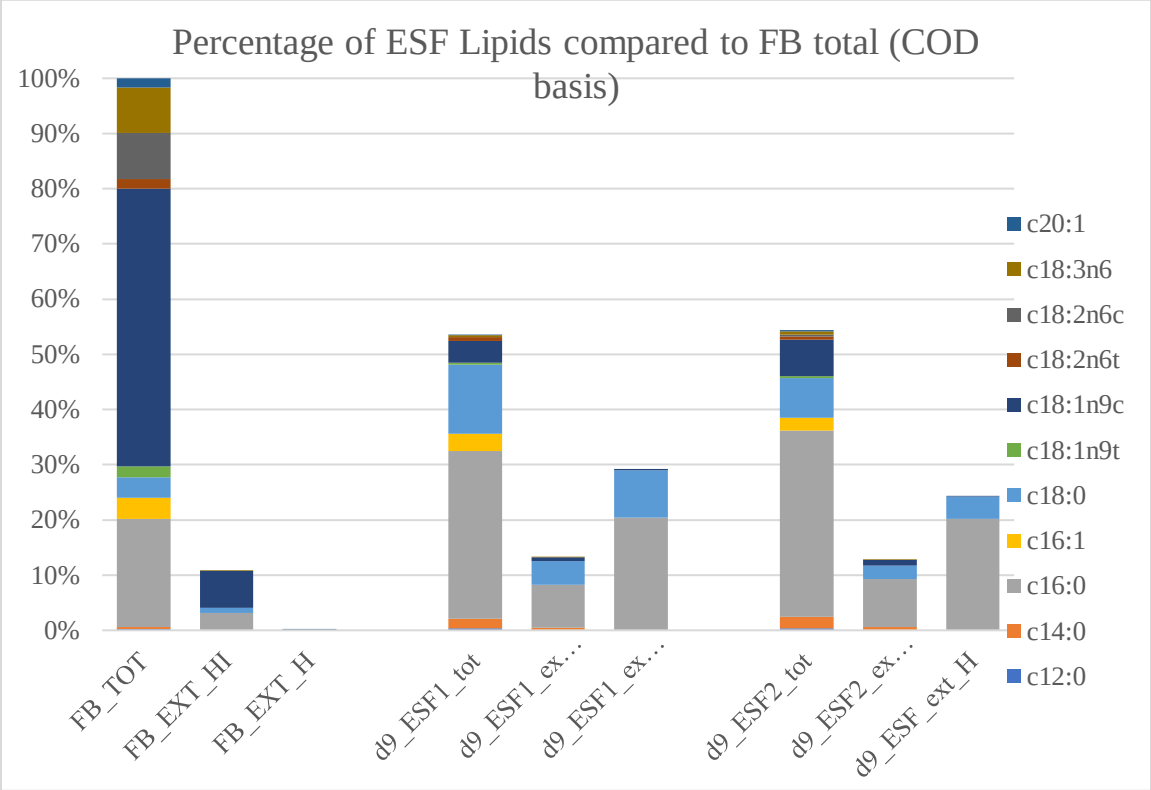

Figure 3.7. Percentages of lipids extraction for the FB and after ESF by the two solvents. All data are normalized to total lipids in FB or in ESF.

3.4 Conclusion

ESF carried out in a flat-plate MEC with a high anode surface area converted up to 18% of total

COD from *S. acutus* biomass to coulombs, significantly higher than in the previous ESF study with a low anode surface area (< 1% to coulombs). Because SCFAs were efficiently converted to current, minimal concentrations of SCFAs remained after 9 days of batch operation. ESF for 9 days significantly enhanced algae-lipid wet extraction, achieving 56% extraction from ESF total lipids, compared to < 1% for the FB. Enhanced lipid wet-extraction occurred in parallel to "biohydrogenation" of long-chain fatty acids: a shift of FAME profile from C18:1 to C16:0. Hexane was superior to hexane/isopropanol in lipid wet-extraction, and it also showed strong selectivity towards saturated fatty acids. Thus, ESF improved the quantity and quality of extractable FAME-based biofuel from *S. acutus*, while directing electron equivalents in SCFAs to current and H_2 generation at the cathode.

CHAPTER 4 FEEDING BIOMASS AFFECTS HOW WELL ELECTRO-SELECTIVE FERMENTATION ENHANCES LIPID EXTRACTION AND BIOHYDROGENATION

This work, in a slightly modified format, will be submitted to the Journal of Power Sources, titled:

Liu Y, Lai Y-JS, Rittmann BE. 2019. Feeding biomass affects how Electro-Selective Fermentation enhances lipid-extraction and biohydrogenation, *Journal of Power Sources.*

4.1 Introduction

Microalgae-based biofuel has been recognized as a potential long-term replacement for fossil fuels (Chisti, 2007; Rittmann, 2008) due to the potentially high weight ratio of lipids stored in their biomass (Adeniyi et al., 2018; Hallenbeck et al., 2016). However, most oil-producing microalgae form tough protection layers outside their oleosomes, preventing extraction with environmentally friendly, but relatively weak solvents, such hexane (HEX) or 1:1 v/v Hexane : Isopropanol (HI) (Huang, 1996). The stronger "gold-standard" solvents, e.g., Folch (1:1 chloroform : methanol, v/v) and Bligh-Dyer (1:1:0.5 chloroform : methanol : water, v/v) (Bligh and Dyer, 1959; Folch et al., 1957), are effective in rupturing microalgal cell structure and exposing the content in oleosomes for easy extraction, but they pose serious environmental and worker hazards (Laurens et al., 2015; Sheng et al., 2011).

In Chapter 2, I created the concept of Electro-Selective Fermentation (ESF) by combining Selective Fermentation (SF) with the Microbial Electrolysis Cell (MEC). SF exploits the fact that carbohydrate and protein are biodegraded faster than lipids by anaerobic microbial communities (Rittmann and McCarty, 2001). Thus, SF conserves lipids, while making them more readily extracted from algal biomass using HI solvent (Lai et al., 2016b). Another benefit of SF is biohydrogenation of the lipids to more saturated forms (Lai et al., 2016). Adding the anode of an MEC to SF, i.e., ESF, enhanced protein degradation, electron utilization, "biohydrogenation", and lipid extraction compared to SF as shown in Chapter 2, due in part to the oxidation of short-chain fatty acids (SCFAs) by anode-respiring bacteria (ARB). However, ESF also led to

greater lipid degradation due to β-oxidation that was associated with "biohydrogenation" (Cavaleiro et al., 2016; Liu et al., 2019a, b).

The results of Lai et al. (2016) and Chapter 2 disagreed about the effects of SF and ESF on lipid extraction of biomass of *Scenedesmus acutus*. Lai et al. (2016) found that SF increased

S. acutus lipid extraction by several-thousand-fold at 37℃, compared to directly applying wet-extraction to the feeding biomass (FB). In contrast, in Chapter 2, I using a different batch of *S. acutus* and 25℃, found that ESF was ineffective at enhancing lipid wet-extraction. These discrepancies suggest that different batches of algal FB may have been at the root of the very different effects, although effects of temperature or SF versus ESF cannot be discounted.

Here, I carried out semi-continuous ESF tests on four different batches of *S. acutus* biomass. All tests were performed at 25℃, using a flat-plate MEC with enhanced anode respiration (Liu et al. 2019b), a hydraulic retention time of 6 days, and neutral pH. The total test duration was

102 days, which gave 17 hydraulic retention times (*HRTs*). The four batches of *S. acutus* FB were supplied by the photobioreactor laboratory of Arizona State University, Tempe, AZ. I hypothesize that a long-term ESF experiment will achieve steady state between biofilm attachment or detachment, as well as suspended biomass and attached biofilm; thus, the biomass loss to attachment, shown in Chapter 3, can be avoided over the long run.

The main goals of this study were (1) to evaluate how different algae FBs affected ESF performance and (2) to link changes in the microbial community to lipids extraction during ESF.

4.2 Material and Methods

4.2.1 *Scenedesmus acutus* Feeding Biomass

Four different batches of *Scenedesmus acutus* biomass were collected from a photobioreactor in the microalgae laboratory of the Biodesign Swette Center for Environmental Biotechnology, Arizona State University, Tempe Campus (Tempe, AZ, USA). All biomass batches had a Volatile Suspended Solid (VSS) concentration of ~1.5 g VSS /L. The biomass was exposed to nutrient starvation in order to enrich it in triacylglyderides (TAGs) (Griffiths and Harrison, 2009; Rodolfi et al., 2009). The harvested biomass was stored in a cold room at 4°C for approximately 48 hours to allow settling. After settling, part of the supernatant was removed, and then the remaining suspension was thoroughly mixed to make a homogenous slurry. All slurry batches of feeding biomass (FB) had a final VSS concentration of approximately 5.9 g VSS /L, as shown in Table 4.1. Nitrate (NO_3^-), a potential electron acceptor, was not detected in the algae slurry's supernatant, due to elongated nutrient starvation. Before its addition to the ESF reactors, the algae FB was sparged with N_2 gas for 15 minutes to remove dissolved oxygen.

4.2.2 Semi-continuous ESF Setup and Operation

ESF was carried out in a flat-plate MEC reactor (Liu et al., 2019b) that followed the design of Ki et al. (2017), but with the serpentine structure in the cathode chamber removed. The MEC, constructed from acrylic plates (McMaster-Carr, Santa Fe Springs, CA, USA), had an anode chamber volume of 200 mL and a cathode chamber of 60 mL. The anode was carbon fiber (0.01-mm strand diameter, 2000 filaments, Goodfellows Cambridge Limited, Huntingdon, England) woven through a perforated titanium-plate mesh. The cathode was stainless-steel mesh (SS, type 316, mesh 80 x 80, 0.014cm of wire diameter, McMaster-Carr, Santa Fe Springs, CA, USA). The anode and cathode had geometric areas of 49 cm^2, but the actual biofilm area on the anode may have been larger due to high specific area provided by the carbon fiber. The anode and cathode were separated by an anode-exchange membrane (AEM, AMI-7001, Membranes International, New Jersey, USA).

Prior to the ESF experiment with the first batch of FB, an ARB biofilm was accumulated on the anode carbon fibers by batch feeding of 1970 mg/L sodium acetate, 380 mg/L sodium propionate, 200 mg/L sodium butyrate, 90 mg/L glucose, 140 mg/L Bovine Serum Albumin, and 1 mL/L of trace element solution (Lee et al., 2008b) in a 80-mM Phosphate Buffer (pH = 7.5). Anaerobic digester sludge was used as an inoculum. This acclimation step was in batch mode with an anode potential set at -0.3V (vs Ag/AgCl, -0.078V vs the standard hydrogen electrode (SHE)) using a VSP potentiostat (BioLogic Science Instruments SAS, Claix, France). EC-Lab software (v 11.21, Bio-Logic SAS) was used to set the electrical parameters and record current density, coulombs collected,

and power data during operation of the MEC. Current densities (based on the geometric area) of the MEC reached 5 A/m^2 after 7 days, and this concluded the startup period.

The ESF experiments were started by adding 180 mL of *S. acutus* biomass batch "A" (characteristics shown in Table 4.1) and 20 mL of Waste Activated Sludge (WAS, Northwest wastewater reclamation plant, Mesa, AZ). The WAS was provided to ensure that the ESF reactor contain hydrolytic and fermenting bacteria. NaH_2PO_4 and $NaHPO_4$ were added to the biomass-WAS mixture to achieve an 80-mM phosphate buffer with a starting pH of 7.0. Then, the mixture was transferred to the MEC anode chamber using a 60-mL syringe, sparged with N_2 gas for 15 minutes to remove dissolved oxygen, and moved to a room with a stable temperature of 25 ± 1.0°C. The overall ESF experiment was run for 102 days. Over this time, four batches of FB (all nutrient starved to be lipid rich) was used. The four batches, named "A," "B," "C," and "D," are characterized in Table 4.1. Sampling the FB and the effluent suspended biomass was conducted every 6 – 8 days.

Table 4.1 Properties and time periods for the four FB batches

Batch	Time period (days)	Initial VSS (g VSS /L)	Initial FAME % (g COD / g COD)	Carbohydrates % (g COD /g COD)	Protein% (g COD /g COD)	SCFAs % (g COD /g COD)
"A"	0 - 25	5.9 ± 0.1	42	15	14	3
"B"	26 - 50	4.9 ± 0.1	41	11	11	1
"C"	51 - 85	5.4 ± 0.1	43	6	10	1
"D"	86 - 102	5.1 ± 0.0	41	6	10	4

4.2.3 Analytical Methods

Total Chemical oxygen demand (TCOD), total suspended solids (TSS), volatile suspended solids (VSS), total carbohydrate, and total protein were determined directly from FB and effluent-slurry samples. TSS and VSS were determined by methods documented in sections 2540 B and E of *Standard Methods*, respectively; TCOD was determined by an HR+ HACH chemical oxygen demand (COD) kit (concentration range 150 – 15000 mg /L); ammonium-N was determined by a high range HACH ammonium-N kit (range 2 – 47 mg N /L) (HACH Co., Loveland, CO, USA). Carbohydrates were analyzed using a modified phenol sulfuric acid method developed by Laurens et al. (Laurens et al., 2014); protein was determined by Bio-Rad Bradford protein assay kit (BioRad Life Science, Hercules, CA, USA). Short-chain fatty acids (SCFAs) were assayed after centrifuging and filtering the slurry using a 0.2-μm membrane filter (Pall

Science, NY, USA), then measured using a an high-performance liquid chromatography (HPLC) (Shimadzu Corp, Columbia, MD, USA) equipped with an Bio-Rad Aminex HPX-87H column (BioRad Life Science, Hercules, CA, USA) (Parameswaran et al., 2009). Total and extractable lipids in the biomass were quantified using the approach of Lai et al (2016), resulting in fatty-acid methyl ester (FAME) concentrations. The FAME concentrations were then converted to mg COD /L to make values consistent. The saturation ratios of the FB and ESF biomasses were quantified by dividing the sum of COD values of saturated LCFAs by the total FAME-COD value.

Centrifuged pellets and scraped anode biofilm were used for DNA analysis (Liu et al., 2019a). DNA extraction was performed with PowerSoil DNA isolation Kits (MoBio Laboratories, Inc, Carslbad, CA, USA). Amplification, and sequencing were performed by the Microbiome Analysis Laboratory, Arizona State University, Tempe, AZ, USA, using a MiSeq Illumina Sequencer, targeting the V4 Region of the 16S rRNA gene with primer set 515f/806r. 16S rRNA gene sequences were analyzed using the Quantitative Insights into Microbial Ecology software version 2 package (QIIME 2, version 2018.11, http://qiime2.org/, Bolyen et al., 2018). To compare microbial communities between samples, principal component analysis were performed using the EMPeror software package in the QIIME 2 system. (Vázquez-Baeza et al., 2013).

4.2.4 Calculations

COD distributions of the FB and ESF suspended biomass were established by converting all concentration values to COD values. Conversion factors for carbohydrate and protein were obtained from Lee et al. (2008) and Chapter 2, and FAME-to-COD ratios were calculated using the same methods as in Chapter 2. From FAME-COD concentration values, the extractable lipid ratio from FB and ESF suspended biomass was calculated by dividing the value of extractable FAME of the sample by the total FAME concentration of the FB sample on the same day. The saturation ratios were calculated from the sum of a sample's saturated FAME-COD concentration, dividing by the total FAME-COD concentration of the total FAME-COD of the corresponding FB on the same day. Coulombic Efficiency (CE), the fraction of electrons recovered as electric current at the anode compared to electron equivalent removed from the substrate, was calculated from:

$$\mathrm{CE} = \frac{\frac{Coulombs}{96485\left(\frac{C}{mol}\right)} * 8g\ COD/mol}{\left(COD_{IN} - COD_{eff}\right) * V_{feed}} \qquad \textit{(Eq. 4.1)}$$

where COD_{in} is the total COD concentration of FB influent (mg COD/L); COD_{eff} is the total COD in the ESF effluent on the same day CE is calculated; Coulombs represents the Coulomb number collected on the same day; 96485 C/mol is the Faraday's constant; 8g COD/mol represent that 1 mol of electrons corresponds to 8 g of COD equivalent; V_{eff} is the volume of FB fed on the same day in liters; and CE expresses the efficiency by which the ARB remove electrons for the organic (COD) and respire the electrons to the anode.

4.3 Results and Discussion

4.3.1 ESF Performance for FB Degradation

The trends for current density were similar for each batch: A high current density was recorded shortly after a new batch was added; then the current gradually declined until FB addition the next day. The peak current density was 3.5 A/m^2 for batch "A." When batch "B" replaced "A," an immediate decrease of maximum current density was recorded, 2.3 A/m^2, but the peak current slowly increased over 25 days, reaching 2.7 A/m^2 on day 33. The maximum current density immediately decreased to 2.2 A/m^2 when batch "C" replaced "B," but it increased to 3.8 A/m^2 at day 86, when "D" replaced "C." The maximum current density for "D" immediately dropped to 2.5 A/m^2, and it decreased with time, to 2.3 A/m^2 at the end of the experiment (day 102). Taken as a whole, the current densities were similar to those obtained in Liu et al. (2019a) and modest compared to maximum current densities of ~10 A/m^2 achieved using acetate as electron donor (Torres et al., 2008).

The key finding is that the FB affected the peak current density, with "B" and "D" having noticeably lower current densities than "A" and "C." This is illustrated by the current densities for the last day of each cycle, namely days 24, 50, 84, and 102, shown in Table 4.2. (All current-density results are in Figure 4.S1 in the Supplementary Information (SI).) This trend means that the FB in the "A" and "C" tests was more readily biodegradable by ESF than in the "B" and "D" tests, as the "A" and "C" batches generated more acetate from fermentation.

Table 4.2 also gives the CEs, influent and effluent total COD concentrations, and COD removals on the last day of each test. ESF achieved modest COD removals for all algae FB batches

(25 – 38%), and the removal rates tended to increase as time progressed: from 25% for A to 38% and 35% for batches C and D, respectively. The overall trend suggests that the ESF consortia were acclimating to *S. acutus* FB over time. The CE values of all four batches were in the range of 69 to 81%, similar to the values obtained by Mahmoud et al. (2014) in batch treatment of landfill leachate, another complex organic substrate. The CEs were lower than 95% obtained by Ki et al.(2015) using pre-fermented primary sludge centrate, but much higher than 19% obtained by Zhang et al. (2012) using untreated sewage sludge. A CE lower than about 85% means that some of the electrons removed from the input COD were going to sinks other than anode respiration and ARB synthesis (Parameswaran et al., 2009; Rabaey et al., 2009). Since the feeding biomass did not contain nitrate or sulfate as alternative electron acceptors, the other sinks could include synthesis of non-ARB biomass (e.g., fermenters), fermentation products (e.g., SCFAs), and methanogenesis. Because measurements of the composition of the gas using gas chromatography with thermal conductivity detector (GC 2010, Shimadzu, Pleasanton, CA, USA) (Esquivel-Elizondo et al., 2017)) detected negligible methane, the non-ARB sinks likely were fermenter biomass and SCFAs.

Table 4.2. COD removal and electrochemical performances for ESF using all four FB batches. The values are for the last day of each test.

Batches	Influent COD (mg/L)	Effluent COD (mg/L)	COD Removal %	Maximum Current density (A/m^2)	CE %
A	11400±50	8550±300	25±3	3.5	69±3
B	10400±100	7300±100	30±1	2.7	81±1
C	11800±50	7350±50	38±1	3.8	70±1
D	10300±100	6660±100	35±1	2.3	72±1

4.3.2 Ammonium-N Accumulation and Protein Degradation

The trends in ammonium-N accumulation for all four batches are shown in Figure 4.1 (a). The FB had close to zero ammonium-N, except between days 12 and 24 and between days 80 and 86, where FB ammonium-N accumulation reached ~10 mg N/L and ~4 mg N/L, respectively. These two periods of relatively high FB ammonium-N were in the latter stages of FB batch storage for batches "A" and "C." This small buildup of ammonium-N, despite the FB being stored at 4°C, is consistent with the relatively greater biodegradability of the "A" and "C" batches based on COD removal and higher extractability from FB shown at the end of stage "C." However, batches "B" and "D," which were more recalcitrant, did not show ammonium-N accumulation in storage.

The ammonium-N concentration in the ESF effluent rose quickly to ~75 mg N /L on day 12. A small drop occurred on day 18, but ammonium-N again rose and peaked at day 24, at ~90 mg N/L, on the final day of batch "A." After batch "B" replaced batch "A" on day 25, the ammonium-N concentration in the ESF effluent drastically decreased to ~50 mg N /L on day 30 and continually fell to ~18 mg N/L on day 36. Clearly, ammonium-N accumulation, which originated from protein fermentation and degradation of other nitrogeneous biomass components, slowed with batch "B." Ammonium-N accumulation showed a slow increase after FB batch "C" replaced "B" on day 50, rising to ~35 mg N/L on day 72 and reaching ~70 mg N/L on day 84, a value approaching the peak ammonium-N accumulation at the end of batch "A" (day 24, ~80 mg N/L). The ammonium-N accumulation rapidly fell after batch "D" replaced "C" on day 84, ultimately to ~20mg N/L on day 102.

4.3.3 FAME Extractability Ratios and Saturation Ratios

Figure 4.1 (b) summarizes the FAME extractabilities for ESF and the FB biomasses over the course of the 102 days. For all batches, the FB biomass had low FAME extractability: 0% for FB batches "A" and "B" and 2 – 3% for batches "C" and "D." The FAME profiles of the four batches of FB, effluent suspended biomass, and extractable lipids are shown in Figure 4.S2 in the Supplemental Information.

The extractability of ESF suspended biomass with batch "A" increased to ~6% on day 6 and had a big hike to ~20% on day 12. While the ESF "B" suspended biomass gave high extractability (~22%) for the first sample after the FB was switched to batch "B," it fell rapidly to ~10% on day 38 and subsequently to 0% on day 44. The extractability of the "B" effluent suspended biomass did not fall immediately after the change of FB, because some of the effluent suspended biomass of "A" was still in the reactor on days 30 and 38 due to semi-continuous feeding. When suspended biomass from "A" reached a low-enough concentration, the extractability of the "B" suspended biomass reached zero (day 44). The ultimately poor extractability of "B" indicates that FB "B" was resistant to ESF treatment for improving FAME extractability.

When FB batch "C" replaced "B" on day 50, the effluent suspended biomass's extractability immediate rose to ~3% on day 58 and continued to increase to ~13% out to day 84. The peak extractability of batch "C" (~13%) never obtained the level with batch "A" (~20%), and the rate of extractability increase also was lower than that experienced with batch "A." This difference may be due in part to a change in the ESF microbial communities during the "B" feeding, a factor evaluated in a later section. The

extractability after batch “D” replaced “C” (day 94) dropped to the level similar to FB extractability (~3%) by day 102.

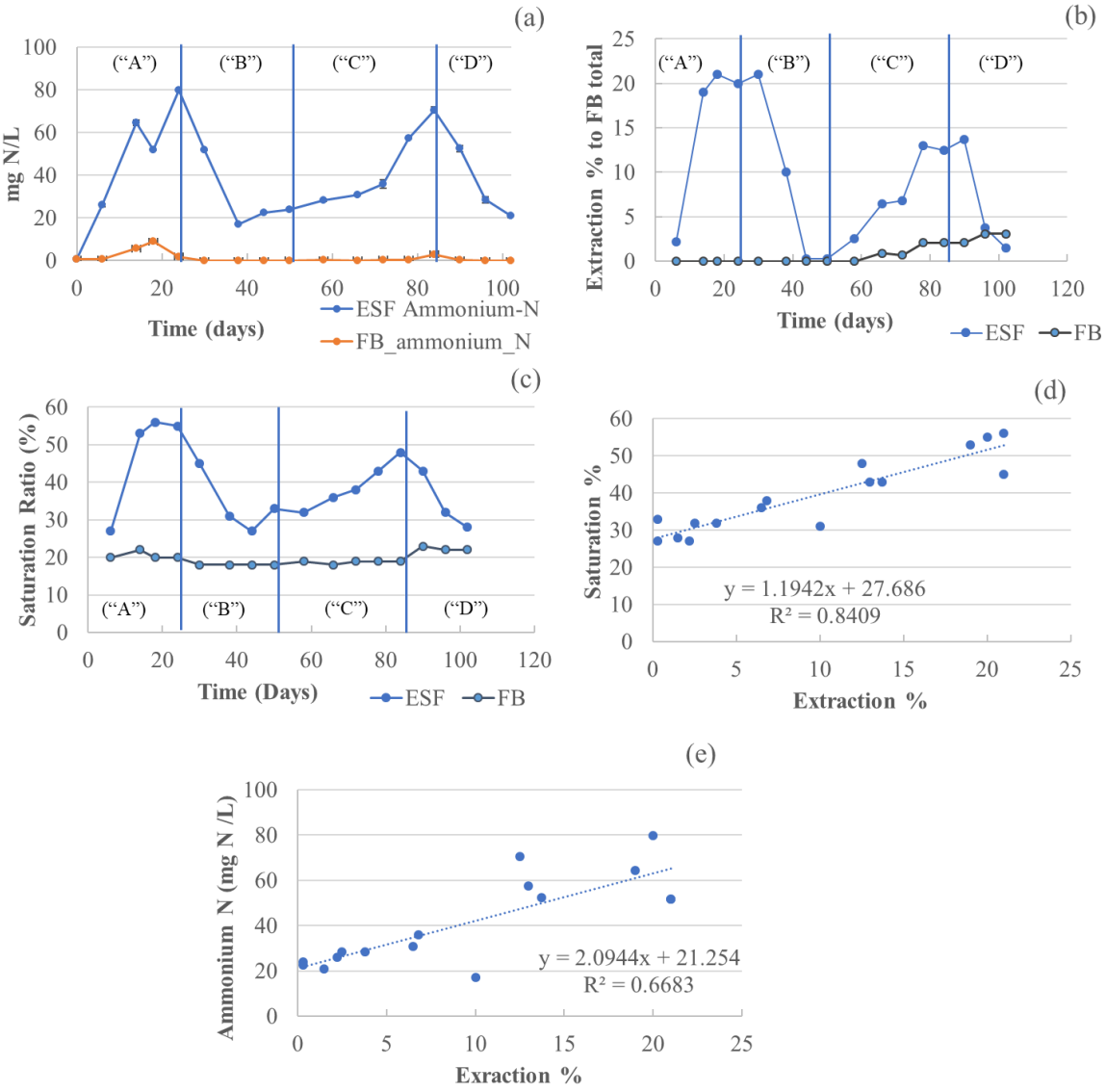

Figure 4. 1. Trends of ammonium-N concentration (a), extractability (b), and FAME saturation (c) and over the course of 102 days of SF. The four segments of different FB batches were divided by lines and annotated with representative letters "A," "B," "C," and "D." (d) The correlation between extractability and FAME saturation; and (e) the correlation between extractability and ammonium-N concentration.

The trends of FAME-saturation ratio of ESF suspended biomass and FB batches, shown in Figure 4.1 (c), are similar to those shown by the ammonium-N concentration (Figure 4.1(a)) and extraction ratios (Figure 4.1(b)). When the FB saturation ratio was stable at ~20%, the saturation ratio of ESF suspended biomass with FB "A" rose to ~53%. When batch "B" replaced "A," the saturation ratio fell to ~30% on day 44, consistent with weakened extractability enhancement for "B." The saturation ratio slowly recuperated after batch "C" replaced "B," up to 49% on day 84, but dropped to ~30% after batch "D" replaced "C," a trend parallel with the extractability dropping to ~3%. Figure 4.1(d) shows that the extractability and saturation ratios were strongly correlated: a high R^2 (0.84) and no systematic errors. Likewise, the ammonium-N concentration strongly and positively correlated with the extractability ratio (R^2 =0.67), as shown in Figure 4.1 (e). The results in Figure 4.1 and Table 4.1 clearly demonstrate the protein degradation, FAME extractability, FAME saturation, and current density depended strongly and in the same way on characteristics of the FB and that strong protein degradation was the key factor.

4.3.4. Microbial Community Analysis

Ten 16S rRNA gene libraries were created from Illumina sequencing of the four FB batches, the four ESF effluents' suspended biomass, and two biofilm samples collected from the anode at the end of batches "B" and "D."

To determine if different samples had distinct community structures, I performed Principal Coordinates Analysis (PCoA) using the weighted Unifrac method in the Qiime 2 software; the results shown in Figure 4.2. Three clusters are clearly evident: ESF suspended biomass cluster slightly to the left of the origin on the PC1 axis (65.0%), FB are to the far right of the PC1 axis, and biofilm samples are to the far left. The FB samples are scattered along the PC2 axis, with FB "A" and "D" clustering near the bottom of the PC2 axis, but FB "B" and "C" being near the top of the PC2 axis. The fact that neither "A" and "C" nor "B" and "D" FB samples clustered support that the endogenous microbial community was not a main factor determining ESF performances. Thus, it is more likely that the biochemical composition of the algal batches determined the performance. The key characteristics of the biochemical composition may be the proteins or lipids in the membranes, although the structure of cell wall also may play an important role in determining the difference behaviors of the "recalcitrant" and "degradable" batches.

For the effluent suspended biomass samples, "B" and "D" cluster closest to the PC2 axis. "A" and "C" are separated, and "A" was farthest to the left, perhaps because "A" had a stronger influence of the initial WAS inoculum. The two biofilm samples were well

separated from each other along the PC2 axis (24.3%), but similar along the more dominant PC1 axis. This indicates that the "recalcitrant" batches

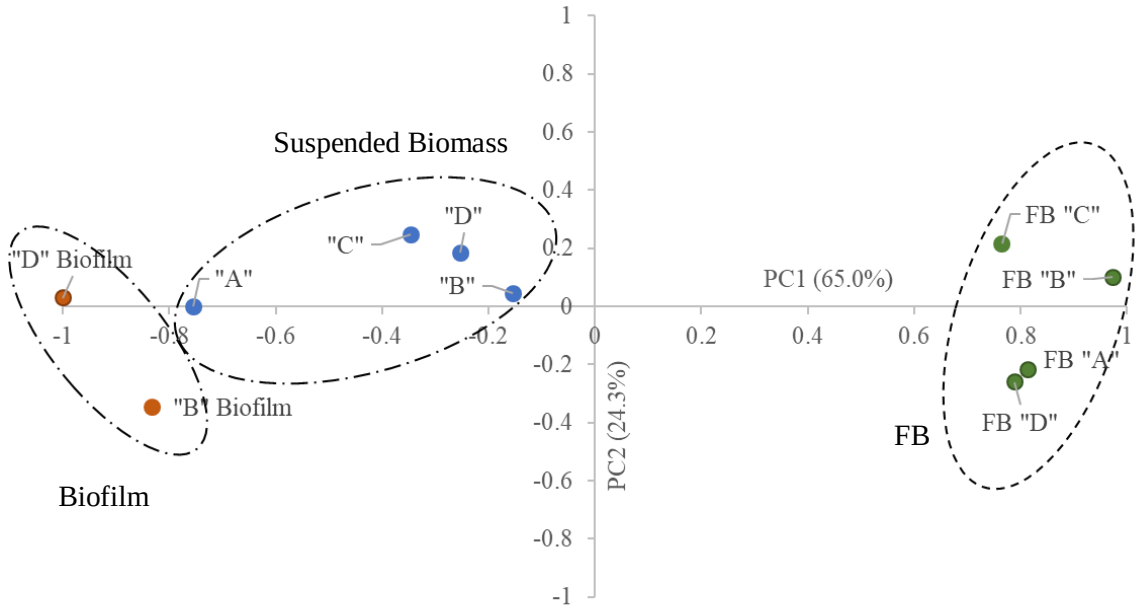

Figure 4. 2. Principle coordinates analyses (PCoA) for microbial communities of the different FB samples and different suspended biomass samples from different FBs. Samples from FB are represented by green dots, biofilms presented by brown dots, and suspended biomass are represented by blue dots. The names of the respective samples are labeled next to the dots. The percentages in the axis labels represents the percentages of variations explained by the principal coordinates, with minimum and maximum limits being -1 and 1, respectively.

I looked more closely at the what types of microorganisms caused the differences among the communities. Based on ESF performance and the PCoA analysis of the ESF-suspended biomass samples, I separate the "A" and "C" communities from the "B" and "D" communities. I present in Figure 4.3 (b) the detailed results for "A" and "B" ESF suspended biomass. In the same figure, I also show the detailed results for the "A" and "B" FB samples and the "B" biofilm samples. Results are presented at the genus level, although some names are at the family level when the item could not be identified to the genus level. Figures 4.S4 present the parallel information for the "C" and "D" samples for FB, ESF suspended biomass, and "D" biofilm.

Both batches of FB had high abundance of *Acutodesmus*, which is from the chloroplast DNA of *S. acutus*. "B" had lower *Acutodesmus* abundance than "A." One known lipid biohydrogenater, *Porphyromonadaceae* (family level) (Liu et al., 2019a), was in both batches of FB. Seven major genera of fermenters (*Aeromonadaceae* family) (>1% abundance) were found in FB "A," but were absent in "B."

The suspended biomasses of "A" and "B," which showed vastly different community structures compared to FB, differed from each other in important ways. *Acutodesmus* still were present, but, compared to the FB, lower in "B" (14%) and much lower in "A" (2%), supporting that more *S. acutus* chloroplast DNA was degraded in "A." This agrees with higher extraction ratio in Figure 4.1 (b). Two known biohydrogenaters, *Erysipelotrichaceae* and *Porphyromonadaceae*, were present in both suspended biomasses; *Erysipelotrichaceae* was higher in "A," and *Porphyromonadaceae* was higher in "B." Given that lipid was not readily extractable in "B," it is possible that

Porphyromonadaceae was utilizing other substrates when lipids were not available (Hahnke et al., 2015a)). All major fermenters, except *Syntrophomonas* and *Anaerovibrio*, had higher abundances with "A." Given the stronger protein degradation in "A" (Figure 4.1(a) and Figure 4.S3(c)), it is possible these fermenters preferred to ferment protein when it was available. It is possible that *Syntrophomonas* and *Anaerovibrio* were weak carbohydrate fermenters, as a substantial fraction of carbohydrates were endogenously degraded during cold storage (Figure 4.S3 (b)), particularly for the "A" FB. The only methanogen detected was *Methanocorpusculum*, a H_2-oxidizing genus; no acetate-cleaving methanogens were detected. *Geobacter*, the only detected genus of ARB, had higher abundance in the "A" suspended biomass than in the "B" suspended biomass, suggesting stronger ARB growth on and detachment from the anode with "A."

The microbial communities of anode biofilms for "B" are shown in Figure 4.3 (c). The largest abundances belonged to *Geobacter*, a typical ARB genus (Bond, 2002; Miceli et al., 2014). The *Geobacter* abundance was 35%, a value greater than in the "D" biofilm (15%, Fig 4.S3 (c)), which is consistent with the higher current density in "B" over "D" (Table 4.1). The "D" biofilm had a much higher abundance of *Methanocorpusculum*, suggesting that, upon long-term ESF, hydrogenotrophic methanogens could colonize the anode's biofilm and becomes an undesired electron sink; however, I never detected methane in the headspace gas.

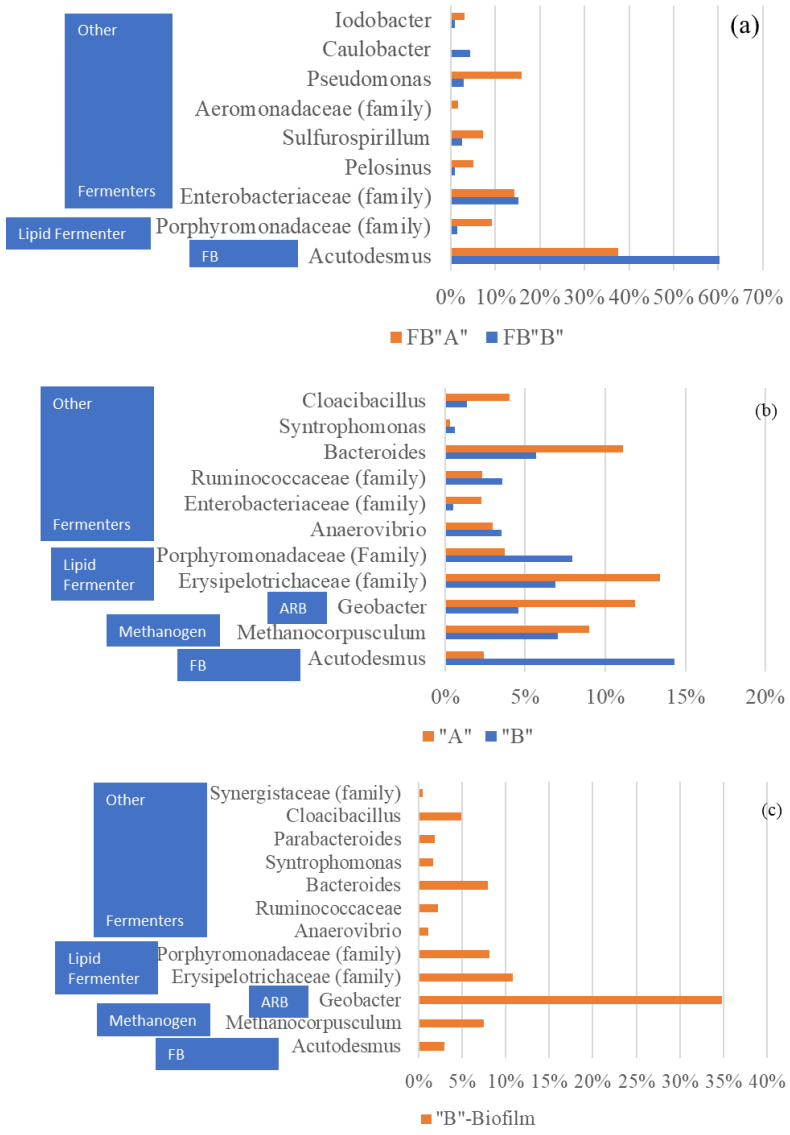

Figure 4. 3 Phylogenetic profiling of the suspended biomass in the FB of "A" and "B" (a), ESF suspended biomass of "A" and "B" (b) and biofilm of "B" (c) at the genus level. Items that could not be identified at the genus level are named at the family level and noted by "(family)." The horizontal axis presents the percentage abundance of the families based on the total reads of the 16S rDNA gene. Functions associated with each family are shown to the left.

4.4 Conclusion

ESF carried out in a flat-plate MEC fed four different batches of *S. acutus* biomass yielded different and consistent trends in terms of current density, lipid extractability, and saturation ratio. Batches "A" and "C" had higher values for each factor, compared to batches "B" and "D." The strong correlation between lipid extractability and saturation ratio suggests that "biohydrogenation" by β-oxidation occurred once intracellular lipids became more exposed and bioavailable to lipid-fermenting bacteria, which also were relatively enriched in the "A" and "C" batches. Increased protein removals and ammonium-N release occurred in parallel with higher lipid extractability and saturation ratio for "A" and "C." Principal coordinates analysis suggests that the FB endogenous microbial community had little impact on performance, but the community of the ESF-had a strong relationship. Key bacteria associated with the better performance of the "A" and "C" batches were *Bacteroides, Porphyromonadaceae*, and *Erysipelotrichaceae*. Taken together, all the trends reinforce that ESF was effective for enhancing lipid extraction and saturation when it increased protein degradation, which removed the barriers protecting the lipids from extraction and saturation. The effect depended on as-yet-undefined characteristics of the FB, which affected the community structure of the ESF suspended biomass.

Supplemental Information for Chapter 4

4.S1. Daily Maximum and Average Current Densities of the MEC

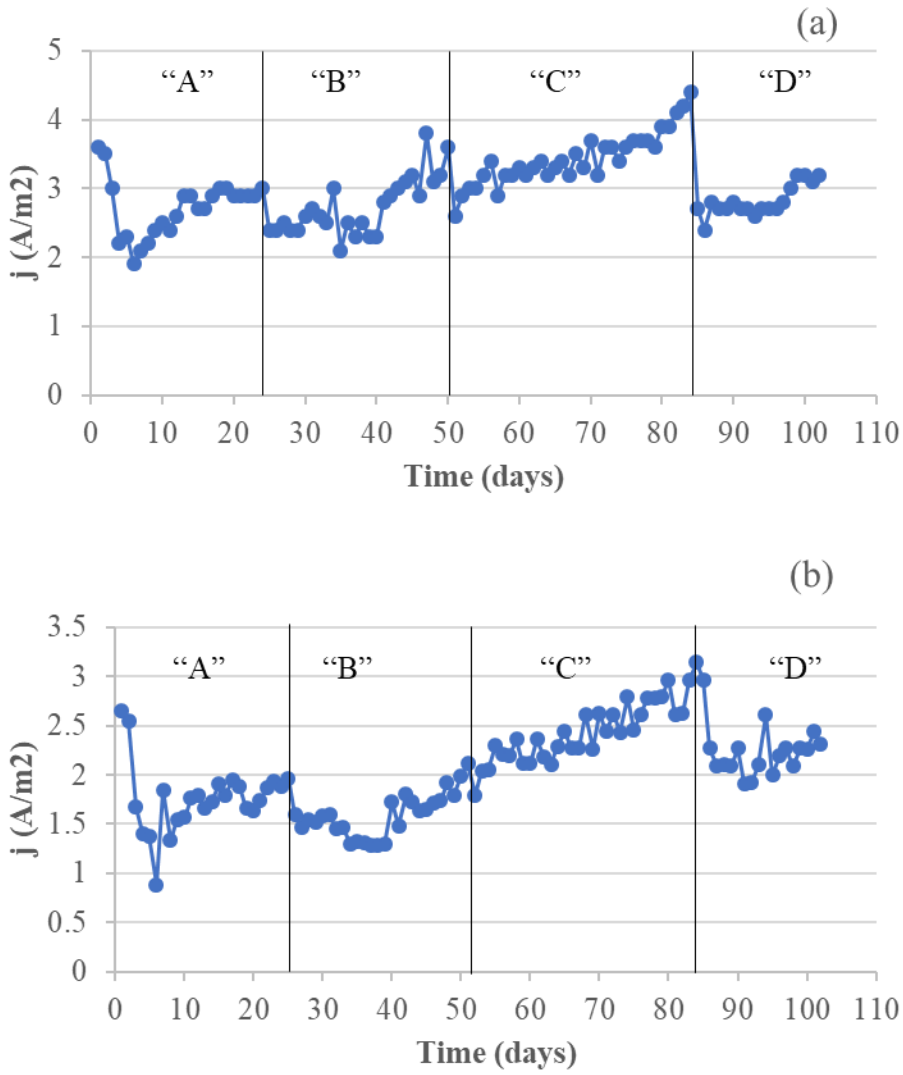

Figure 4.S1 Maximum current density (a) and Average current density trends of the ESF. The four segments of different FB batches were divided by lines and annotated with representative letters, "A," "B," "C," and "D."

4.S2. FAME Profiles of the Four Batches

The FAME profiles for the four sampling days -- 24, 50, 84, 102 for "A," "B," "C," and "D," respectively -- are shown in Figure 4.S2. Since "A" and "C" behaved differently from "B" and "D" in terms of anode respiration, ammonium-N release, FAME extractability, and FAME saturation, these two groups are discussed separately.

For "A" and "C," ESF led to net loss of lipids and strong "biohydrogenation". "A" showed losses of C18:1c (57%) and several poly-unsaturated species (C18:2c, 69%; C18:2t, 57%; and C18:3, 71%). In contrast, the saturated LCFA species, C16:0, the main product of ESF lipid transformation, had an increase of 116%. As documented by Cavaleiro et al. (2016) and in Chapter 2, β-oxidation of C18:1 to C16:0 should result in a 9% decrease in COD: for example, 1000 mg COD/L of C18:1 becomes 910 mg COD/L by β-oxidation to C16:0. In ESF, a 1460 mg COD/L decrease was observed in C18:1 of batch "A," while 940 mg COD/L of C16:0 was generated, a ratio of 64%. This means that C16:0 was further β-oxidized to smaller molecules, resulting in more lipid loss. The additional β-oxidation is partly accounted for by the increase of C14:0 in ESF effluent, from 21 mg COD/L in the FB to 162 mg COD/L. Additional β-oxidation probably was the cause of the remaining COD loss.

For batches "B" and "D," all LCFA-species concentrations decreased, except C14:0. In batch "B," C18:1c decreased from 2200 mg COD/L to 1590 mg COD/L (a 28% decrease). However, C16:0 also showed a decrease, from 620 mg COD/L to 580 mg COD/L (a 7% decrease). C14:0, which is the product of β-oxidation of C16:1 and C16:0, was the only species that saw an increase in concentration, but the increase was minimal

(15 mg COD/L to 21 mg COD /L, 36%). Poly-unsaturated species (C18:2c, C18:2t, and C18:3) showed decreases in concentrations

(35%, 30%, and 32%, respectively). Similar trends in lipid-profile change also occurred in batch "D," where the decrease of C18:1c, C18:2c, C18:2t and C18:3 (33%, 35%, 27%, 37%) did not result in an increase of C16:0 (decreased by 8%). The trends for "B" and "D" show that lipid was lost, but not through a β-oxidation route that led to "biohydrogenation". Given "B" and "D" showed near-zero extractability shown in Figure 4.1. (b), the cause of lipid loss in "B" and "D" was likely attachment of suspended biomass to the anode biofilm, as pointed out in Chapter 3.

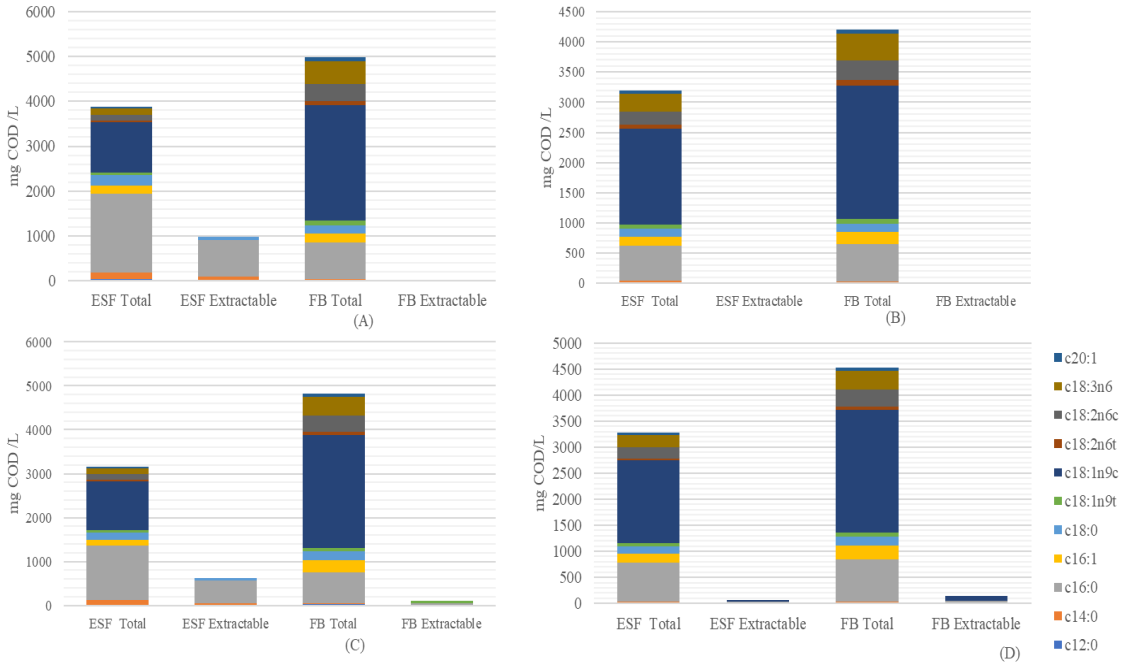

Figure 4.S2. LCFA profiles (in mg COD/L) for ESF effluents from batches "A," "B," "C," and "D" in panels (A), (B), (C), and (D), respectively.

4.S3. Protein / Carbohydrate Degradation

Figure 4.S3 shows the trends in carbohydrate and protein degradation in all periods of ESF. The degradation ratio for carbohydrates in ESF effluents (Fig. 4.S2 (a)) increased as the experiment advanced, but carbohydrates in FB (Fig. 4. S3 (b)) revealed endogenous degradation during storage at 4°C: e.g., the FB carbohydrate concentration decreased from an initial value of ~1600 mg COD /L to ~700 mg COD /L on day 24 for "A", a degradation ratio of ~55%. Endogenous degradation of carbohydrates occurred to a smaller degree for the other batches. The consistently low degree of lipid extraction for FB (lower than 3%, Figure 4.1 (b)) means that carbohydrate degradation did not lead to improved lipid extraction.

Figure 4.S3 (c) displays protein degradation during ESF for *S. acutus*. Batches "A" and "C" showed relatively higher degradation ratios compared to "B" and "D," and this difference corresponded to the higher lipid extractability by "A" and "C", and lower values for "B" and "D" (Figure 4.1 (b)) Also, FB protein concentration was largely stable in storage (Fig. S3(d)), which reinforces that the high extraction ratios displayed by "A" and "C" were affected by protein degradation, as shown in Chapter 2 and Chapter 3.

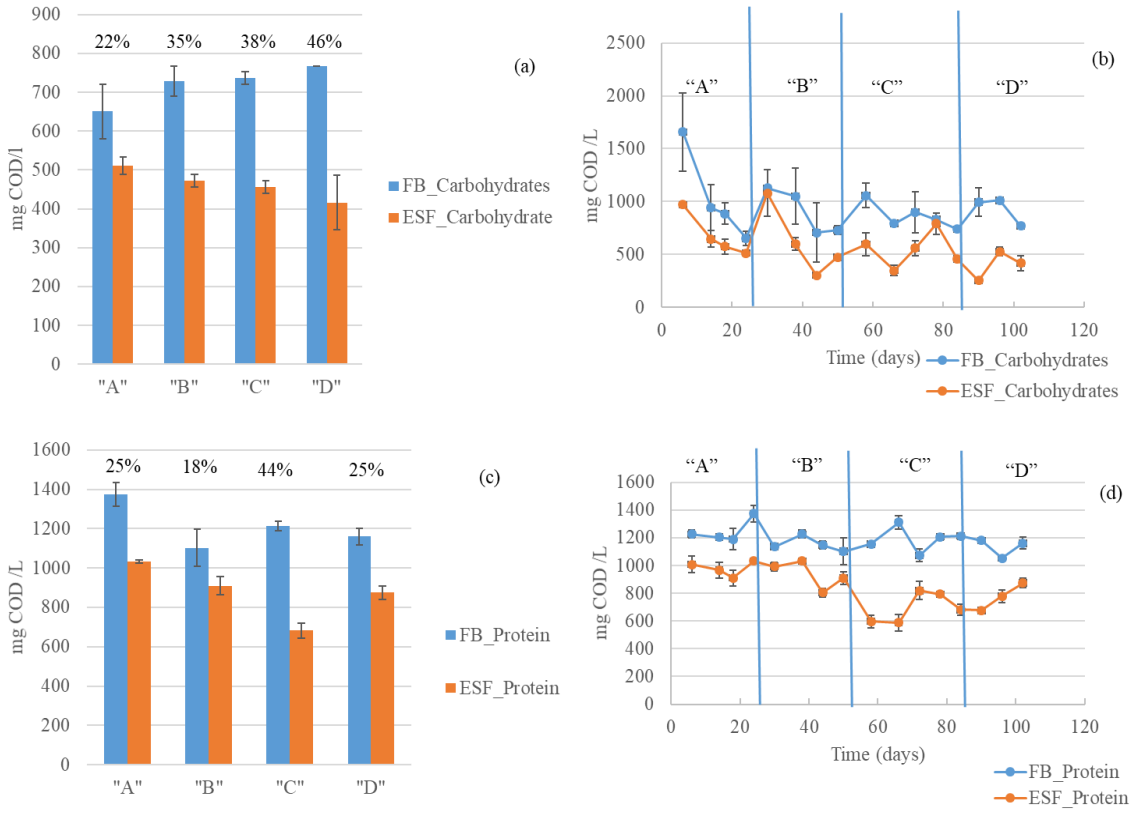

Figure 4.S3. Trends of total carbohydrate and protein concentrations for FB and ESF for all four batches. (a) and (c) show carbohydrate and protein concentrations at the end of each stages respectively, and removal ratios are shown on top of bar diagrams; (b) and (d) show overall trends of protein and carbohydrate concentrations. Error bars indicate high and low values.

4.S4. Microbial Community Analysis

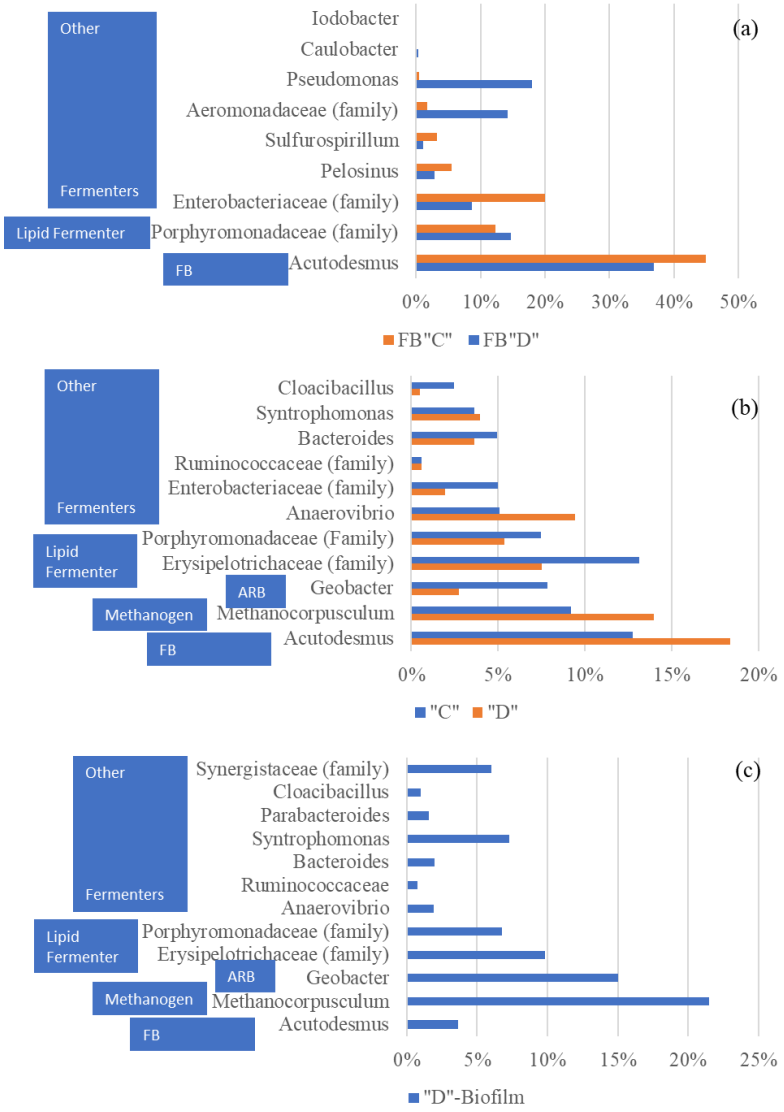

Figure 4.S4. Phylogenetic profiling of the suspended biomass in the FB "C" and "D" (a), ESF suspended biomass of "C" and "D" (b) and biofilm of "D" (c) at the genus level. Items that could not be identified at the genus level are named at the family level and noted by "(family)." The horizontal axis presents the percentage abundance of the families based on the total reads of the 16S rDNA gene. Functions associated with each family are shown to the left.

CHAPTER 5 EFFECTS OF SOLIDS RETENTION TIMES ON ELECTRO-SELECTIVE FERMENTATION USING *SCENEDESMUS ACUTUS* BIOMASS

This work, in a slightly modified format, will be submitted to the ACS Sustainable Chemistry & Engineering*, titled:*

Liu Y, Lai Y-JS, Rittmann BE. 2019. Effects of solids retention times on Electro-Selective Fermentation using *Scenedesmus acutus* biomass , *ACS Sustainable Chemistry & Engineering.*

5.1 Introduction

Electro-Selective Fermentation (ESF) is a novel technology that combines Selective Fermentation (SF) and Microbial Electrolysis Cells (MECs) to enhance lipid-wet extraction and "biohydrogenation" by β-oxidation from microalgae feeding biomass (FB) (Liu et al., 2019a, 2019b). The cell wall of *Scenedesmus*, composed of trilaminar structure of glycosylated polypeptide, poses a strong barrier to the extraction of internal components, such as lipids and proteins (Allard and Templier, 2001; Voigt et al., 2014). Hence, breaking down cell-wall carbohydrates and proteins can make the intracellular lipids more readily extractable. ESF has proven effective in degrading cellular protein of *Scenedesmus* biomass, thus exposing the lipids for wet extraction (Liu et al., 2019a). In ESF, anode-respiring bacteria (ARB), which reside as a biofilm on an anode surface of a microbial electrolytic cell (MEC), scavenge the short-chain fatty acids (SCFA) generated in the fermentation process, and this lowers the SCFA concentrations. The electrons that ARB remove from the SCFAs flow from the anode to the cathode through the MEC's

external circuit, ultimately reaching cathode where they reduce H_2O to generate H_2. Thus, ARB in ESF maximize electron utilization to energy-embodying products.

In Chapter 2, I showed that ESF improved lipid wet extraction to about 25%, but this benefit came with a significant loss of total lipids (~30%). The loss of lipids was associated with "biohydrogenation" through β-oxidation of unsaturated fatty acids, such as C18:1 and C18:3.

β-oxidation cleaved off two carbon atoms from long-chain fatty acid (LCFA) molecules to form acetate and H_2 (Cavaleiro et al., 2016). Acetate is the preferred substrate for ARB (Ki et al., 2015; Mahmoud et al., 2014a; Miceli et al., 2014), and the generated acetate was converted to current at the anode, with H_2 harvested at the cathode. Thus, β-oxidation in ESF led to the benefits of additional saturated LCFA production, but also to the disbenefit of loss of total lipids. An improved ESF system would reduce total-lipid loss and maintain the enhancements to lipid extraction and saturated-LCFA production.

A critical variable that determines performance of any microbiological system is the solids retention time (*SRT*), which is defined as the average time that biomass spends in the system (Rittmann and McCarty, 2001). When the system is at steady state, *SRT* equals the reciprocal of the specific growth rate (μ). In ESF, the *SRT* of planktonic biomass can be manipulated by changing the hydraulic retention time (*HRT*) via changing the flow rate. In Chapter 2 and Chapter 4, I proved ESF to be effective in enhancing lipid-wet extraction and lipid "biohydrogenation" with *Scenedesmus acutus* biomass, when the *HRT* was 5 or 6 days. As pointed out by Rittmann and McCarty (2001), lipid fermenters have a slower growth rate compared to carbohydrate and protein fermenters.

This means that a short *SRT*, associated with a short *HRT*, should selectively wash out planktonic lipid fermenters, while keeping protein and carbohydrate fermenters.

A potentially important factor is that the actual *SRT* in a system may be larger than the *HRT* due to biofilm growth and accumulation. ESF involves a biofilm that is dominated by ARB, although other bacteria, such as protein and lipid fermenters, can inhabit the biofilm as well. For example, high-throughput sequencing results documented in Chapter 2 showed that *Geobacteraceae* (ARB), *Erysieplotrichaceae* (lipid fermenter), *and Porphyromonadaceae* (protein fermenter and lipid biohydrogenater) were present in the ESF biofilm in relatively high abundance. Thus, *SRT* values must be calculated on the basis of *HRT* and biofilm detachment in ESF. I hypothesize that establishing a proper *SRT*, achieved by implementing a specific *HRT*, will allow removal of carbohydrates and protein, but conserve lipids. The ultimate outcome will be improved lipid wet-extraction, additional saturated fatty acid production, and better lipid conservation.

The specific goals of this research were to: 1) compare extractable-lipid production from *S. acutus* biomass for ESF with relatively long and short *SRTs*; 2) identify *SRT*s required for enhancing lipid extraction in *S. acutus* biomass, while minimizing lipid loss; and 3) link different lipid extractabilities with changes in the microbial community.

5.2 Material and Methods

Two flat-plate MEC reactors followed the design of Ki et al. (2017), but with removal of the cathodic serpentine structure. The MEC was constructed with multiple layers of transparent acrylic plates. The anode chamber had a volume of 200 mL, and the cathode chamber had a working volume of 66 mL. The anode was a carbon fiber (0.01-mm strand diameter, 2000 filaments, Goodfellows Cambridge Limited, Huntingdon, England) woven through a perforated titanium-plate mesh. The cathode was made of stainless-steel mesh (SS, type 316, mesh 80 * 80, 0.014cm of wire diameter, McMaster-Carr, Santa Fe Springs, CA, USA). The anode and cathode had geometric areas of 49 cm^2, but the actual area for biofilm attachment on the anode may have been greater than its geometric area due to the high specific area of the carbon fiber. An Ag/AgCl reference electrode (BASI Electrochemistry, West Lafayette, IN, USA) was installed at the center of the anode chamber from the top through a butyl-stopper with its tip ~3 cm above the bottom of the anode chamber and ~1cm from the surface of the carbon-fiber anode. An anion-exchange membrane (AEM) (AMI - 7001, Membranes International, New Jersey, USA) separated the anode and the cathode.

A biofilm dominated by ARB was accumulated on the anode surface of both MECs, prior to the experiments fed *S. acutus* biomass, by feeding a synthetic medium with a mixture of organic substrates (1970 mg/L sodium acetate, 380 mg/L sodium propionate, 200 mg/L sodium butyrate, 90 mg/L glucose, 140 mg/L Bovine Serum Albumin) and 1 mL/L of trace element solution (Lee et al., 2008a) in a 80-mM phosphate buffer (pH = 7.5)). Initially, the feed synthetic medium (180 mL) was inoculated with anaerobic digester

sludge (20 mL) from the Mesa Northwest Wastewater Reclamation Plant (MNWWRP, Mesa, AZ). Then, autoclaved synthetic medium was continuously fed with an initial flow rate of 0.1 mL / min (*HRT* = 1.4 d), and the current was be monitored using the potentiostat connected to a computer with the EC-Lab software package. When the two reactors achieved a stable current density (~2 A/m^2), the flow rate was increased in increments of 0.1 mL/min to increase the available flux of organic substrate to the biofilm, up to 0.5 mL/min (*HRT* = 0.3d). Both reactors accumulated an active ARB biofilm with stable current density of ~5 A/m^2.

The two MECs (denoted MEC-A and MEC-B) were operated with different *HRT* patterns. MEC-A had a 6-d *HRT* for 36 days and then a 2-d *HRT* for 12 days. MEC-B had a 2-d- *HRT* for 12 days and then a 6-d *HRT* for 36 days. The A experiment was begun by filling the anode chamber with 180 mL of newly collected *S. acutus* biomass (80 mM PBS, pH = 7.0, 4.8 g VSS /L, Arizona State University, Tempe Campus, Tempe, AZ) inoculated with 20 mL WAS to ensure a diverse community of bacteria able for hydrolysis and fermentation. To achieve a 6-d *HRT*, 33 mL of anode effluent was removed at the end of each day, and 33 mL of fresh *S. acutus* feeding biomass (FB) was added immediately to re-establish the volume in the anode chamber. The 6-d *HRT* stage lasted for 36 days. From day 37 onwards, the *HRT* of MEC A was switched to 2 days, where 100 mL of effluent was replaced with FB each day until day 48. For MEC B, the reactor started with a 2-d *HRT*, where 100 mL of effluent were replaced daily from day 1 to 12. Then, the *HRT* was switched to 6 days, where the volume of effluent replacement

was 33 mL per day until day 48. FB and effluent samples were collected every three days for the 2-d HRT stages and every six days at the 6-d *HRT* stages.

I assayed volatile suspended solid (VSS), total chemical oxygen demand (TCOD), ammonia-nitrogen, protein, lipids, and short-chain fatty acids (SCFAs) in the FB and MEC effluent. VSS was determined by methods described in sections 2540 B and E of *Standard Methods* (Rice et al., 2012). Total COD was measured using a HACH COD kit (HR+, concentration range 200-1,5000 mg/L). NH_4^+ was measured using HACH ammonium-N kit (concentration range 2 - 47 NH_4^+-N /L) (HACH Co., Loveland, CO, USA). After a sample was filtered through a 0.2-μm membrane (Pall Science, NY, USA), SCFAs were measured by high-performance liquid chromatography (HPLC) (Shimadzu Corp, Columbia, MD, USA) equipped with an Aminex HPX-87H column (Parameswaran et al., 2009).

Total and extractable lipids, characterized as fatty acid methyl esters (FAME) and expressed as COD values, were quantified for the solids using the method of Lai et al. (2016a). Total lipids were assayed by direct-transesterification, which converted all algal triacylglycerides (TAGs) and diacylglycerides (DAGs) to fatty acid methyl esters (FAME). FAME concentrations were determined using a Shimadzu gas chromatography equipped with a Bio-Rad Animex HPX-87H column (Bio Rad Life Science, Hercules, CA, USA). Extractable lipids were measured by extraction with 100% hexane (H) (Lai et al., 2016b; Liu et al., 2019b) followed by FAME analysis. Extractability was computed by dividing the extractable FAME by the total FAME of the corresponding FB; saturation was computed by dividing the saturated FAME in the FB or effluent by the total FAME

in the same sample; and FAME recovery was computed by dividing the total FAME in an effluent sample by the total FAME of its corresponding FB.

Total carbohydrates were determined by a modified phenol-sulfuric acid method developed (Laurens et al., 2012b). Total Protein was determined using a Bio-Rad protein kit (Bio-Rad, Hercules, CA, USA).

SCFAs, total protein, total carbohydrates, and total FAME concentrations obtained from these methods were converted mg COD /L to quantify the electron distribution in the solids.

DNA samples from the FB, both reactor effluents, and both anode biofilms were extracted and analyzed for community analysis on day 36 (6-d *HRT* transition to 2-d *HRT*) and day 48 for MEC-A and on day 12 (2-d *HRT* transition to 6-d *HRT*) and day 48 for MEC-B. DNA was extracted using PowerSoil DNA isolation Kits (MoBio Laboratories, Inc, Carslbad, CA, USA). Amplification and sequencing were performed by the Microbiome Analysis Laboratory, Arizona State University, using a MiSeq Illumina Sequencer, targeting the V4 Region of the 16S rRNA gene with primer set 515f/806r. 16S rRNA gene sequences were analyzed using the Quantitative Insights into Microbial Ecology software package (QIIME 2, version 2019.4, http://qiime2.org/). Principal coordinates analysis (PCoA) of the community structure in different samples was performed using EMPeror software package in the QIIME 2 system using weighted Unifrac method (Vázquez-Baeza et al., 2013).

5.3. Results and Discussion

5.3.1 ESF Performance and *SRT*

The average current densities, obtained by dividing daily collected coulombs (1 d = 86400 s) and anode area (49 cm^2), are shown in Figures 5.1 (a) and (b). While both reactors, started up with fresh *S. acutus* FB, gave initial current densities of ~ 3A/m^2, the current densities of the two reactors quickly diverged: For MEC-A (6-d *HRT*), the current density stabilized at ~1.2 A/m^2 at day 5, while the current density for MEC-B (2-d *HRT*) stabilized at ~ 2.0 A/m^2 at day 3. The average current densities had dramatic changes when the *HRT* was changed. For MEC-A, switching the *HRT* to 2d on day 37 led to an immediate increase in the current density to ~3 A/m^2; the current density slightly rose to ~3.3 A/m^2 on day 40 and then stayed stable for the rest of the experiment. For MEC-B, the *HRT* change to 6 d on day 12 caused a drop in the current density to ~1.3 A/m^2, although it gradually increased to ~2 A/m^2 by about day 37. The over-arching trend is that the 6-d *HRT* yielded lower current density than 2-d HRT, which indicates that a higher FB loading rate (caused by a shorter *HRT*) led to greater ARB activity brought about by a higher substrate flux to the ARB biofilm.

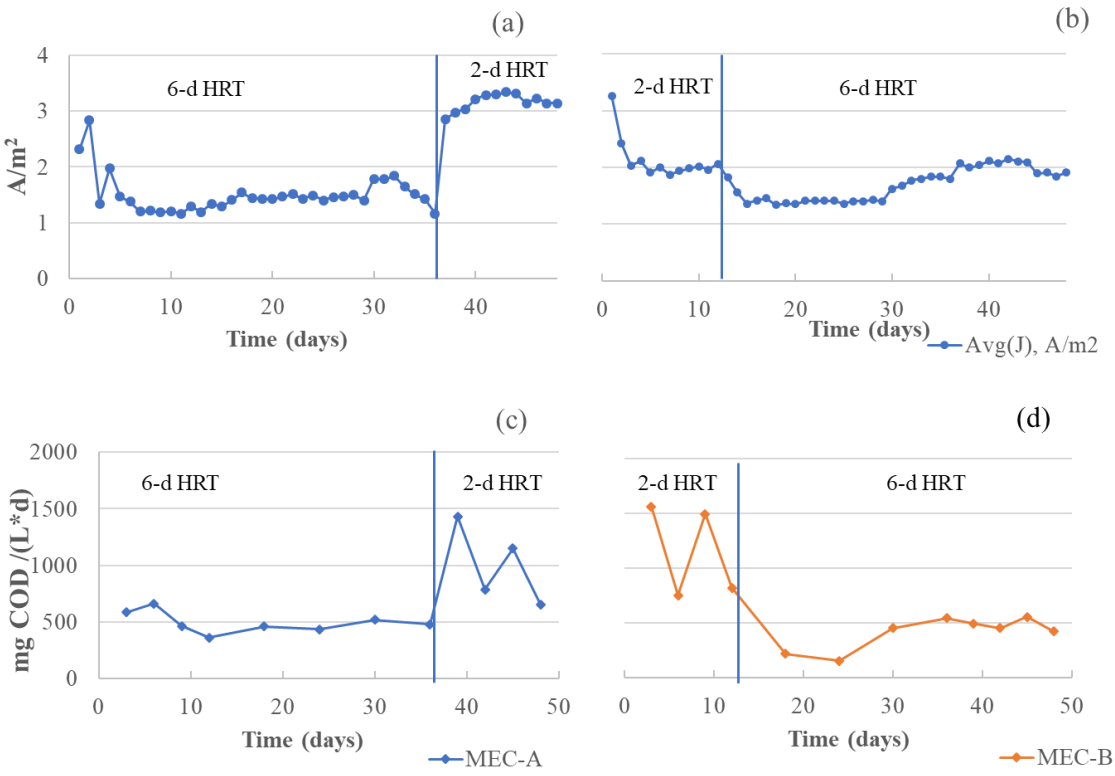

Figure 5. 1. Trends of daily average current density for MEC-A (a) and MEC-B (b). Trends of daily COD removal rates for MEC A (c) and MEC- B (d). The *HRT*s and the times of *HRT* switches are shown.

The COD-removal rate was calculated by dividing the difference between FB-COD and effluent-COD (on the same day) by the *HRT*:

$$COD_{rate} = \frac{COD_{FB} - COD_{Eff}}{HRT} \qquad (Eq.\ 5.1)$$

where COD_{FB} (mg /L) is the FB-COD, COD_{Eff} (mg /L) is the effluent-COD on the same day, and *HRT* (d) is for same day. Figures 1 (c) and (d) shows COD removal rates of MECs A and B. For MEC-A, the 6-d-*HRT* had an average COD removal rate of 500 ± 90 mg COD / L*d, but the *HRT* change to 2 d on day 36 increased the COD removal rate to 1010 ± 350 mg COD /L*d. Similarly for MEC-B, the average COD removal rate of 2-d *HRT* was 1160 ± 430 mg COD /L*d, but was 410 ± 150 mg COD /L*d for the 6-d *HRT*.

Calculations in part 5.S1 of the Supplemental Information show that the overall *SRT*s of the ESF reactors were almost equal to the *HRT*s, since suspended biomass dominated biofilm biomass. Thus, *HRT* is an appropriate surrogate for the overall ESF's *SRT*.

5.3.2 FAME Extractability and Volumetric Productivity

FAME extractability for the biomass in the effluents of both MECs, along with the FB, are shown in Figure 5.2 (a) and (b). FB had low extractability for the whole period, ~ 5%. For MEC-A, the extractability rose rapidly after day 9, roughly increased linearly increased to ~25% at day 24, and then stayed stable to day 36, the end of the 6-d *HRT*. When the *HRT* of MEC-A was decreased to 2 d, the extractability decreased immediately to ~13% on day 39 and then stabilized at ~19%. For MEC-B, the extractability in the first 12 days, with the 2-d *HRT*, was similar to the FB, ~5%, which is different from the results obtained with 2-d *HRT* with MEC-A. After the *HRT* was switched to 6 d on day 13, the extractability began climbing, reaching ~11% on day 18 and eventually ~22% by day 36. The lack of enhancement with the initial *HRT* of 2 d suggests that the key hydrolytic and fermentative bacteria needed to degrade the protective layers of *S. acutus* could not accumulate but were washed out with the 2-d *HRT*. When the longer *HRT* replaced the shorter HRT, these microorganisms were able to accumulate, which led to a breakdown of *S. acutus*'s protective structures. This explanation is consistent with the higher lipid extractability with the 6-d *HRT* for MEC-B than for MEC-A, because key hydrolytic and fermentative bacteria had been partially washed out during the 2-d stage of MEC A.

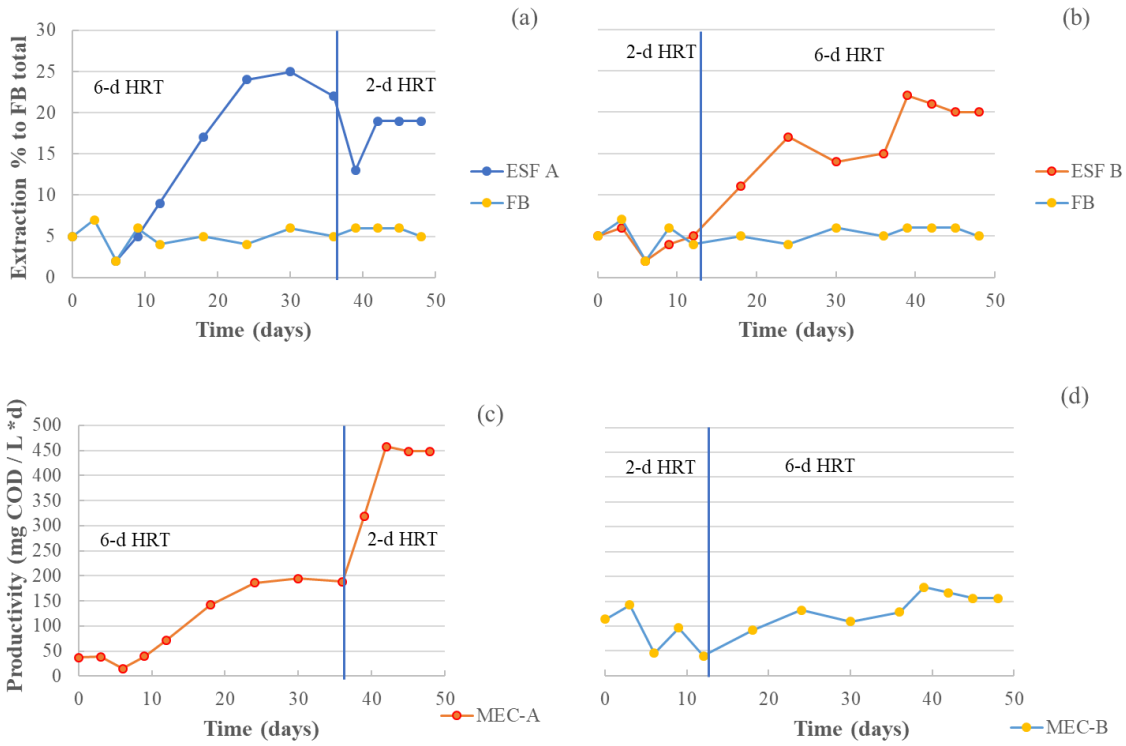

Figure 5. 2. Trends of extractability for MEC-A (a) and MEC-B (b) and of FAME volumetric productivity for MEC-A (c) and MEC-B (d). The times of *HRT* switches are indicated.

For a specific day and reactor volume, the volumetric productivity of lipids ($Prod_{lipids}$, in mg COD / L•d), was calculated from:

$$Prod_{lipids} = COD_{FB} * Ext\% * Q_{eff} / V_r \qquad (Eq.\ 5.2)$$

where COD_{FB} is the total concentration of FAME in *S. acutus* FB (mg COD /L); Ext% is the extractability percentage for that day; Q_{eff} is the volume of effluent produced on the day (for a 6-d *HRT*, Q_{eff} = 33 mL / d; for a 2-d *HRT*, Q_{eff} = 100mL / d); and V_r is the volume of the reactor (200 mL). Figures 2 (c) and (d) shows that the trends of FAME recovery differed from the trends for extractability. For MEC-A, the FAME productivity was stable between days 0-12 at ~50 mg COD /L*d and then increased to ~240 mg COD /L*d on day 24. Switching the *HRT* to 2 d caused an immediate increase in productivity, reaching ~450 mg COD/L*d on day 39, the top productivity achieved by MEC-A. For MEC-B, the productivity was 120 mg COD /L*d at the start, declining to ~40 mg COD /L*d on day 12 before the *HRT* was switched to 6d. Then, the productivity increased and reached peak at 180 mg COD /L*d between day 39 and day 48. The lipid productivity in MEC-B never reached the values of MEC-A with a 6-d *HRT*. This reinforces that having the 6-d *HRT* after the 2-d *HRT* in MEC-B did not restore a microbial community as effective at hydrolytic and fermentative functions. In general, a lower *HRT* supported higher volumetric productivity, but low lipid extractability; however, starting the MEC with a short *HRT* flushed out fermenters, which were not restored once the *HRT* was extended to 6 d. Thus, as long as the MEC had been started with a long *HRT*, which selected a suitable microbial community that was able to ferment protective layer and expose lipids, switching to a shorter *HRT* retained the fermenters so that high

extractability could continue. Thus, volumetric lipid productivity was higher, since the extractability did not dramatically shrink.

HRT also had an influence on FAME recovery for the two MECs, as shown in Figure 5.3. The FAME recovery percentage started low for MEC-A, with a 6-d *HRT*, possibly caused by algae biomass attachment to the anode biofilm, as seen in Chapter 3. Then, it increased to and peaked at ~95% on day 30. At this point, MEC-A had the highest FAME extractability

(Fig. 5.2(a)) and low FAME loss, perhaps because the newly exposed algal-lipid has not accumulated a substantial amount of lipid fermenters. After the *HRT* switch to 2 d, the FAME recovery again approached 100% on day 48, when extractability was high at ~20%. Perhaps the lipid fermenters (but not protein and carbohydrate fermenters) were washed out by the *HRT* of 2 d, fulfilling the potential to achieve high extractability and high lipid recovery, with a short-enough *SRT* (2 d).

MEC-B displayed high, but unstable FAME recovery with the 2-d *HRT* (~65 to ~100%). The lower values may have been due to a combined effect of biomass attachment to the anode and low lipid degradation with a short *HRT*. After the *HRT* switch to 6 d, FAME recovery initially rose to >100% (day 24), and this may have been caused by removal of lipids that had attached to the anode. FAME recovery then decreased and stabilized at ~80% on day 30. Similar to MEC-A, the trends for MEC-B suggest that lipid degraders and fermenters were washed out with the 2-d *HRT*. However, the fermenters were able to regrow after the *HRT* was switched to 6 d.

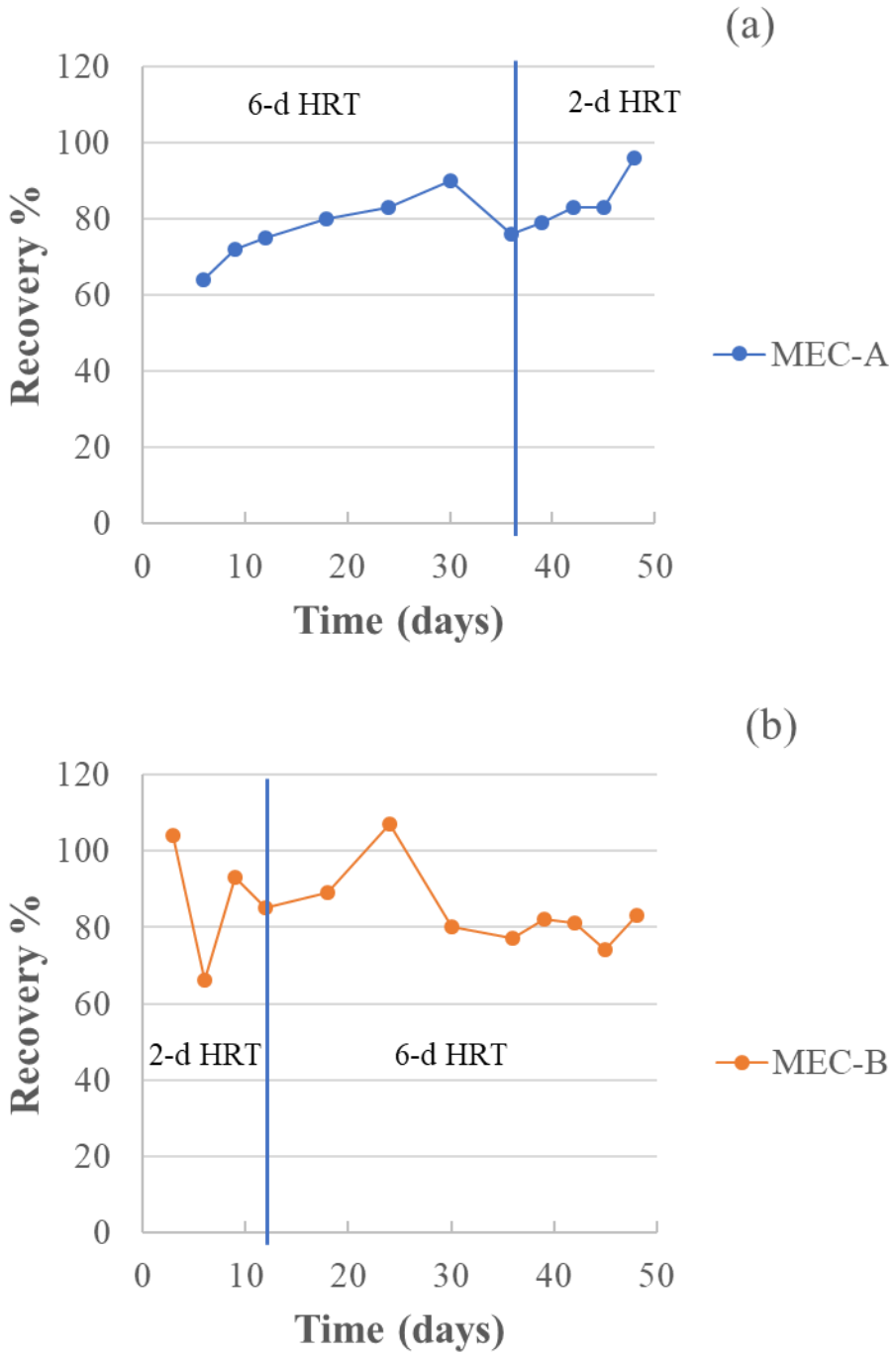

Figure 5. 3. Trends of FAME recovery percentage for MEC-A (a) and MEC-B (b). The times of *HRT* switches, with *HRT*s applied are shown.

5.3.3 Short-Chain Fatty Acids (SCFAs)

Concentrations of SCFAs in the effluents of MEC-A and MEC-B, expressed in mg COD /L, are shown in Figure 5.4. Significant SCFA species were formate, acetate, propionate, butyrate, valerate, and caproate. Since caproate exhibited unique trends, Figures 5.4 (b) and (d) shows caproate and total SCFAs excluding caproate.

In MEC-A, total SCFA was high at the start,1600 mg COD /L, and >90% of was caproate. Total SCFA decreased rapidly, mostly caused by the decrease of caproate, reaching nearly zero after 36 days of operation at the 6-d*HRT* reaction; the almost-complete removal of SCFAs demonstrates strong ARB activity. After the *HRT* was switched to 2 d, total SCFA modestly increased, to ~400 mg COD /L on day 48, and caproate contributed ~ 50%. The total SCFA concentration rebounded, and current density was higher after the *HRT* switch (Figure 5.1. (a)). Both factors demonstrate that the 2-d *HRT* allowed a higher volumetric fermentation rate (Figure 5.1 (c)) that produced more SCFAs and, consequently, more current.

For MEC-B, total SCFA started lower (~800 mg COD /L) than MEC-A, and the majority (~75%) was caproate. The initial 2-d *HRT* in MEC-B showed a modest declining trend of total SCFA and caproate out to day 12, and this may indicate a gradual accumulation of more ARB. After the *HRT* was increased to 6 d, the declining trend of total SCFA accelerated, again mostly caused by rapidly declining caproate. Total SCFA reached ~200 mg COD /L on day 48, and the majority was still caproate (up to 90%).

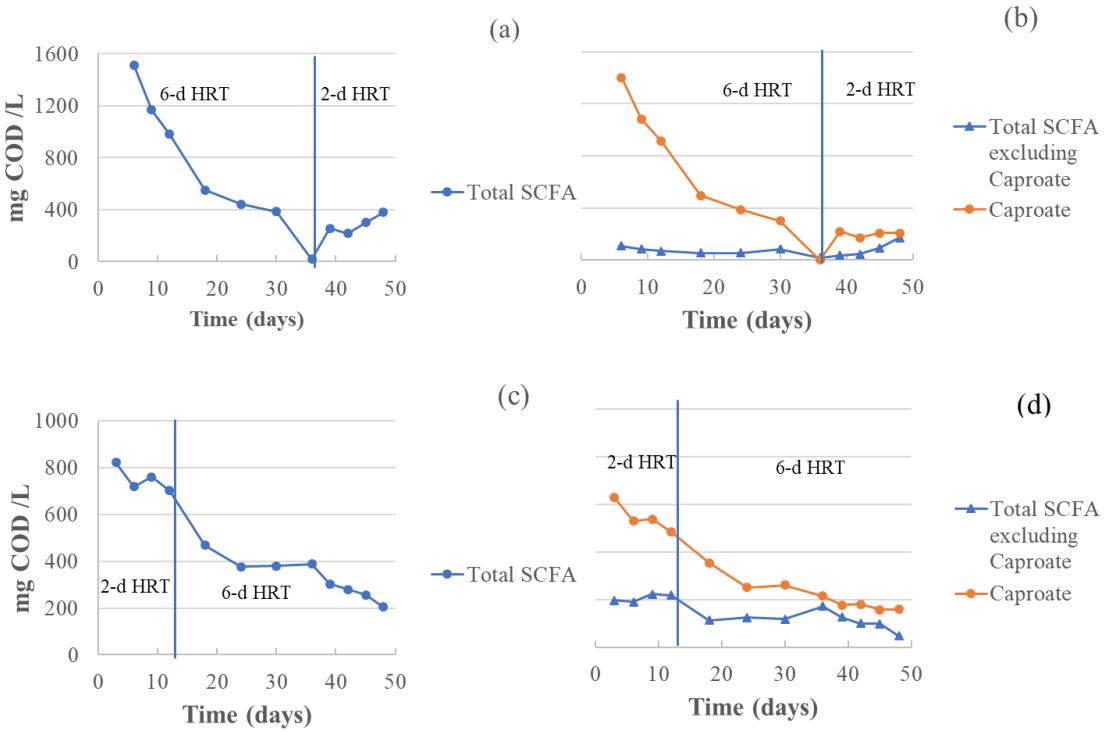

Figure 5. 4. Trends of SCFA concentrations, in mg COD/L: total SCFA in MEC-A (a), Caproate and SCFA excluding caproate in MEC-A (b), total SCFA in MEC-B (c), Caproate and SCFA excluding caproate in MEC-B (d). The points of *HRT* switch, as well as respective *HRT* implemented where shown.

5.3.4 Microbial Community Analysis

Microbial community structures at the family level for the FB, the MEC effluents, and MEC biofilms using high-throughput sequencing. To determine if the different sources had distinct community structures, I performed principal coordinates analysis (PCoA). The results, shown in Figure 5.5, clearly show three clusters: FB to the far right on the PC1 axis (56.8%), the biofilms on the far left on the PC1 axis, and the MEC effluents in the middle of the PC1 axis, but higher on the PC2 axis (19.1%), showing the communities in FB, MEC effluent suspended biomass, and MEC biofilms were distinct.

Some trends appear within the three groups. FB had a systematic movement down on the PC2 axis due to its storage, but almost no movement along the PC1 axis. Because the PC2 axis presented a small portion of the total variance (19.1%), the movement was not a sign of a major change in community structure.

In the cluster of the effluent suspended biomass, MEC-A shifted significantly on both axes between d12 and d36 with 6-d *HRT*, but the subsequent shift between d36 and d48 (to a 2-d *HRT*) was smaller along the PC1 axis and almost negligible along the PC2 axis. This indicates that 6-d *HRT* was causing bigger shift in the microbial community than 2-d *HRT*. The MEC-B community clearly moved left along the PC1 axis between d12 and d36, but the subsequent move between d36 and d48 was negligible. The moves in MEC-B was all smaller than in MEC-A with 6-d *HRT*, especially between d36 and d48, indicating smaller change in the microbial community had occurred even though the *HRT* was extended. This indicates that the recovery of slow-growing bacteria with a later-implemented long *HRT* was small in MEC-B.

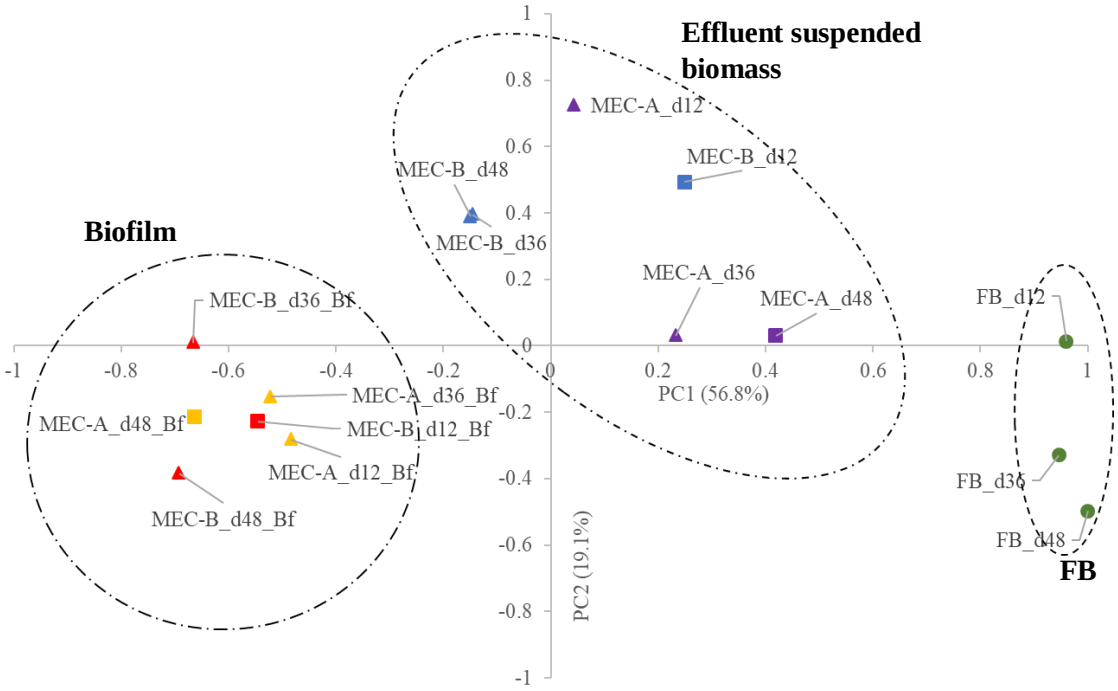

Figure 5. 5. Principal coordinates analyses (PCoA) for microbial communities of FB, MEC effluents, and biofilms. Symbol shapes denote the *HRT* at the time the sample was taken: 6 d (▲) or 2 d (■). Color denotes the sample type: purple for MEC-A effluent, blue for MEC-B effluent, orange for MEC-A biofilm, and red for MEC-B biofilm. A green circle denotes FB. The designation dxx indicates the day on which the sample was taken. The percentages in the axis labels represents the percentages of variations explained by the two principal coordinates; axes values denote degree of variance within the range of -1 and 1.

Microbial community structures at the family level in the MEC-A effluents, MEC-A biofilm, and the FB are presented in Figure 5.6, which also identifies known functions of each family. Parallel presentations for MEC-B are in the Supplemental Information.

The FB (Fig. 5.6(a)) had a high abundance of *Chlamydomonadaceae*, which corresponds to the chloroplast DNA of *S. acutus*; however, endogenous degradation occurred during FB storage, and the DNA of *Chlamydomonadaceae* decreased between days 12 and 48. The abundance of *Pseudomonadace* greatly increased with time. *Pseudomonadaceae* potentially includes cryophilic bacteria capable of degrading *S. acutus* cellular structure (Reddy et al., 2004).

In both MECs (Fig. 5.6(b) and Fig. 5.S1(a), *Chlamydomonadaceae* was substantially less with the 6-d *HRT*, compared to the 2-d *HRT*. Lower *Chlamydomonadaceae* abundance also was associated the higher lipid extractability with the longer *HRT* (Fig. 5.1). Both trends are consistent with greater breakdown of the cell wall of *Chlamydomonadaceae* with the longer *HRT*.

One known lipid hydrogenator, *Erysipelotrichaceae* (Liu et al., 2019a) was in the FB. It, along with the other known lipid fermenter, *Porphyromonadaceae*, greatly increased in both MECs on day 12, although they declined after day 12. The decline may have been due to these two lipid hydrogenators being slow growers that were washed out regardless of *HRT* being 6 d or 2 d. Hence, these lipid fermenters' population could be controlled via an adequate *HRT*. *Porphyromonadaceae* had less decline than *Erysipelotrichaceae*, probably due to the fact that it can also metabolize sugars when usable lipids are not available as substrates (Hahnke et al., 2015b).

All the known fermenters present in the FB, except *Cytophaceae*, accumulated in MECs, especially *Pseudomonadaceae*, which had a dramatic increase up to as high as 28% in MEC-A. These FB-indigenous fermenters accumulated in the MECs regardless of long or short *HRT*, since they had a fast-enough growth rate to withstand washout. In contrast, *Synergistaceae* and all *Bacteroidiales*, including *Porphyromonadaceae*, which are non-indigenous fermenters, were important for an *HRT* of 6 d, then slightly declined for the 2-d *HRT*. This indicates that these fermenters were promoted to grow with a long *HRT* (6-d). A shorter *HRT* (2-d), though not supportive for their growth, did not have a strong flush-out effect for them. In summary, the fermenters' growth was strongly supported by 6-d *HRT*, but they could withstand complete washout in 2-d *HRT*. The high lipid extractability in MEC-A with both 6-d and 2-d *HRTs* may have been associated with the continued persistence of these fermenters.

The anodes of both MECs displayed typical ARB biofilms, with by far the largest number of sequences belonged to *Geobacteraceae*, a widely recognized ARB (Bond, 2002; Jung and Regan, 2007; Miceli et al., 2014). The abundance of *Geobacteraceae* was at least 31%, similar to the value in Chapter 2, indicating a healthy and electrochemically active biofilm. The biofilms also harbored small fractions of all of the microbial types detected in the suspension, while the effluents of both MECs had small numbers of *Geobacteraceae* that were not in the FB. Hence, the biofilm and suspended communities exchanged microorganisms. The biofilms also hosted increasing abundance of *Erysipelotrichaceae* and *Porphyromonadaceae*, showing that these lipid fermenters were thriving in the biofilm. Abundance of bioavailable lipid substrates attached to the

anode might be the cause to this phenomenon, which is similar to my observation in Chapter 2.

The only methanogen detected was *Methanocorpusculaceae*, a H_2-oxidizing family, and it always comprised less than 10%. No acetate-consuming methanogens were present, as they were out-competed by the ARB. This indicates that the ARB most likely prevailed in the competition between it and acetate-consuming methanogens, leaving H_2-consuming methanogens as the only remaining methanogens.

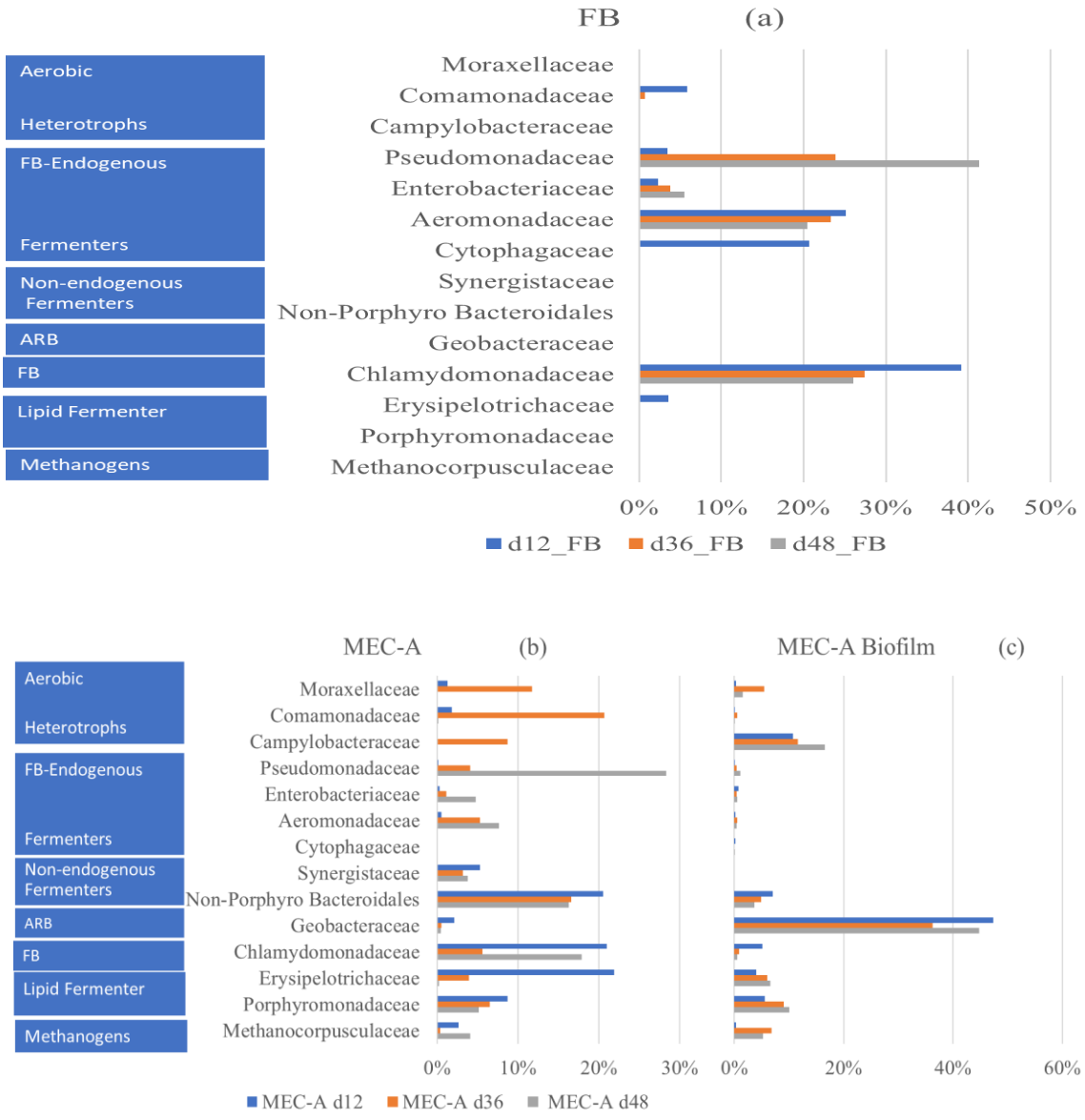

Figure 5. 6. Phylogenetic profiling of the suspended biomass in the FB (a), MEC-A effluent suspension (b), and MEC-A biofilm (c) at the family level. Parallel phylogenic profiles of MEC-B effluent and biofilm are shown in Figure 5.S1 in the Supplemental Information. The horizontal axis presents the percentage abundance of the families based on the total reads of the 16S rRNA gene. Functions associated with each family are shown to the left.

5.4. Conclusions

ESF enhanced lipid extraction from *S. acutus* biomass, and different MEC *HRT*s, which were almost equal to the overall *SRT*s, led to different results for lipid extraction and other performance parameters. The 6-d *HRT* attained higher lipid extractability, but the 2-d *SRT* attained higher lipid productivity per unit reactor volume. Starting the MEC with a 2-d *HRT* impaired the enhancement of lipid extractability because protein fermenters, such as *Syneristaceae*, *Pseudomonadaceae*, and *Enterobacteriaceae* were flushed out and could not recover after the switch to a longer *HRT*. Principal coordinates analysis revealed that the communities of the FB, MEC effluent, and MEC biofilms were distinct, but 6-d *HRT* caused greater change in microbial community structures than 2-d *HRT*. Only the microbial community in the MEC effluent was systematically affected by the change in *HRT*, the 6-d *HRT* had more lipid fermenters, but both *HRT* were able to flush out these lipid fermenters due to their nature as a slow grower. By far the largest part of the microbial community of the biofilms were well-known ARB, and the biofilm community was not affected systematically by the *HRT*.

Supplemental Information for Chapter 5

5. S1. Estimating the Solids Retention Time (SRT)

The *SRT* of an ESF reactor is not the same as its Hydraulic Retention Time (*HRT*) due to the biofilm on the anode. Likewise, the *SRT* of the entire ESF system is a composite of the *SRT*s of the suspended biomass and the biofilm. Thus, a change to the *HRT* does not necessarily equal a change to the *SRT* system.

A biofilm's average *SRT* is the reciprocal of the biofilm's average first-order detachment rate (b_{det}) (Rittmann and McCarty, 2001), which can be estimated *a priori* by

$$b_{det} = 8.42 * 10^{-2}\left(\frac{\sigma}{1+433.2\left(L_f-0.003\right)}\right)^{0.58} \qquad \textit{(Eq. 5.S1)}$$

where L_f is the biofilm thickness (cm), X_f is the biofilm density (mg / cm^3), and σ is the shear stress in dyne / cm^2 (the same as g/cm^2-s). The σ values in the MECs can be bracketed by 0.02 dyne /cm^2 to 1 dyne/cm^2, based on modest to strong mixing intensity (Rittmann and McCarty, 2001). By using values this σ range, X_f = 40 mg /cm^3, and L_f = 0.01 cm, I computed a b_{det} range of 0.004 d^{-1} to 0.4 d^{-1}. which leads to range of biofilm *SRT*s of 260 d to 27 d.

Detachment of biofilm biomass augments the suspended biomass. When the suspension receives input active biomass, its *SRT* increases according to (Rittmann and McCarty, 2001):

$$SRT_{planktonic} = \frac{X_a V}{QX_a - QX_a^0} = \frac{X_a V}{QX_a - b_{det} X_f L_f A_b} \qquad \textit{(Eq 5.S2)}$$

where X_a is the concentration of active biomass of the planktonic biomass, V is the ESF reactor's working volume, Q is the volumetric flow rate, $Q^* X_a^0$ is the detachment rate of the biofilm (and the rate of biomass addition to the suspension), $X_f L_f$ is the mass of biofilm per unit surface area, and A_b is the biofilm surface area.

An overall *SRT* can be computed for all of the biomass in the ESF reactor: planktonic + biofilm. Starting from the definition of *SRT* and combining planktonic active biomass and biofilm active biomass, the $SRT_{overall}$ is:

$$SRT_{overall} = \frac{X_a V + X_f L_f A}{Q X_a} = HRT + \frac{X_f L_f A}{Q X_a} \qquad \textit{(Eq. 5.S3)}$$

Eq. 5.S3 shows that the total *SRT* is always larger than the *HRT* due to the accumulation of biofilm biomass.

Assuming an active-biomass concentration (X_a) of 3000 mg VSS /L in the suspended phase, a biofilm density (X_f) of 40 mg /cm^3, and a biofilm thickness (L_f) of 0.01cm, along with known biofilm area of 49 cm^2 and an anode chamber volume of 200 mL, Equations 5.S2 and 5.S3 yield the SRT values in Table 5.S1. The overall *SRTs* are only slightly greater than the the *HRTs*, regardless of long or short *HRTs* (6 d vs 2d) and different shear stress caused by different mixing intensities (b_{det} = 0.004 or 0.04 d^{-1}), because the suspended biomass ($X_a V$) dominated the biofilm biomass ($X_f L_f A$). Thus, it accurate to use the *HRT* as a surrogate of the overall *SRT* of the ESF reactors.

Table 5.S 1 Calculated values of $SRT_{planktonic}$, $SRT_{biofilm}$, and $SRT_{overall}$ using assumptions of high and low shear stress. All SRT values are in d.

	Low shear stress (0.02 dyne/cm^2)	High shear stress (1 dyne/cm^2)
	6-d HRT	
$SRT_{biofilm}$	250	25
$SRT_{planktonic}$	6.1	6.6
$SRT_{overall}$	6.2	6.2
	2-d HRT	
$SRT_{biofilm}$	250	25
$SRT_{planktonic}$	2.0	2.1
$SRT_{overall}$	2.1	2.1

5.S2. Profiling of Microbial Communities in MEC-B

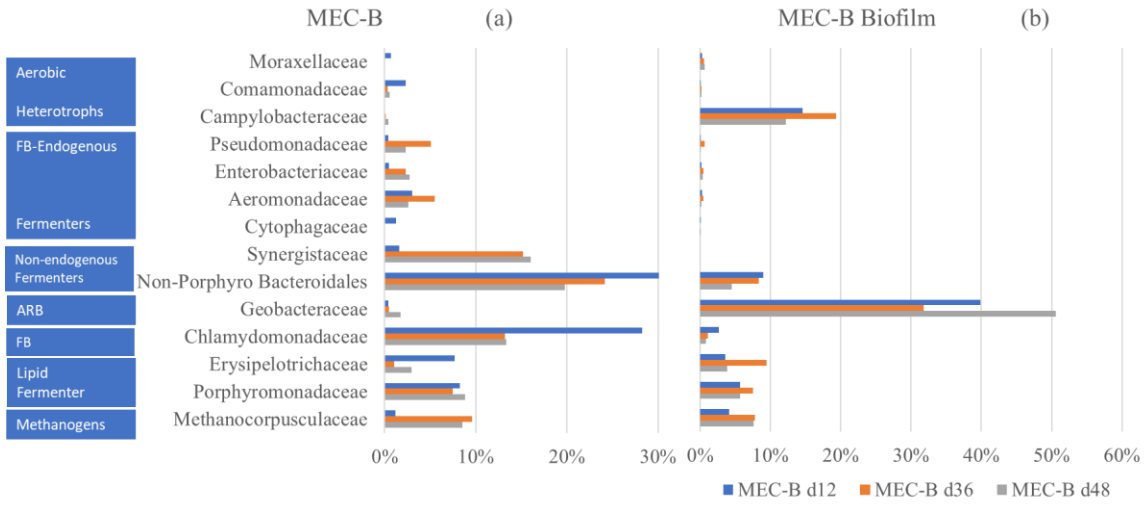

Figure 5.S 1. Phylogenetic profiling of the ESF anode effluent in MEC-B (a) and biofilm in MEC-B (b). The horizontal axis presents the percentage abundance of the families based on the total reads of the 16S rRNA gene. Functions associated with each family are shown to the left.

CHAPTER 6 SUMMARY AND FUTURE RESEARCH

6.1 Summary

MECs have well-known uses: degrading complex organics while producing hydrogen, electricity, or chemicals (Lu et al., 2012; Mahmoud et al., 2014b; Parameswaran et al., 2011; Young et al., 2016). A less-well-recognized feature of MECs is that they can accelerate protein degradation (Lu et al., 2012). Taking advantage of the protein angle, I created the concept of Electro-Selective Fermentation (ESF), a combination of the MEC with Selective Fermentation (SF) of lipid-rich microalgae, such as *Scenedesmus acutus*. SF selectively degrades carbohydrates and proteins, while leaving the lipids intact for wet extraction. SF generally worked to enhance lipid-extraction, and a bonus was biohydrogenation of the lipids (Lai et al., 2016b). However, much of the biomass was converted to short chain fatty acids (SCFAs), which were lost in the effluent. Also, protein degradation was not extensive. So, I combined SF with the anode of an MEC in order to avoid losing the electrons in SCFAs and to increase protein degradation. This dissertation documents the value of ESF and the mechanisms underlying it.

In Chapter 2, I proved the ESF concept by feeding *S. acutus* biomass directly to the anode chamber of an MEC at room temperature. The anode produced modest current density (1 - 2.5 A/m^2), lipid extraction was enhanced, and protein degradation was significantly increased compared to SF. "Biohydrogenation" produced saturated lipids as a bonus, although it was brought about by by β-oxidation that caused loss of total lipids. An important result is the at the suspended microbial community contained one known

biohydrogenater, *Porphyromonadaceae*, and one new biohydrogenater, *Erysipelotrichaceae*.

The MEC I used in Chapter 2 had a very small anode area, and it was unable to oxidize much of the SCFAs produced by fermentation. In Chapter 3, I used a flat-plate MEC with a carbon fiber anode having much larger surface area. In batch experiments, I found that the higher anode area allowed anode respiration to scavenge SCFA concentrations to minimum levels. Lipid extraction and saturation continued to be strong, but the microalgae biomass and its lipids attached to the biofilm, which wasted a substantial amount of electrons in the batch experiments. Thus, a continuous or semi-continuous feeding should overcome this problem.

In Chapter 4, I fed four batches of *S. acutus* biomass semi-continuously to an ESF reactor for 102 days and with an *HRT* of 6 d. Lipid extraction was enhanced by ESF, "biohydrogenation" again occurred by β-oxidation, and SCFA concentrations were minimized. The most important result was that the four FB batches had very different outcomes for lipid extraction and other performance parameters: "A" and "C" batches had high lipid-extraction ratios, but "B" and "D" batches yielded nearly zero lipid extraction. Lipid-extraction ratios were strongly correlated to protein loss, ammonium-N release, and lipid saturation. Principal Coordinates Analysis (PCoA) revealed that, while the FBs of "A" and "C" were not closely related (nor were "B" and "D", the ESF effluents of "A" and "C" were closely related, as were "B" and "D". Thus, the endogenous microbial community of the FB did not determine the different extraction

performances. Instead, FB composition and cellular structure were more likely the cause, although how the cause-and-effect remain unknown.

My research has shown that ESF is effective for enhancing lipid wet-extraction and "biohydrogenation" by β-oxidation. However, lipid loss was not always accompanied by enhancement of lipid extraction. In Chapter 5, I tried to find the minimum *SRT* that provides maximum lipid extraction, but has minimum lipid loss. I compared two MECs with different shifting *SRTs*, 6 d to 2 d versus 2 d to 6 d. A 6-d *SRT* successfully achieved high extraction ratio, but still had high lipid loss. Shortening the *SRT* to 2 d from 6 d continued good lipid extraction, and lipid loss was reduced. The 2-d *SRT* also led to an almost tripling of the volumetric rate of lipid production. In contrast, starting with a short *SRT* of 2 d flushed our key fermenters early, and extending the *SRT* to 6 d only partially restored lipid extraction. Thus, I conclude that ESF must be started with a long-enough *SRT* to allow accumulation of fermenters that lead to enhanced lipids extraction; a short *SRT* can be implemented later to achieve maximum lipid production and minimum lipid loss.

6.2 Suggestions for Future Research

6.2.1 Pursuing a Higher Lipid-Extraction Ratio

In my work, I achieved 25% to 30% lipid extraction with respect to the total lipid concentration in the FB. Given that most of the microalgal-lipids are intracellular globules that can be released once the cell structures are completely ruptured, I am convinced of the potential for big improvement to the lipid-extraction ratio. Chapter 2's ESF process removed 45% of total carbohydrate and 45% of protein of the *S. acutus* cell, which yielded ~ 25% lipid extraction. To achieve total degradation of protein and carbohydrate components of *S. acutus* biomass, a semi-continuous experiment with a long *SRT* to see maximum degradation of carbohydrates, protein and lipid extraction / loss. Then, experiment with a shorter *SRT* may be able to maximize volumetric lipid production by taking advantage of fermenters accumulated from the previous long-*SRT* stage.

Another approach to maximize carbohydrate / protein removal and lipid extraction is to pre-inoculate the FB with protein fermenters; this is a form of bioaugmentation. As described in Chapter 2, the family of *Bacteroidaceae* contains protein fermenters that were accumulated in ESF; in Chapter 5, *Pseudomonadaceae* also accumulated in the MEC effluent. Therefore, I suggest pre-inoculating the FB with these microorganisms instead of the waste-activated sludge, to initiate a stronger kick-start to the fermentation process in the ESF.

6.2.2 Find Out Why the ARB Biofilm Enhances Protein Degradation

It is apparent from that the ARB biofilm enabled greater degradation of protein, which consequently led to high lipid extraction via exposure of lipids to solvent extraction. Lu et al. (2012) was first to observe enhanced protein degradation with MEC, and they brought upon the concept of "cascade degradation" in an attempt to explain the mechanism. However, the concept of cascade degradation was not explained in the article, nor has it been explained in any later works. It is possible that the low concentration of SCFAs caused by ARB respiration lowered the thermodynamic barriers of protein fermentation reaction by minimizing product concentrations, but the protein degradation and lipid extraction was still enhanced with high SCFA concentrations in Chapter 2. To solve this conundrum, the mechanism of accelerated protein degradation in MECs must be solved *a priori*. I suggest using Bovine Serum Albumin (BSA) as the sole substrate in an MEC pre-inoculated with an ARB biofilm to start. I also propose that the ARB biofilm should be pre-inoculated with pure *Geobacter* culture to eliminate fermenters within the biofilm. If the mechanism behind enhanced protein degradation is low SCFA concentrations, I can artificially increase acetate concentration by spiking acetate into the anode chamber, which should in turn build a thermodynamic barrier by increasing the product concentration, thus slowing the protein degradation process. If *Geobacter* cannot directly use BSA, then its augmentation to protein degradation might be related to its acetate consuming current producing activities. I propose running multiple MECs with open circuit and closed circuit respectively to see their respective performance on protein degradation.

6.2.3 Find Out the Cause of the Different Performances Associated with Different FB Batches

In Chapter 4, I documented that four batches of FB yielded quite different performances on lipid extraction and many other parallel effects. I concluded that these performance differences were caused by the biochemical compositions of the FB, but not the endogenous microbial community. The question is then, "what caused the differences?" In most of my experiments, I successfully achieved high lipid extraction; it was only with the long-term experiment described in Chapter 4 in which I identified "recalcitrant" FB batches. If I were to expand upon my earlier findings, I would try different batches of FBs having well defined different grow stages and lipid contents. As the algae I used in all Chapters had ~ 30 - 40 % lipid by weight, algae batches with lower lipid content might be used to potentially identify "recalcitrant" FB with respect to lipid content. Once a "recalcitrant" FB is found, I propose analyzing its intracellular and membrane lipid composition to find the differences between "recalcitrant" FBs and "degradable" FBs. The results, in turn, can help algae producers avoid producing recalcitrant FB batches, which has much lower economic values due to its resistance to ESF treatment.

REFERENCES

Adeniyi OM, Azimov U, Burluka A. 2018. Algae biofuel: Current status and future applications. Renew. Sustain. Energy Rev. 90:316–335.

Allard B, Templier J. 2001. High molecular weight lipids from the trilaminar outer wall (TLS)-containing microalgae Chlorella emersonii, Scenedesmus communis and Tetraedron minimum. Phytochemistry 57:459–467.

Andersen ME. 2002. Lessons Learned in Applying the U.S. EPA Proposed Cancer Guidelines to Specific Compounds. Toxicol. Sci. 53:159–172.

APHA. 2016. Standard Methods for the Examination of Water & Wastewater, 20th edition. Washington DC: American Public Health Association.

Bermingham EN, Maclean P, Thomas DG, Cave NJ, Young W. 2017. Key bacterial families (Clostridiaceae, Erysipelotrichaceae and Bacteroidaceae) are related to the digestion of protein and energy in dogs. PeerJ 5:e3019.

Bligh EG, Dyer WJ. 1959. A rapid method of total lipid extraction and purification. Can. J. Biochem. Physiol. 37:911–917.

Bolyen E, Rideout JR, Dillon MR, Bokulich NA, Abnet C, Al-Ghalith GA, Alexander H, Alm EJ, Arumugam M, Asnicar F, others. 2018. QIIME 2: Reproducible, interactive, scalable, and extensible microbiome data science.

Bond DR. 2002. Electrode-Reducing Microorganisms That Harvest Energy from Marine Sediments. Science. 295:483–485.

Brown RE, Jarvis KL, Hyland KJ. 1989. Protein measurement using bicinchoninic acid: elimination of interfering substances. Anal. Biochem. 180:136–139.

Castro-Carrera T, Toral PG, McEwan NR, Hervas G, Abecia L, Pinloche E, Girdwood SE, A B. 2014. Rumen bacterial community evaluated by 454 pyrosequencing and terminal restriction fragment length polymorphism analyses in dairy sheep fed marine algae. J. Dairy Sci. 97:1661–1669.

Cavaleiro AJ, Pereira MA, Guedes AP, Stams AJM, Alves MM, Sousa DZ. 2016. Conversion of Cn-Unsaturated into Cn-2-Saturated LCFA Can Occur Uncoupled from Methanogenesis in Anaerobic Bioreactors. Environ. Sci. Technol. 50:3082–3090.

Chisti Y. 2007. Biodiesel from microalgae. Biotechnol. Adv. 25:294–306.

Cho S, Park S, Seon J, Yu J, Lee T. 2013. Evaluation of thermal, ultrasonic and alkali pretreatments on mixed-microalgal biomass to enhance anaerobic methane production. Bioresour. Technol. 143:330–336.

Christ O, Wilderer PA, Angerhofer R, Faulstich M. 2000. Mathematical modeling of the hydrolysis of anaerobic processes. Water Sci. Technol. 41:61–65.

Cooney M, Young G, Nagle N. 2009. Extraction of Bio-oils from Microalgae. Sep. Purif. Rev. 38:291–325.

Dejoye C, Vian MA, Lumia G, Bouscarle C, Charton F, Chemat F. 2011. Combined extraction processes of lipid from Chlorella vulgaris microalgae: Microwave prior to supercritical carbon dioxide extraction. Int. J. Mol. Sci. 12:9332–9341.

Dong T, Knoshaug EP, Davis R, Laurens LML, Van Wychen S, Pienkos PT, Nagle N. 2016. Combined algal processing: A novel integrated biorefinery process to produce algal biofuels and bioproducts. Algal Res. 19:316–323.

DuBois M, Gilles KA, Hamilton JK, Rebers PA, Smith F. 1956. Colorimetric Method for Determination of Sugars and Related Substances. Anal. Chem. 28:350–356.

Ehimen EA, Connaughton S, Sun Z, Carrington GC. 2009. Energy recovery from lipid extracted, transesterified and glycerol codigested microalgae biomass. GCB Bioenergy 1:371–381.

Esquivel-Elizondo S, Delgado AG, Krajmalnik-Brown R. 2017. Evolution of microbial communities growing with carbon monoxide, hydrogen, and carbon dioxide. FEMS Microbiol. Ecol. 93:1–12.

Folch J, Lees M, Sloane Stanley GH. 1957. A simple method for the isolation and purification of total lipids from animal tissues. J. Biol. Chem. 226:497–509.

Gao Y, Ryu H, Santo JW, Lee H. 2014. Syntrophic interactions between H 2 -scavenging and anode-respiring bacteria can improve current density in microbial electrochemical cells. Bioresour. Technol. 153:245–253.

Greiner T, Bäckhed F. 2011. Effects of the gut microbiota on obesity and glucose homeostasis. Trends Endocrinol. Metab. 22:117–123.

Griffiths MJ, Harrison STL. 2009. Lipid productivity as a key characteristic for choosing algal species for biodiesel production. J. Appl. Phycol. 21:493–507.

Guo K, Prévoteau A, Rabaey K. 2017. A novel tubular microbial electrolysis cell for high rate hydrogen production. J. Power Sources 356:484–490.

Hahnke S, Maus I, Wibberg D, Tomazetto G, Pühler A, Klocke M, Schlüter A. 2015a. Complete genome sequence of the novel Porphyromonadaceae bacterium strain ING2-E5B isolated from a mesophilic lab-scale biogas reactor. J. Biotechnol. 193:34–36.

Hahnke S, Maus I, Wibberg D, Tomazetto G, Pühler A, Klocke M, Schlüter A. 2015b. Complete genome sequence of the novel Porphyromonadaceae bacterium strain ING2-E5B isolated from a mesophilic lab-scale biogas reactor. J. Biotechnol. 193:34–36.

Halim R, Gladman B, Danquah MK, Webley PA. 2011. Bioresource Technology Oil extraction from microalgae for biodiesel production. Bioresour. Technol. 102:178–185.

Hallenbeck PC, Grogger M, Mraz M, Veverka D. 2016. Solar biofuels production with microalgae. Appl. Energy 179:136–145.

Holmes DE, Bond DR, O'Neil RA, Reimers CE, Tender LR, Lovley DR. 2004. Microbial communities associated with electrodes harvesting electricity from a variety of aquatic sediments. Microb. Ecol. 48:178–190.

Hu Q, Sommerfeld M, Jarvis E, Ghirardi M, Posewitz M, Seibert M, Darzins A. 2008. Microalgal triacylglycerols as feedstocks for biofuel production: Perspectives and advances. Plant J. 54:621–639.

Huang H. A. 1996. Oleosins and Oil bodies in Seeds and Other Organs. Plant Physiol.:1055–1061.

Huws SA, Kim EJ, Lee MRF, Scott MB, Tweed JKS, Pinloche E, Wallace RJ, Scollan ND. 2011. As yet uncultured bacteria phylogenetically classified as Prevotella, Lachnospiraceae incertae sedis and unclassified Bacteroidales, Clostridiales and Ruminococcaceae may play a predominant role in ruminal biohydrogenation. Environ. Microbiol. 13:1500–1512.

IPCC. 2018. Summary for Policymakers of IPCC Special Report:13–16.

John Wallace R, Chaudhary LC, McKain N, McEwan NR, Richardson AJ, Vercoe PE, Walker ND, Paillard D. 2006. Clostridium proteoclasticum: A ruminal bacterium that forms stearic acid from linoleic acid. FEMS Microbiol. Lett. 265:195–201.

Jung S, Regan JM. 2007. Comparison of anode bacterial communities and performance in microbial fuel cells with different electron donors. Appl. Microbiol. Biotechnol. 77:393–402.

Kaspar H, Wuhrmann K. 1977. Product inhibition in sludge digestion. Microb. Ecol. 4:241–248.

Ki D, Parameswaran P, Popat SC, Rittmann BE, Torres CI. 2015. Effects of pre-fermentation and pulsed-electric-field treatment of primary sludge in microbial electrochemical cells. Bioresour. Technol. 195:83–88.

Knothe G. 2011. A technical evaluation of biodiesel from vegetable oils vs. algae. Will algae-derived biodiesel perform? Green Chem. 13:3048.

Lai YJS, McCaw A, Ontiveros-Valencia A, Shi Y, Parameswaran P, Rittmann BE. 2016a. Multiple synergistic benefits of selective fermentation of Scenedesmus biomass for fuel recovery via wet-biomass extraction. Algal Res. 17:253–260.

Lai YS, Parameswaran P, Li A, Aguinaga A, Rittmann BE. 2016b. Selective fermentation of carbohydrate and protein fractions of Scenedesmus , and biohydrogenation of its lipid fraction for enhanced recovery of saturated fatty acids. Biotechnol. Bioeng. 113:320–329.

Lai Y, Parameswaran P, Li A, Baez M, Rittmann BE. 2014. Effects of pulsed electric field treatment on enhancing lipid recovery from the microalga , Scenedesmus. Bioresour. Technol. 173:457–461.

Laurens LML, Nagle N, Davis R, Sweeney N, Van Wychen S, Lowell A, Pienkos PT. 2015. Acid-catalyzed algal biomass pretreatment for integrated lipid and carbohydrate-based biofuels production. Green Chem. 17:1145–1158.

Laurens LML, Van Wychen S, McAllister JP, Arrowsmith S, Dempster TA, McGowen J, Pienkos PT. 2014. Strain, biochemistry, and cultivation-dependent measurement variability of algal biomass composition. Anal. Biochem. 452:86–95.

Laurens LML, Dempster TA, Jones HDT, Wolfrum EJ, Wychen S Van, Mcallister JSP, Rencenberger M, Parchert KJ, Gloe LM. 2012. Algal Biomass Constituent Analysis: Method Uncertainties and Investigation of the Underlying Measuring Chemistries. Anal. Chem. 84:1879–1887.

Lee H-S, Parameswaran P, Kato-Marcus A, Torres CI, Rittmann BE. 2008a. Evaluation of energy-conversion efficiencies in microbial fuel cells (MFCs) utilizing fermentable and non-fermentable substrates. Water Res. 42:1501–1510.

Lee HS, Parameswaran P, Kato-Marcus A, Torres CI, Rittmann BE. 2008b. Evaluation of energy-conversion efficiencies in microbial fuel cells (MFCs) utilizing fermentable and non-fermentable substrates. Water Res. 42:1501–1510.

Lee HS, Rittmann BE. 2009. Evaluation of metabolism using stoichiometry in fermentative biohydrogen. Biotechnol. Bioeng. 102:749–758.

Liu Y, Lai Y-JS, Barbosa TS, Chandra R, Parameswaran P, Rittmann BE. 2019. Electro-selective fermentation enhances lipid extraction and biohydrogenation of Scenedesmus acutus biomass. Algal Res. 38:101397.

Logan BE, Call D, Cheng S, Hamelers HVM, Sleutels THJA, Jeremiasse AW, Rozendal RA. 2008. Microbial Electrolysis Cells for High Yield Hydrogen Gas Production from Organic Matter. Environ. Sci. Technol. 42:8630–8640.

Lu L, Xing D, Liu B, Ren N. 2012. Enhanced hydrogen production from waste activated sludge by cascade utilization of organic matter in microbial electrolysis cells. Water Res. 46:1015–1026.

Lu L, Xing D, Xie T, Ren N, Logan BE. 2010. Hydrogen production from proteins via electrohydrogenesis in microbial electrolysis cells. Biosens. Bioelectron. 25:2690–2695.

Mahmoud M, Parameswaran P, Torres CI, Rittmann BE. 2014a. Fermentation pre-treatment of landfill leachate for enhanced electron recovery in a microbial electrolysis cell. Bioresour. Technol. 151:151–158.

Mahmoud M, Parameswaran P, Torres CI, Rittmann BE. 2014b. Fermentation pre-treatment of landfill leachate for enhanced electron recovery in a microbial electrolysis cell. Bioresour. Technol. 151:151–158.

Markou G, Nerantzis E. 2013. Microalgae for high-value compounds and biofuels production: A review with focus on cultivation under stress conditions. Biotechnol. Adv. 31:1532–1542.

Miceli JF, Parameswaran P, Kang DW, Krajmalnik-Brown R, Torres CI. 2012. Enrichment and analysis of anode-respiring bacteria from diverse anaerobic inocula. Environ. Sci. Technol. 46:10349–10355.

Miceli JF, Garcia-peña I, Parameswaran P, Torres CI, Krajmalnik-brown R. 2014. Combining microbial cultures for efficient production of electricity from butyrate in a microbial electrochemical cell. Bioresour. Technol. 169:169–174.

Miron Y, Zeeman G, van Lier JB, Lettinga G. 2000. The role of sludge retention time in the hydrolysis and acidification of lipids, carbohydrates and proteins during digestion of primary sludge in CSTR systems. Water Res. 34:1705–1713.

National Centers for Environmental Information. 2019. Global Climate Report - Annual 2018.

Parameswaran P, Torres CI, Lee HS, Rittmann BE, Krajmalnik-Brown R. 2011. Hydrogen consumption in microbial electrochemical systems (MXCs): The role of homo-acetogenic bacteria. Bioresour. Technol. 102:263–271.

Parameswaran P, Torres CI, Lee H-S, Krajmalnik-Brown R, Rittmann BE. 2009. Syntrophic interactions among anode respiring bacteria (ARB) and Non-ARB in a biofilm anode: electron balances. Biotechnol. Bioeng. 103:513–23.

Parameswaran P, Zhang H, Torres CI, Rittmann BE, Krajmalnik-Brown R. 2010. Microbial community structure in a biofilm anode fed with a fermentable substrate: The significance of hydrogen scavengers. Biotechnol. Bioeng. 105:69–78.

Rabaey K, Angenent L, Schröder U, Keller J. 2009. Bioelectrochemical Systems: From Extracellular Electron Transfer to Biotechnological Application. IWA Publishing.

Ramsay IR, Pullammanappallil PC. 2001. Protein degradation during anaerobic wastewater treatment: Derivation of stoichiometry. Biodegradation 12:247–257.

Reddy GSN, Matsumoto GI, Schumann P, Stackerbrandt E, Shivaji S. 2004. Psychrophilic pseudomonads from Antarctica: Pseudomonas antartica sp. nov., Pseudomonas meridiana sp. nov. and Pseudomonas proteolytica sp. nov. Int. J. Syst. Evol. Microbiol. 54:713–719.

Reguera G, McCarthy KD, Mehta T, Nicoll JS, Tuominen MT, Lovley DR. 2005. Extracellular electron transfer via microbial nanowires. Nature 435:1098–1101.

Rittmann BE, McCarty PL. 2001. Environmental Biotechnology: Principles and Applications. Tata McGraw Hill Education Private Limited. McGraw-Hill series in water resources and environmental engineering.

Rittmann BE. 2008. Opportunities for renewable bioenergy using microorganisms. Biotechnol. Bioeng. 100:203–212.

Rodolfi L, Zittelli GC, Bassi N, Padovani G, Biondi N, Bonini G, Tredici MR. 2009. Microalgae for oil: Strain selection, induction of lipid synthesis and outdoor mass cultivation in a low-cost photobioreactor. Biotechnol. Bioeng. 102:100–112.

Rozendal RA, Hamelers HVM, Rabaey K, Keller J, Buisman CJN. 2008. Towards practical implementation of bioelectrochemical wastewater treatment. Trends Biotechnol. 26:450–459.

Sayre R. 2010. Microalgae: The Potential for Carbon Capture. Bioscience 60:722–727.

Sheng J, Vannela R, Rittmann BE. 2011a. Evaluation of cell-disruption effects of pulsed-electric-field treatment of Synechocystis PCC 6803. Environ. Sci. Technol. 45:3795–3802.

Sheng J, Vannela R, Rittmann BE. 2011b. Evaluation of methods to extract and quantify lipids from Synechocystis PCC 6803. Bioresour. Technol. 102:1697–1703.

Sheng J, Vannela R, Rittmann BE. 2011c. Evaluation of methods to extract and quantify lipids from Synechocystis PCC 6803. Bioresour. Technol. 102:1697–1703.

Siegert I, Banks C. 2005. The effect of volatile fatty acid additions on the anaerobic digestion of cellulose and glucose in batch reactors. Process Biochem. 40:3412–3418.

Taipale S, Strandberg U, Peltomaa E, Galloway AWE, Ojala A, Brett MT. 2013. Fatty acid composition as biomarkers of freshwater microalgae: Analysis of 37 strains of microalgae in 22 genera and in seven classes. Aquat. Microb. Ecol. 71:165–178.

Torres CI, Krajmalnik-Brown R, Parameswaran P, Marcus AK, Wanger G, Gorby YA, Rittmann BE. 2009a. Selecting anode-respiring bacteria based on anode potential: Phylogenetic, electrochemical, and microscopic characterization. Environ. Sci. Technol. 43:9519–9524.

Torres CI, Lee H, Krajmalnik-brown R, Rittmann BE. 2009b. A Kinetic Perspective on Extracellular Electron Transfer by Anode-Respiring Bacteria. FEMS Microbiol. Rev. 34:2–17.

Torres CI, Marcus AK, Rittmann BE. 2008. Proton transport inside the biofilm limits electrical current generation by anode-respiring bacteria. Biotechnol. Bioeng. 100:872–881.

Torres CI, Marcus AK, Rittmann BE. 2007. Kinetics of consumption of fermentation products by anode-respiring bacteria:689–697.

U.S. Energy Information Administration. 2018. U.S. Energy Facts Explained.

US Department of Commerce NOAA. 2019. Trends in Atmospheric Carbon Dioxide.

Vázquez-Baeza Y, Pirrung M, Gonzalez A, Knight R. 2013. EMPeror: A tool for visualizing high-throughput microbial community data. Gigascience 2:2–5.

Velasquez-Orta SB, Curtis TP, Logan BE. 2009. Energy from algae using microbial fuel cells. Biotechnol. Bioeng. 103:1068–1076.

Voigt J, Stolarczyk A, Zych M, Malec P, Burczyk J. 2014. The cell-wall glycoproteins of the green alga Scenedesmus obliquus. The predominant cell-wall polypeptide of Scenedesmus obliquus is related to the cell-wall glycoprotein gp3 of Chlamydomonas reinhardtii. Plant Sci. 215–216:39–47.

Van De Vossenberg JLCM, Joblin KN. 2003. Biohydrogenation of C18 unsaturated fatty acids to stearic acid by a strain of Butyrivibrio hungatei from the bovine rumen. Lett. Appl. Microbiol. 37:424–428.

Wang L, Li Y, Sommerfeld M, Hu Q. 2013a. A flexible culture process for production of the green microalga Scenedesmus dimorphus rich in protein, carbohydrate or lipid. Bioresour. Technol. 129:289–295.

Wang L, Li Y, Sommerfeld M, Hu Q. 2013b. A flexible culture process for production of the green microalga Scenedesmus dimorphus rich in protein, carbohydrate or lipid. Bioresour. Technol. 129:289–295.

Yang Y, Xu M, Guo J, Sun G. 2012. Bacterial extracellular electron transfer in bioelectrochemical systems. Process Biochem. 47:1707–1714.

Young MN, Links MJ, Popat SC, Rittmann BE, Torres CI. 2016. Tailoring Microbial Electrochemical Cells for Production of Hydrogen Peroxide at High Concentrations and Efficiencies. ChemSusChem 9:3345–3352.

Zbinden MDA, Sturm BSM, Nord RD, Carey WJ, Moore D, Shinogle H, Stagg-Williams SM. 2013. Pulsed electric field (PEF) as an intensification pretreatment for greener solvent lipid extraction from microalgae. Biotechnol. Bioeng. 110:1605–1615.

Zhang G, Zhao Q, Jiao Y, Wang K, Lee D-J, Ren N. 2012. Efficient electricity generation from sewage sludge usingbiocathode microbial fuel cell. Water Res. 46:43–52.